

AD-A089 792

HAZELTINE CORP GREENLAWN NY  
METAL-GRID SPATIAL FILTER, VOLUME I.(U)  
JUL 80 P W HANNAN, P L BURGHYER

F/G 9/1

F19628-78-C-0152

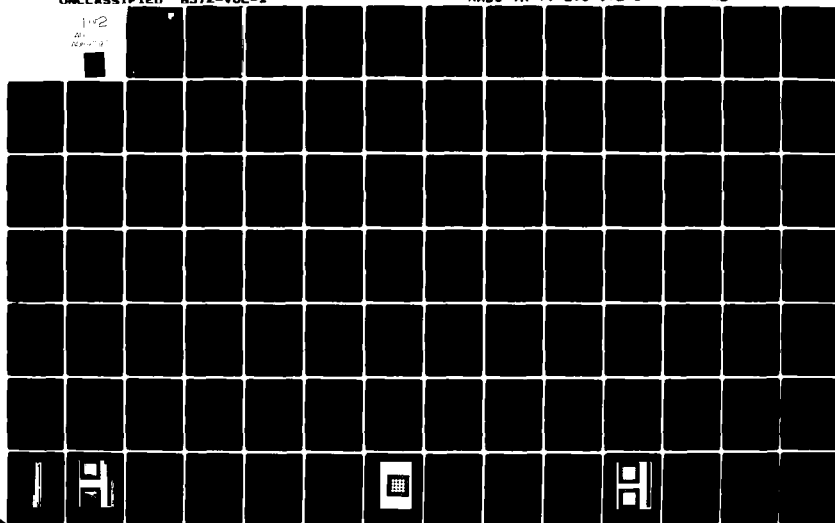
UNCLASSIFIED

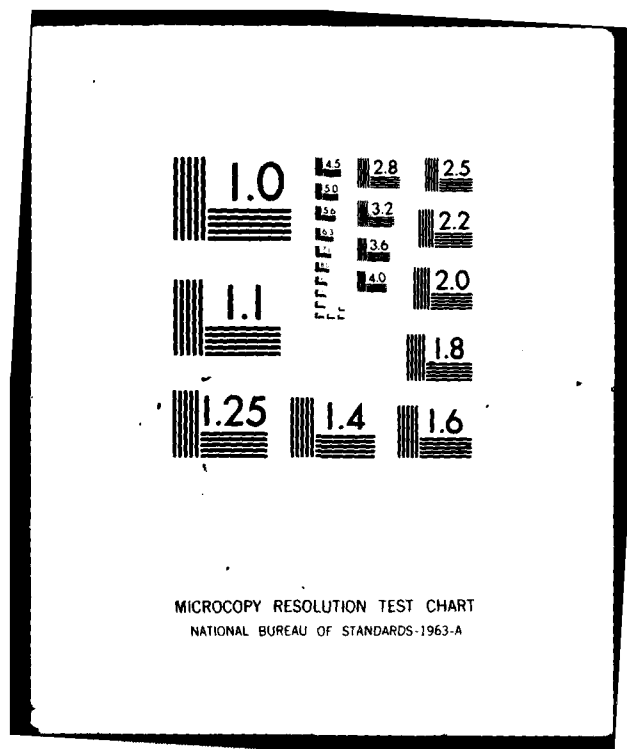
6372-VOL-1

RADC-TR-79-295-VOL-1

NL

1-2  
AD-A089 792





MICROCOPY RESOLUTION TEST CHART  
NATIONAL BUREAU OF STANDARDS-1963-A

✓  
RADC-TR-79-295, Vol I (of two)  
Interim Technical Report  
July 1980

12  
LEVEL

A089756



## METAL-GRID SPATIAL FILTER

Hazeltine Corporation

P. W. Hannan  
P. L. Burgmyer

AD A089792

DTIC  
ELECTE  
OCT 1 1980  
S C D

APPROVED FOR PUBLIC RELEASE; DISTRIBUTION UNLIMITED

ROME AIR DEVELOPMENT CENTER  
Air Force Systems Command  
Griffiss Air Force Base, New York 13441

FILE COPY

80 9 29 157

This report has been reviewed by the RADC Public Affairs Office (PA) and is releasable to the National Technical Information Service (NTIS). At NTIS it will be releasable to the general public, including foreign nations.

RADC-TR-79-295, Vol I (of two) has been reviewed and is approved for publication.

APPROVED:




PETER R. FRANCHI  
Project Engineer

APPROVED:



ALLAN C. SCHELL  
Chief, Electromagnetic Sciences Division

FOR THE COMMANDER:



JOHN P. HUSS  
Acting Chief, Plans Office

#### SUBJECT TO EXPORT CONTROL LAWS

This document contains information for manufacturing or using munitions of war. Export of the information contained herein, or release to foreign nationals within the United States, without first obtaining an export license, is a violation of the International Traffic in Arms Regulations. Such violation is subject to a penalty of up to 2 years imprisonment and a fine of \$100,000 under 22 U.S.C 2778.

Include this notice with any reproduced portion of this document.

If your address has changed or if you wish to be removed from the RADC mailing list, or if the addressee is no longer employed by your organization, please notify RADC (EEA) Hanscom AFB MA 01731. This will assist us in maintaining a current mailing list.

Do not return this copy. Retain or destroy.

UNCLASSIFIED

SECURITY CLASSIFICATION OF THIS PAGE (When Data Entered)

| 19 REPORT DOCUMENTATION PAGE  |   | READ INSTRUCTIONS<br>BEFORE COMPLETING FORM         |  |
|---|---|---|--|
| 1. REPORT NUMBER<br>(18) RADC-TR-79-295, Vol-1 (of two)   | 2. GOVT ACCESSION NO.<br>AD-A089792   | 3. RECIPIENT'S CATALOG NUMBER                       |  |
| 4. TITLE (and Subtitle)<br>(6) METAL-GRID SPATIAL FILTER.<br>Volume I.  | 5. TYPE OF REPORT & PERIOD COVERED<br>(9) Interim Report.<br>Sep 1978 - Aug 1979                | 6. PERFORMING ORG. REPORT NUMBER<br>(14) 6372-VOL-1 |  |
| 7. AUTHOR<br>(10) P. W. Hannan<br>P. L. Burgmyer  | 8. CONTRACT OR GRANT NUMBER(s)<br>(15) F19628-78-C-0152   |   |  |
| 9. PERFORMING ORGANIZATION NAME AND ADDRESS<br>Hazeltine Corporation<br>Pulaski Road<br>Greenlawn NY 11740  | 10. PROGRAM ELEMENT, PROJECT, TASK AREA & WORK UNIT NUMBERS<br>(16) 62702F<br>46001436 (17, 14) |   |  |
| 11. CONTROLLING OFFICE NAME AND ADDRESS<br>Deputy for Electronic Technology (RADC/EEA)<br>Hanscom AFB MA 01731  | 12. REPORT DATE<br>(11) Jul 1980  | 13. NUMBER OF PAGES<br>124                          |  |
| 14. MONITORING AGENCY NAME & ADDRESS (if different from Controlling Office)<br>Same (12) 124  | 15. SECURITY CLASS. (of this report)<br>UNCLASSIFIED  | 15a. DECLASSIFICATION/DOWNGRADING SCHEDULE<br>N/A   |  |
| 16. DISTRIBUTION STATEMENT (of this Report)<br><br>Approved for public release; distribution unlimited.   |   |   |  |
| 17. DISTRIBUTION STATEMENT (of the abstract entered in Block 20, if different from Report)<br><br>Same  |   |   |  |
| 18. SUPPLEMENTARY NOTES<br>RADC Project Engineer: Peter R. Franchi (RADC/EEA)   |   |   |  |
| 19. KEY WORDS (Continue on reverse side if necessary and identify by block number)<br><br>Metal-Grid<br>Spatial Filter<br>Angular Filter  |   |   |  |
| 20. ABSTRACT (Continue on reverse side if necessary and identify by block number)<br><br>This interim report presents the results of studies relevant to the design of spatial filters that have metal grids as their basic reflecting element. An analysis of metal-grid spatial filter designs shows the performance that is available. An experimental investigation of various types of metal grids confirms their suitability for spatial filters. |   |   |  |

DD FORM 1 JAN 73 1473 EDITION OF 1 NOV 65 IS OBSOLETE

UNCLASSIFIED

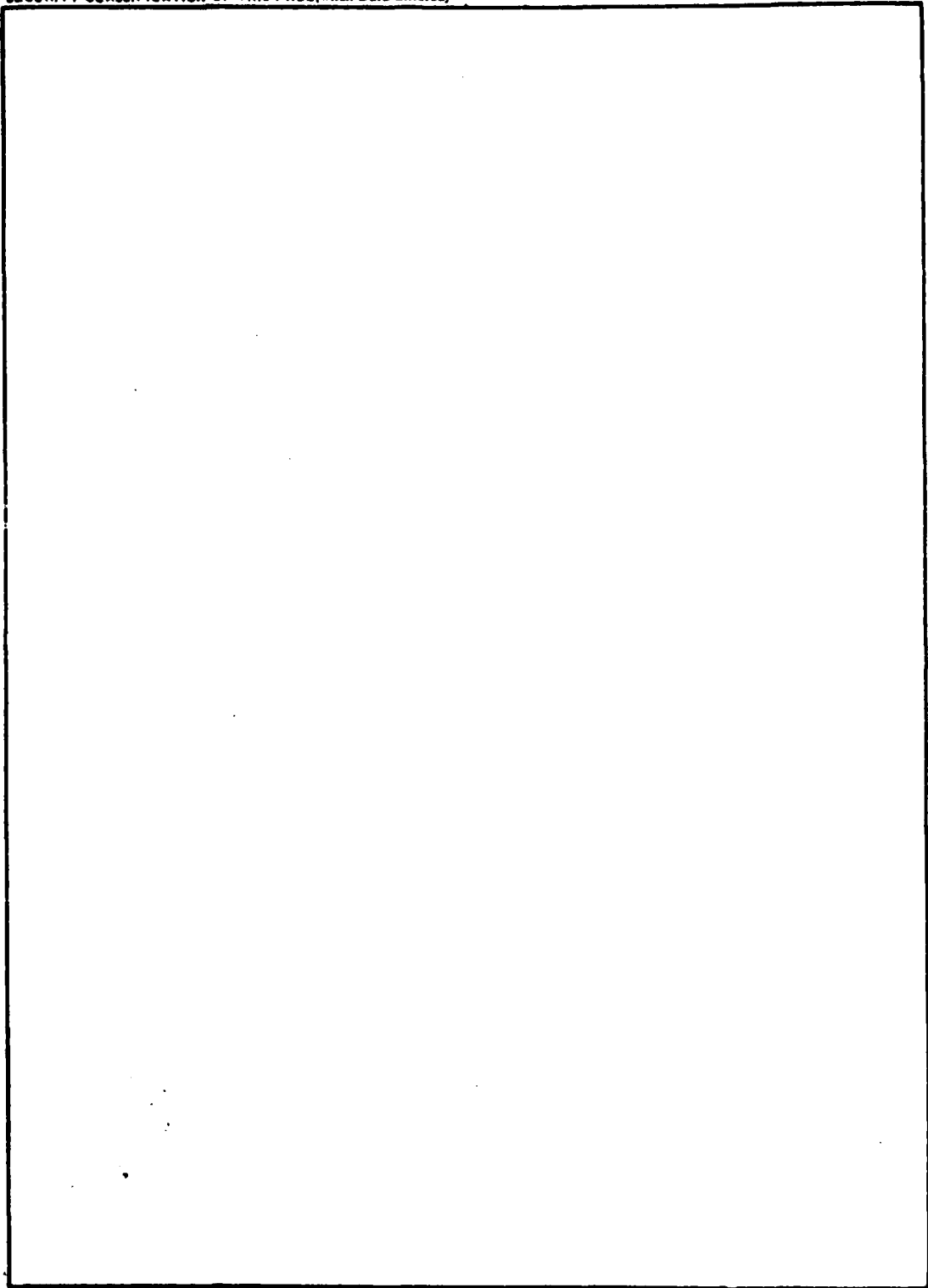
SECURITY CLASSIFICATION OF THIS PAGE (When Data Entered)

446971

1/A

**UNCLASSIFIED**

**SECURITY CLASSIFICATION OF THIS PAGE(When Data Entered)**



**UNCLASSIFIED**

**SECURITY CLASSIFICATION OF THIS PAGE(When Data Entered)**

# TABLE OF CONTENTS

## VOLUME I

## PAGE

|     |   |     |
|-----|---|-----|
| 1.  | INTRODUCTION.....                       | 1   |
| 2.  | THE METAL GRID SPATIAL FILTER.....      | 2   |
| 2.1 | Background.....                         | 2   |
| 2.2 | Purpose of Spatial Filter.....          | 3   |
| 2.3 | Principle of Spatial Filter.....        | 3   |
| 2.4 | Types of Metal Grids.....               | 11  |
| 2.5 | Susceptance of Crossed Metal Grids..... | 18  |
| 2.6 | Dielectric Support for Metal Grids..... | 28  |
| 3.  | SPATIAL FILTER DESIGN ANALYSIS.....     | 35  |
| 3.1 | Purpose of Design Analysis.....         | 35  |
| 3.2 | Basic Filter Design.....                | 35  |
| 3.3 | Nominal Filter Performance.....         | 38  |
| 3.4 | Filter Element Tolerances.....          | 49  |
| 3.5 | Frequency Bandwidth.....                | 62  |
| 3.6 | Available Rejection vs. Frequency.....  | 64  |
| 4.  | SIMULATOR TESTS OF METAL GRIDS.....     | 67  |
| 4.1 | Purpose of Simulator Tests.....         | 67  |
| 4.2 | Near Grazing Simulator Tests.....       | 68  |
| 4.3 | Near Broadside Simulator Tests.....     | 88  |
| 5.  | CONCLUSIONS.....                        | 109 |
| 6.  | REFERENCES.....                         | 112 |

|  |                      |
|--|----------------------|
| Accession For.....                             |                      |
| NTIS GRA&I <input checked="" type="checkbox"/> |                      |
| DTIC TAB..... <input type="checkbox"/>         |                      |
| Unannounced <input type="checkbox"/>           |                      |
| Justification.....                             |                      |
| By.....  |                      |
| Distribution/.....                             |                      |
| Availability Codes                             |                      |
| Dist   | Avail and/or Special |
| A  |                      |

| <u>Figure No.</u> | <u>Description</u>  | <u>Page No.</u> |
|-------------------|---|-----------------|
|                   | Table 3-2, Part 1 of 2<br>Element Values for Broadside-<br>Centered Filters                                 | 40              |
|                   | Table 3-2, Part 2 of 2<br>Element Values for Broadside-<br>Biased (b) and Off-Broadside (o)<br>Filters      | 41              |
| 3-2               | Transmission, Filter B31, H and<br>E-Planes   | 43              |
| 3-3               | Passband Reflection and Transmission,<br>Filter B31, H-Plane  | 44              |
| 3-4               | Passband Reflection and Transmission,<br>Filter B31, E-Plane  | 45              |
|                   | Table 3-3, Part 1 of 2<br>Nominal Performance for Broadside-<br>Centered Filters                            | 46              |
|                   | Table 3-3, Part 2 of 2<br>Nominal Performance for Broadside-<br>Biased (b) and Off-Broadside (o)<br>Filters | 47              |
| 3-5               | Rejection for Filters with Various<br>Parameters  | 48              |
| 3-6               | Rejection vs. Cutoff Slope for Various<br>Filters   | 50              |
| 3-7               | Rejection vs. Susceptance Sum for Vari-<br>ous Filters  | 51              |
| 3-8               | Method for Determination of Tolerance   | 53              |
| 3-9               | Tolerance on Center Length vs. Rejec-<br>tion, for $5^\circ \Delta\phi_i$ Allowable                         | 54              |
| 3-10              | Tolerance on Center Length vs. Rejec-<br>tion for 0.2 $\Delta R$ Allowable                                  | 55              |
| 3-11              | Tolerance on Edge Susceptance vs. Re-<br>jection, for $5^\circ \Delta\phi_i$ Allowable                      | 56              |



## LIST OF ILLUSTRATIONS

| <u>Figure No.</u> | <u>Description</u>   | <u>Page No.</u> |
|-------------------|--|-----------------|
| 2-1               | Purpose of Spatial Filter  | 4               |
| 2-2               | Principle of Metal-Grid Spatial Filter                           | 5               |
| 2-3               | Broadside Passband Options                                       | 7               |
| 2-4               | Off-Broadside vs. Broadside Passbands                            | 9               |
| 2-5               | Shapes of Off-Broadside and Broadside Passbands                  | 10              |
| 2-7               | Crossed and Parallel Inductive Metal Grids                       | 13              |
| 2-8               | Contacting Inductive Crossed Metal Grids                         | 15              |
| 2-9               | Insulated Inductive Crossed Metal Grids                          | 17              |
| 2-10              | Geometry for Contacting Crossed Grid                             | 20              |
| 2-11              | Transmission of One Metal Grid, H-Plane                          | 21              |
| 2-12              | Transmission of One Metal Grid, E-Plane                          | 24              |
| 2-13              | Geometry for Insulated Crossed Grid                              | 26              |
| 2-14              | Dielectric Support Structure for Metal Grids in a Spatial Filter | 29              |
| 2-15              | Transmission of One Metal Grid and Dielectric Core, E-Plane      | 31              |
| 2-16              | Transmission of One Metal Grid and Dielectric Skin, E-Plane      | 34              |
|                   | Table 3-1, Part 1 of 2 Filter Identification Code                | 36              |
|                   | Table 3-1, Part 2 of 2 Filter Identification Code                | 37              |
| 3-1               | Filter Elements for 2-, 3-, and 5-Pole Filters                   | 39              |

| <u>Figure No.</u> | <u>Description</u>   | <u>Page No.</u> |
|-------------------|--|-----------------|
| 3-12              | Tolerance on Edge Susceptance vs. Rejection, for 0.2 $\Delta R$ Allowable          | 58              |
| 3-13              | Tolerance on All Lengths Cumulative vs. Rejection for 5° $\Delta \phi_i$ Allowable | 59              |
| 3-14              | Tolerance on All Lengths Cumulative vs. Rejection, for 0.2 $\Delta R$ Allowable    | 60              |
|                   | Table 3-4<br>Frequency Bandwidth   | 63              |
| 3-15              | Available Rejection vs. Frequency  | 65              |
| 4-1               | Sample Orientations for Near-Grazing Simulator                                     | 70              |
| 4-2               | Diagram for Near-Grazing Simulator   | 72              |
| 4-3               | Near-Grazing Simulator   | 73              |
| 4-4               | Contacting Crossed Strip Samples for Near-Grazing Simulator                        | 74              |
| 4-5               | Data for Contacting Crossed Strip Samples Near Grazing                             | 75              |
| 4-6               | Data for Contacting Crossed Strips with Dielectric Near Grazing                    | 77              |
| 4-7               | Data Comparison for Strips With and Without Dielectric Near Grazing                | 78              |
| 4-8               | Round Hole Sample for Near-Grazing Simulator                                       | 79              |
| 4-9               | Data for Round Holes Near Grazing  | 81              |
| 4-10              | Data for Round Holes With and Without Dielectric Near Grazing                      | 82              |
| 4-11              | Insulated Crossed Wire Samples for Near-Grazing Simulator                          | 83              |
| 4-12              | Data for Insulated Crossed Wire Samples Near Grazing                               | 84              |

| <u>Figure No.</u> | <u>Description</u>   | <u>Page No.</u> |
|-------------------|--|-----------------|
| 4-13              | Data for Insulated Crossed Wires with Dielectric Near Grazing      | 86              |
| 4-14              | Data Comparison for Wires With and Without Dielectric Near Grazing | 87              |
| 4-15              | Sample Orientations for Near-Broadside Simulator                   | 89              |
| 4-16              | Diagram of Near-Broadside Simulator                                | 90              |
| 4-17              | Near-Broadside Simulator   | 91              |
| 4-18              | Contacting Crossed Strip Samples for Near-Broadside Simulator      | 93              |
| 4-19              | Data for Contacting Crossed Strip Samples Near Broadside           | 94              |
| 4-20              | Data for Contacting Crossed Strips with Dielectric Near Broadside  | 95              |
| 4-21              | Round Hole Samples for Near-Broadside Simulator                    | 96              |
| 4-22              | Data for Round Holes Near Broadside                                | 97              |
| 4-23              | Large Round Hole Samples for Near-Broadside Simulator              | 99              |
| 4-24              | Data for Large Round Holes Near Broadside                          | 100             |
| 4-25              | Data for Large Round Holes with Dielectric Near Broadside          | 101             |
| 4-26              | Nearly-Square Hole Sample for Near-Broadside Simulator             | 103             |
| 4-27              | Data for Nearly Square Holes Near Broadside                        | 104             |
| 4-28              | Insulated Crossed Wire Sample for Near-Broadside Simulator         | 105             |
| 4-29              | Data for Insulated Crossed Wire Sample Near Broadside              | 107             |

| <u>Figure No.</u> | <u>Description</u>   | <u>Page No.</u> |
|-------------------|--|-----------------|
| 4-30              | Data for Insulated Crossed Wires<br>with Dielectric Near Broadside | 108             |

SECTION 1  
INTRODUCTION

Spatial filters offer the potential for reducing side-lobes in the radiation patterns of directive antennas. An investigation of metal-grid spatial filters is being conducted by Hazeltine for RADC/ET. The program includes study of metal grids, analysis of spatial filter designs, study of filter/antenna performance, and the design, fabrication and test of a spatial filter.

This interim report presents the results obtained in the first part of the program. The basic features of a metal-grid spatial filter are first described (Section 2). Then the results of a study and computer analysis of metal-grid spatial-filter designs are presented (Section 3 and Appendix A). This analysis includes consideration of passband width, passband ripple, number of grids, cutoff slope, stopband rejection, frequency bandwidth, and the important question of sensitivity to tolerances.

Next, (Section 4) the results of measurements of various types of metal grids in two simulator waveguides are described. These measurements relate to the significant question of the effect of dielectric supporting material on the behavior of various metal grids, particularly near grazing incidence in the E-plane where spurious passbands might exist. Finally, (Section 5) the conclusions reached from the studies are summarized.

## SECTION 2

### THE METAL GRID SPATIAL FILTER

#### 2.1 BACKGROUND

Spatial filters comprising layers of dielectric have been synthesized and analyzed by Mailloux (Ref. 1) and by Raytheon under contract to RADC/ET (Ref. 2). Spatial filters utilizing layers of metal grids have been proposed by Schell et al (Ref. 3). Experiments with spatial filters using a particular type of metal grid have been performed by Rope et al (Refs. 4, 5). The low weight and reasonable fabrication costs of metal grids are important attributes. Also, pure metal grids do not have the dielectric Brewster angle effect that can cause a spurious passband for E-plane incidence. However, metal grids are generally supported by dielectric layers, so the question of spurious passbands remains and is addressed in this investigation.

- Ref. 1 - R. J. Mailloux, "Synthesis of Spatial Filters with Chebyshev Characteristics", IEEE Trans. AP, pp. 174-181; March, 1976.
- Ref. 2 - J. H. Pozgay, S. Zamoscianyk, L. R. Lewis, "Synthesis of Plane Stratified Dielectric Slab Spatial Filters Using Numerical Optimization Techniques", Final Technical Report RADC-TR-76-408 by Raytheon Co., December, 1976.
- Ref. 3 - A. C. Schell et al, "Metallic Grating Spatial Filter for Directional Beamforming Antenna" AD-D002-623; April, 1976.
- Ref. 4 - E. L. Rope, G. Tricoles, O-C. Yue, "Metallic Angular Filters for Array Economy", IEEE AP-S Int. Symp. Digest, pp. 155-157; 1976.
- Ref. 5 - E. L. Rope, G. Tricoles, "An Angle Filter Containing Three Periodically Perforated Metallic Layers", IEEE AP-S Int. Symp. Digest, pp. 818-820; 1979.

## 2.2 PURPOSE OF SPATIAL FILTER

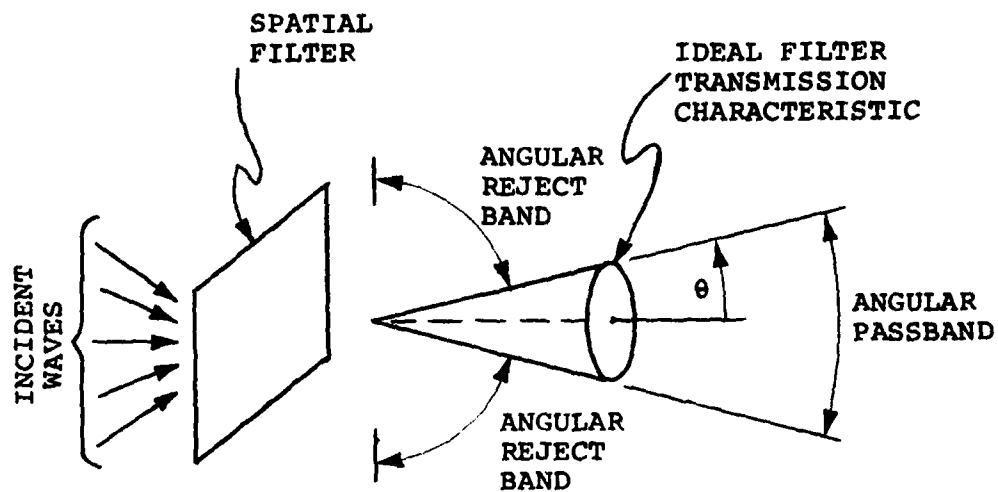
A spatial filter is a device which passes or rejects an electromagnetic wave depending on the angle of incidence of this wave relative to the filter surface. A representative spatial filter is indicated in Figure 2-1(a), in which waves incident at and near broadside (normal incidence) are passed by the filter but waves incident at angles further from broadside are rejected by the filter.

If a spatial filter is placed in front of a directive antenna, it can reduce those sidelobes of the directive antenna that correspond to waves that are incident in the angular reject band of the filter. The main lobe of the antenna corresponds to a wave that is incident in the angular passband of the antenna, and is not substantially affected by the filter. This case is indicated in Figure 2-1(b).

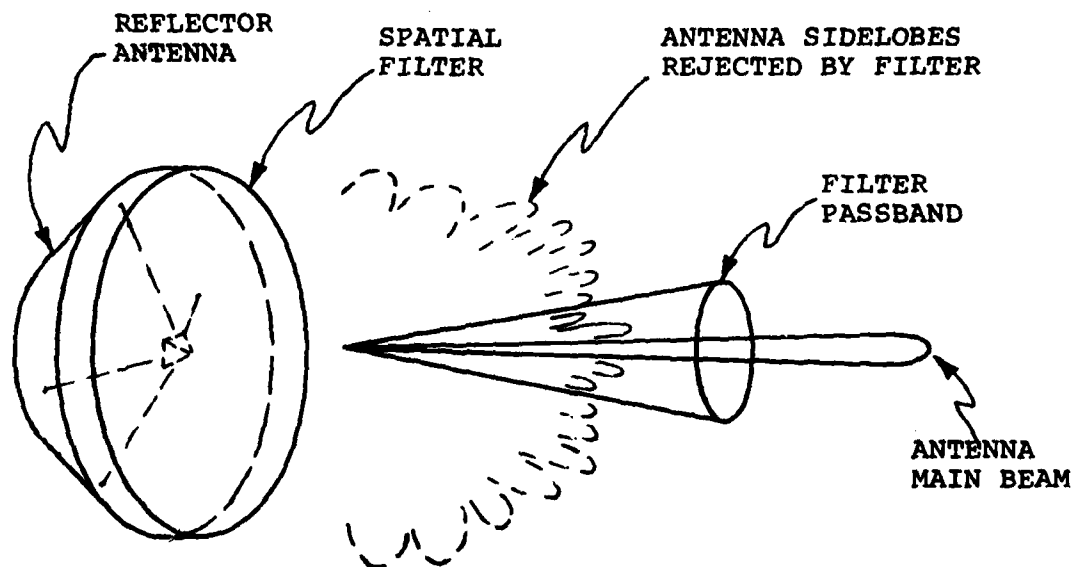
The antenna may have either a fixed main beam or a main beam that is scanning over a limited angular region. For a scanning beam antenna, the angular passband of the spatial filter can encompass the scan region so that the main beam is always passed but potential grating lobes may be rejected. This application was considered by Mailloux (Ref. 1). For a fixed-beam antenna such as the reflector antenna indicated in Figure 2-1(b), the spatial filter can reduce the sidelobes caused by feed spillover, feed-support scattering, and reflector contour errors while retaining a strong main beam. The reflector antenna application is the principal one to be considered in this program.

## 2.3 PRINCIPLE OF SPATIAL FILTER

The spatial filters to be investigated in this program operate in accordance with a single basic principle. This principle appears in Reference 3, and is repeated in the following. As indicated in Figure 2-2 the spatial filter comprises a series of layers. Each layer acts essentially as a



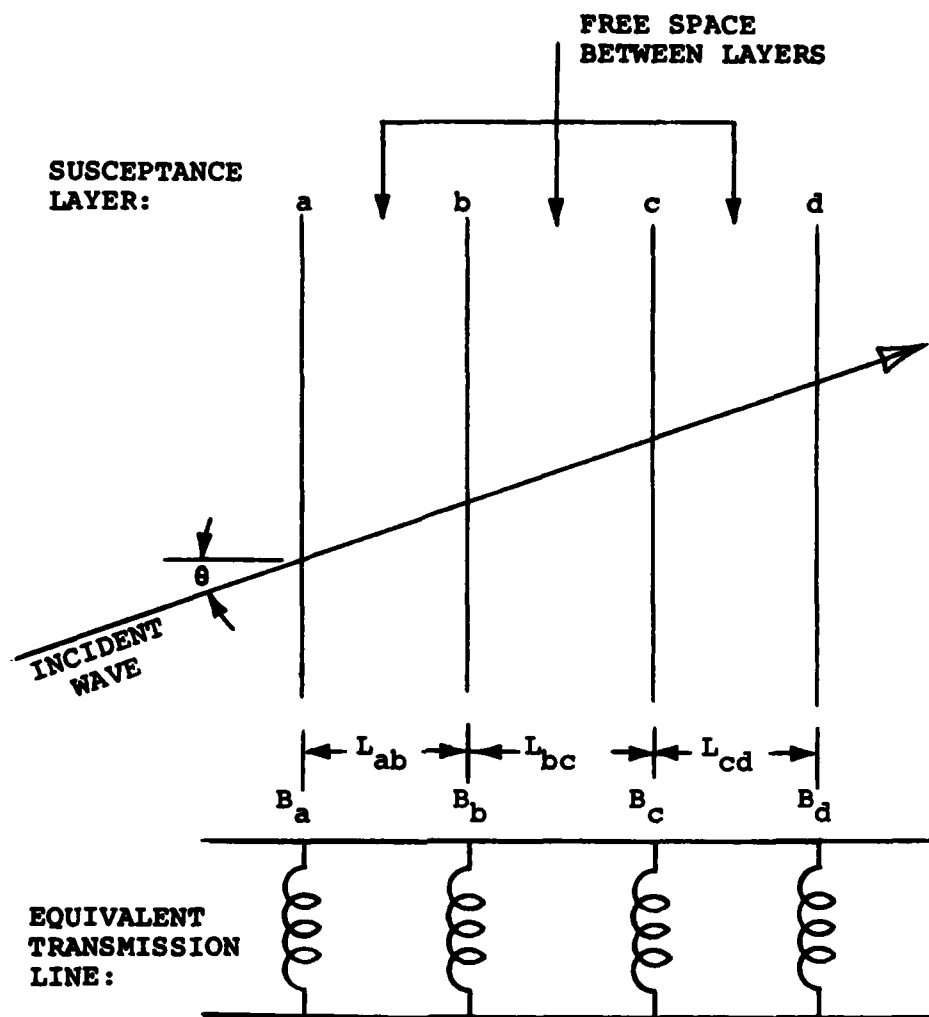
(a) basic function



(b) application to reflector antenna

Figure 2-1 Purpose of Spatial Filter





$$\text{EQUIVALENT WAVELENGTH} = \lambda_g = \frac{\lambda}{\cos \theta}$$

$$\text{EQUIVALENT PHASE SHIFT BETWEEN LAYERS} = \frac{2\pi L}{\lambda_g}$$

$$= \frac{2\pi L \cos \theta}{\lambda} = \frac{2\pi L}{c} f \cos \theta$$

Figure 2-2 Principle of Metal-Grid Spatial Filter

shunt susceptance to an incident plane wave. Between these susceptance layers are regions of essentially free space in which the plane wave travels in almost the same direction as its incidence direction.

In a transmission-line equivalent circuit of this spatial filter the equivalent wavelength or "guide" wavelength ( $\lambda_g$ ) is equal to the free-space wavelength divided by  $\cos \theta$  where  $\theta$  is the angle of incidence. The phase shift between layers is therefore proportional to  $\cos \theta$  as well as to frequency. The nominal values for the susceptance layers and the phase shifts between layers can be specified so as to yield a conventional frequency filter. However, because the phase shifts between layers are proportional to  $\cos \theta$  as well as to frequency, the structure will also act as an angle-sensitive filter in which the term  $\cos \theta$  is the variable of significance. The net result is that the spatial filter can be designed on the basis of a conventional frequency filter.

A choice exists as to where to locate the frequency passband on the curve of  $\cos \theta$ . Figure 2-3 shows two examples of this choice. In one example the center of the frequency passband does not correspond to  $\theta = 0$  but is "biased" away from  $\theta = 0$  so that all of the reflection zeroes of the basic filter response appear in the angle passband. This case yields a spatial filter having a relatively narrow frequency bandwidth of operation because a small change of frequency in one direction will result in the rejection of a wave incident at broadside.

In the other example the center of the frequency passband corresponds to  $\theta = 0$ . This "centered" case yields a spatial filter having the widest frequency bandwidth of operation before a change in frequency causes the filter to reject a wave incident at broadside. This type of spatial filter is the principal type that is investigated in this program.

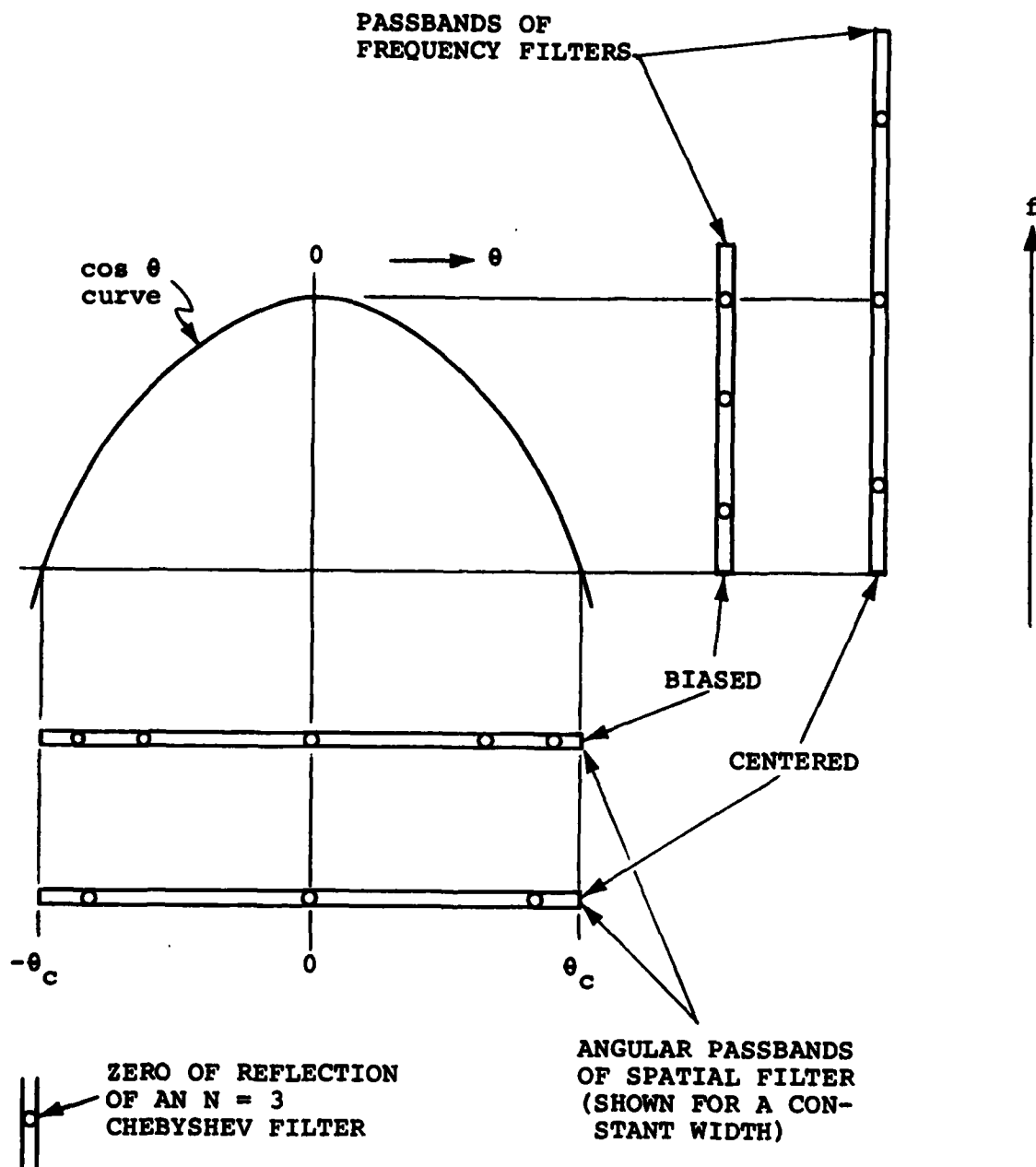


Figure 2-3 Broadside Passband Options

The frequency bandwidth of broadside operation of the centered type of spatial filter can be estimated by consideration of the  $\cos \theta$  curve of Figure 2-3. The resulting relation for bandwidth of this broadside filter is:

$$\begin{aligned} \frac{\Delta f}{f_m} &= \frac{\sin^2 \theta_c}{\cos \theta_c} \approx \theta_c^2 \\ &\approx \frac{1}{\pi} \times \text{passband solid angle} \\ &\approx 2 \times \frac{\text{passband solid angle}}{\text{hemisphere solid angle}} \end{aligned}$$

where  $\Delta f$  is the full frequency band of operation,  $f_m$  is the mid frequency (geometric mean), and  $\theta_c$  is the cutoff angle (edge of angular passband) of the spatial filter at the mid frequency. This simple formula gives the maximum possible bandwidth that could be obtained if the layer susceptances of the spatial filter vary ideally with incidence angle and if the spatial filter need only pass a wave at  $\theta = 0$  (i.e., the spatial filter is used for a very narrow beam antenna). For a  $\theta_c$  of  $20^\circ$  the bandwidth is about 12%, while for a  $\theta_c$  of  $10^\circ$  the bandwidth is about 3%. It is evident that if the spatial filter is to have a reasonably wide frequency band of operation, the spatial filter should not be designed for a very narrow angular passband.

The spatial filters discussed so far have "broadside passbands", i.e., angular passbands that include the broadside direction. It is also possible to design a spatial filter having an angular passband that does not include the broadside direction. Such an "off-broadside passband" is obtained by locating the frequency passband well down on the curve of  $\cos \theta$ , as indicated in Figure 2-4. This off-broadside passband is actually a "ring passband", as illustrated in Figure 2-5. (The more conventional broadside pass-

Diagram illustrating the angular passbands for a constant width spatial filter. The diagram shows a central horizontal axis labeled  $\theta$  with a vertical axis labeled  $0$ . A cosine curve, labeled  $\cos \theta$  curve, is plotted. The curve intersects the horizontal axis at  $0$  and  $\pm \theta_c$ . The curve also intersects horizontal lines at  $\pm \theta_{c1}$  and  $\pm \theta_{c2}$ . The diagram shows the spatial filter's angular passbands for broadside (centered) and off-broadside illumination. The broadside (centered) spatial filter angular passband is indicated by a horizontal line at  $0$ . The off-broadside spatial filter angular passband is indicated by a horizontal line at  $\pm \theta_{c2}$ . The diagram also shows the spatial filter's angular passbands for broadside (centered) and off-broadside illumination. The broadside (centered) spatial filter angular passband is indicated by a horizontal line at  $0$ . The off-broadside spatial filter angular passband is indicated by a horizontal line at  $\pm \theta_{c2}$ .

9

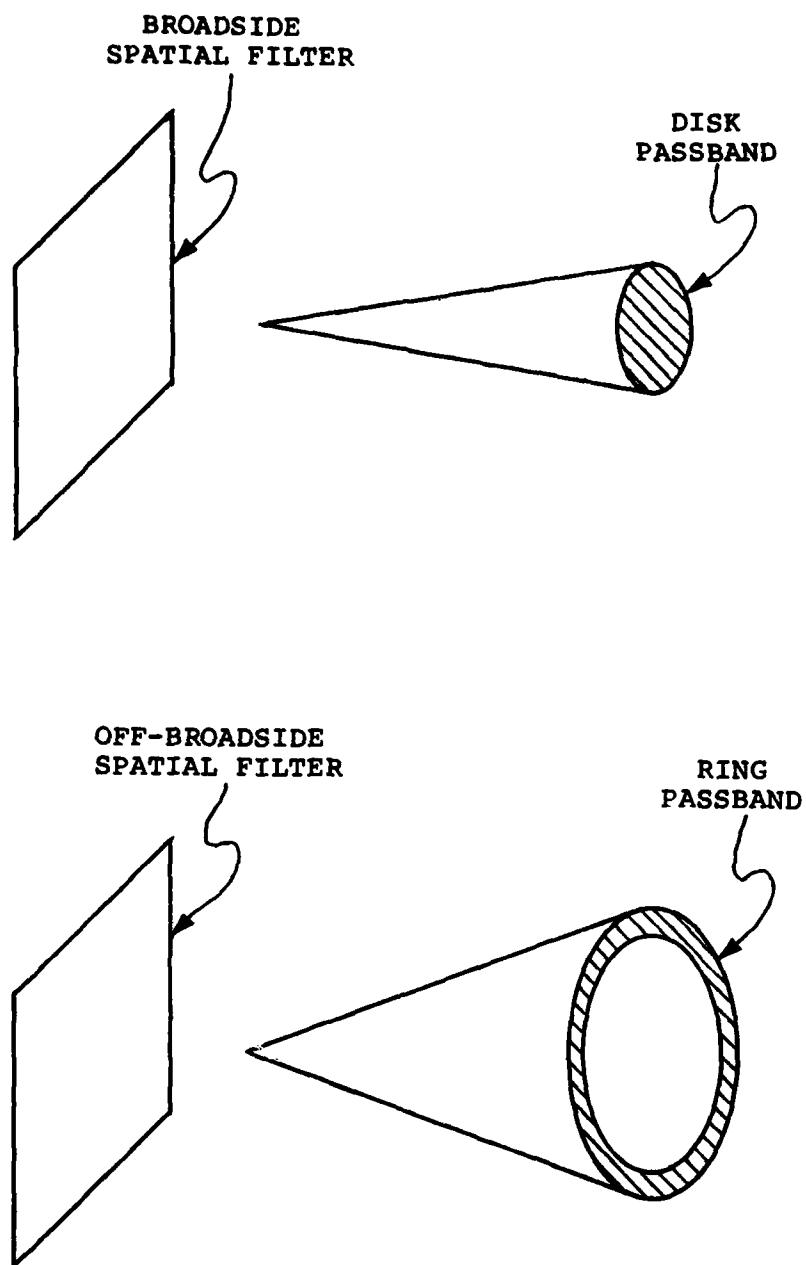


Figure 2-5 Shapes of Off-Broadside and Broadside Passbands

band is a "disk passband".) The ring passband is symmetrical about the broadside direction.

The frequency bandwidth of this off-broadside filter can be estimated for the situation in which the filter must pass a wave incident at the mid angle  $\theta_m$  where  $\cos \theta_m = \frac{\cos \theta_{c1} + \cos \theta_{c2}}{2}$  and where  $\theta_{c1}$  and  $\theta_{c2}$  are the angles corresponding to the two edges of the ring passband. This bandwidth for the off-broadside filter is:

$$\begin{aligned} \frac{\Delta f}{f_m} &= \frac{\cos \theta_{c1} - \cos \theta_{c2}}{\sqrt{\cos \theta_{c1} \cos \theta_{c2}}} \approx \frac{\theta_{c1} + \theta_{c2}}{2} (\theta_{c2} - \theta_{c1}) \\ &= \frac{1}{2\pi} \times \text{passband solid angle} \\ &= \frac{\text{passband solid angle}}{\text{hemisphere solid angle}} \end{aligned}$$

Note that although the angular width ( $\theta_{c2} - \theta_{c1}$ ) of the ring passband may be much narrower than the half-angle ( $\theta_c$ ) of a disk passband, its total solid angle must be about twice that of the disk passband for the same frequency bandwidth of operation.

The off-broadside spatial filter may be appropriate for particular applications where it is desirable for the filter surface to be tilted relative to the wavefront of the antenna main beam. However the off-broadside filter appears to have less general application than the broadside filter. While some study of the off-broadside filter is included in this program, the principal filter that is investigated is the broadside filter.

#### 2.4 TYPES OF METAL GRIDS

There are several types of metal grids that can be considered for a spatial filter. An early selection can be made between certain types in those cases where the performance of one type is clearly preferable to another. In other cases the

selection between types is more complex and warrants further investigation.

#### Inductive or Capacitive Grid

One choice that can be made is between an inductive susceptance or a capacitive susceptance for the metal grid, as indicated in Figure 2-6. The central layers in a spatial filter typically require rather large values of susceptance. These large values are easily obtainable with a non-resonant inductive grid by using a closely-spaced grid. On the other hand large susceptance values with a non-resonant capacitive grid require very small capacitive gaps that would be difficult to control to an acceptable tolerance. The alternative, a resonant capacitive grid, would degrade the frequency behavior of the filter and would also have a problem of tolerance control.

Another factor of significance is the strong potential for spurious passbands in the E-plane of incidence with a capacitive metal grid supported by a dielectric skin. With an inductive metal grid this potential also exists but to a lesser degree. For these reasons the inductive susceptance has been selected for the metal-grid spatial filter to be investigated.

#### Crossed Grid or Parallel Grid

Another choice that can be made is between a crossed inductive grid and a parallel inductive grid, as indicated in Figure 2-7. A spatial filter using crossed grids is capable of providing the desired rejection outside the passband for incident waves of any polarization. With a spatial filter using only parallel grids, incident waves polarized perpendicular to the wires would pass through the filter virtually unaffected.

In a reflector antenna designed for linear polarization, some of the sidelobe radiation can be cross polarized. For example, wide-angle radiation from currents in the feed sup-



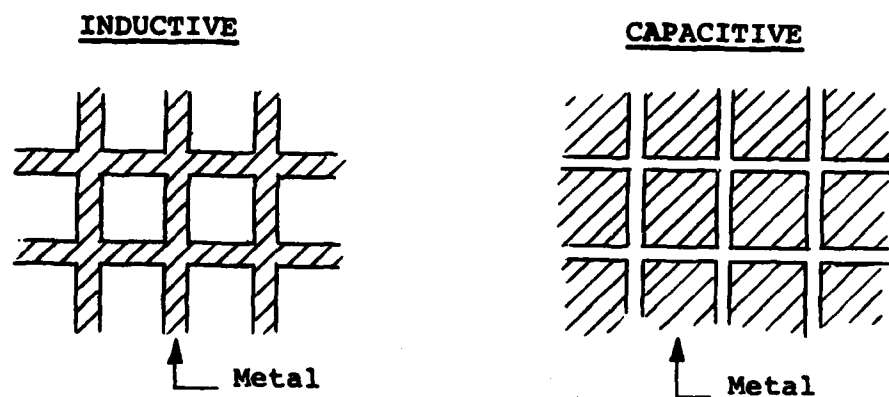


Figure 2-6 Inductive and Capacitive Metal Grids

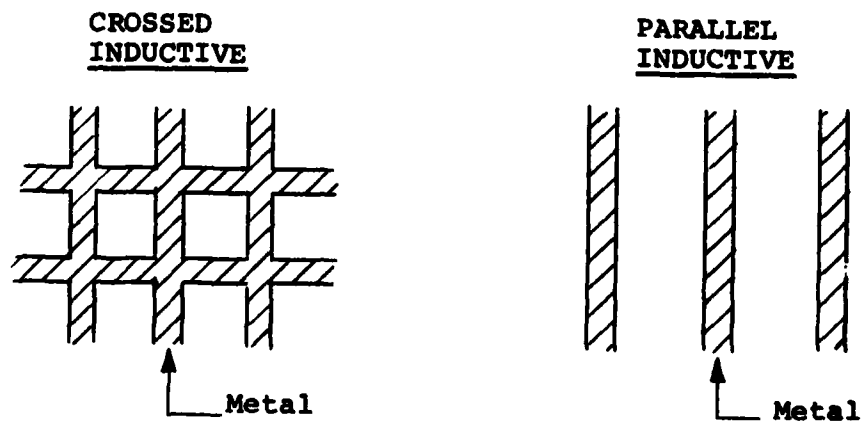


Figure 2-7 Crossed and Parallel Inductive Metal Grids

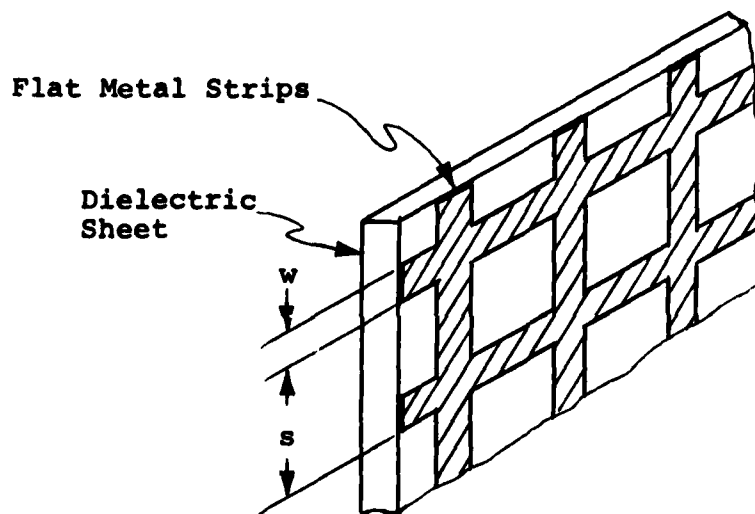
ports and from spillover beyond the edge of the reflector can contain appreciable cross-polarized components. A spatial filter using parallel grids would not reject these cross-polarized sidelobes. Of course, with a reflector antenna designed for circular polarization or dual polarization a spatial filter using parallel wire grids would not adequately reject even the normally-polarized sidelobes. A spatial filter using crossed grids is clearly more effective for these applications.

A crossed inductive grid has some problems of construction in large sizes as well as some complexities of behavior vs. angle of incidence. However, the crossed grid has been selected for the metal-grid spatial filter to be investigated, because of its capability for providing a spatial filter having adequate rejection for all polarizations.

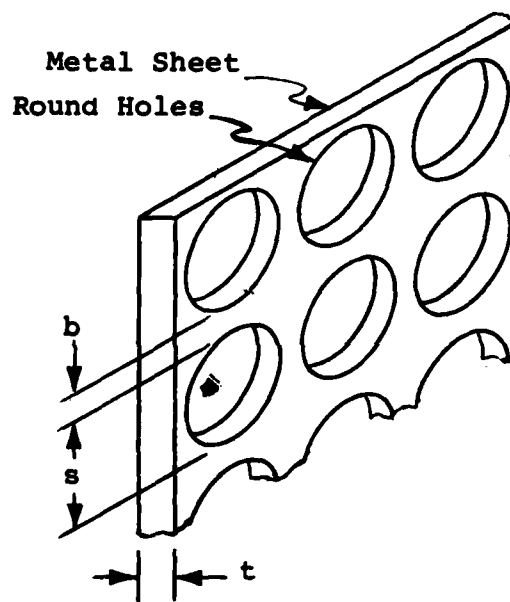
#### Configuration of Crossed Grid

There are several practical configurations that are capable of providing an inductive crossed metal grid. These configurations may be separated into two categories: (1) contacting crossed grids, and (2) insulated crossed grids. With the contacting crossed grids, the crossed sets of parallel conductors have electrical contact at all the crossing points. With the insulated crossed grids there is no conductive path between the crossed sets of parallel conductors, although there is some capacitance. Also the two crossed sets of parallel conductors in an insulated crossed grid are typically slightly displaced from each other.

Two configurations for the contacting crossed grids are of interest. One configuration is flat metal strips on a sheet of dielectric, as indicated in Figure 2-8(a). A good method for obtaining this configuration is to use conventional printed-circuit technology in which a copper-clad



(a) strip configuration



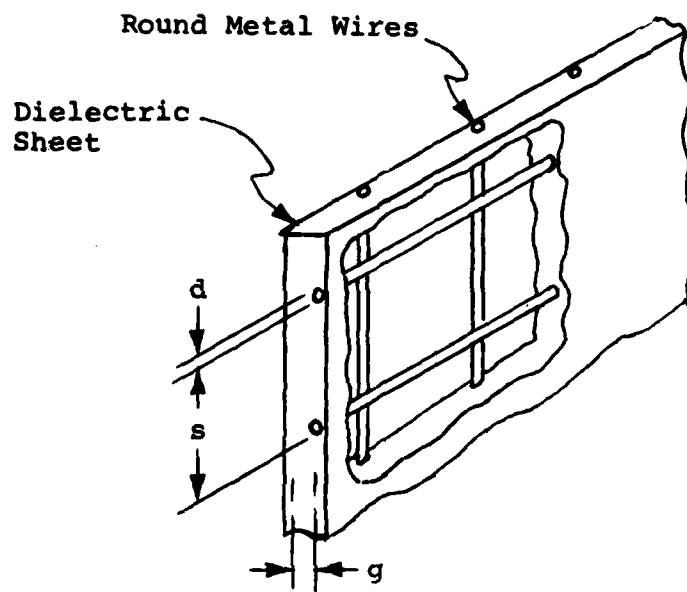
(b) hole configuration

Figure 2-8. Contacting Inductive Crossed Metal Grids

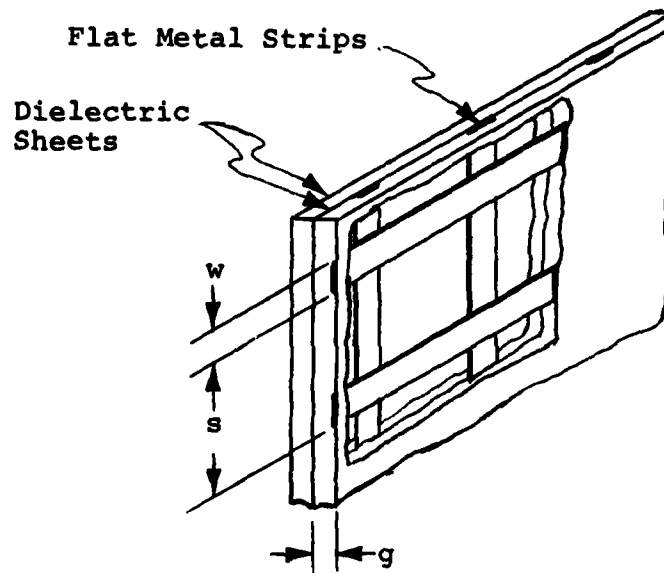
sheet of thin dielectric is selectively etched, leaving the desired pattern of copper on the dielectric sheet. This method is best suited to structures which are flat, which is expected to be the case for a typical spatial filter. A limitation of this method is that an area as large as that typically required for a spatial filter cannot be obtained from a single printed-circuit panel. Assembling several printed-circuit sheets is possible but presents some practical difficulties of securing the necessary electrical contact in all the conductors across adjacent sheets.

The other configuration for a contacting crossed grid is holes in a metal sheet, as indicated in Figure 2-8(b). A thin dielectric sheet bonded to the holed metal sheet may be needed for strength and for assembly in a multi-layer spatial filter. A limitation of the holed metal sheet configuration again is the area that can be constructed with a single sheet; however, this area is typically larger than that available with the strip construction described above. Round holes, as shown in the figure, are easily obtainable with rather good control of tolerances when large susceptance is desired. However, small values of susceptance with round non-resonant holes requires the holes to be nearly touching which may be difficult to achieve reliably. Approaching resonance by the addition of a major amount of dielectric would reduce the susceptance of the round holes but would complicate the frequency behavior of the filter and would create problems of dielectric tolerance control. An approach that can overcome this problem is to use a procedure for constructing the holes that makes them nearly square instead of round.

For the insulated crossed grids there are also two configurations of interest. One configuration is crossed grids of round metal wires embedded in a thin dielectric sheet as indicated in Figure 2-9(a). Many different antennas have used



(a) wire configuration



(b) strip configuration

Figure 2-9 Insulated Inductive Crossed Metal Grids

this type of construction for their reflecting surfaces, and curved as well as flat surfaces can be made. There is not a clear limitation of area with this wire configuration, although very large areas would require special construction techniques. The behavior of this insulated crossed grid for E-plane incidence is more complex than that of a contacting crossed grid, and may be more subject to possible spurious passbands.

The other insulated crossed grid configuration is flat metal strips on different dielectric sheets for the two crossed grids, as indicated in Figure 2-9(b). This configuration avoids some of the area limitation inherent with printed-circuit construction because printed circuits can usually be made longer in one dimension than the other. If the long dimension is parallel to the conductors in each grid, a larger area can be assembled while avoiding the need for providing electrical contact across adjacent sheets. As with the crossed wires, the behavior of this insulated crossed strip grid for E-plane incidence is more complex than that of the contacting crossed strip grid, and may be more subject to possible spurious passbands.

Before selecting a particular one of the four configurations described above, there are a number of aspects that warrant further investigation. Those aspects that are related to the electrical performance of metal grids and spatial filters are considered in later portions of this report.

## 2.5 SUSCEPTANCE OF CROSSED METAL GRIDS

The design and performance of a metal-grid spatial filter is dependent on the susceptance behavior of the metal grids. Outlined in the following are some basic relations that are known for particular inductive crossed metal grids.

### Contacting Crossed Grids

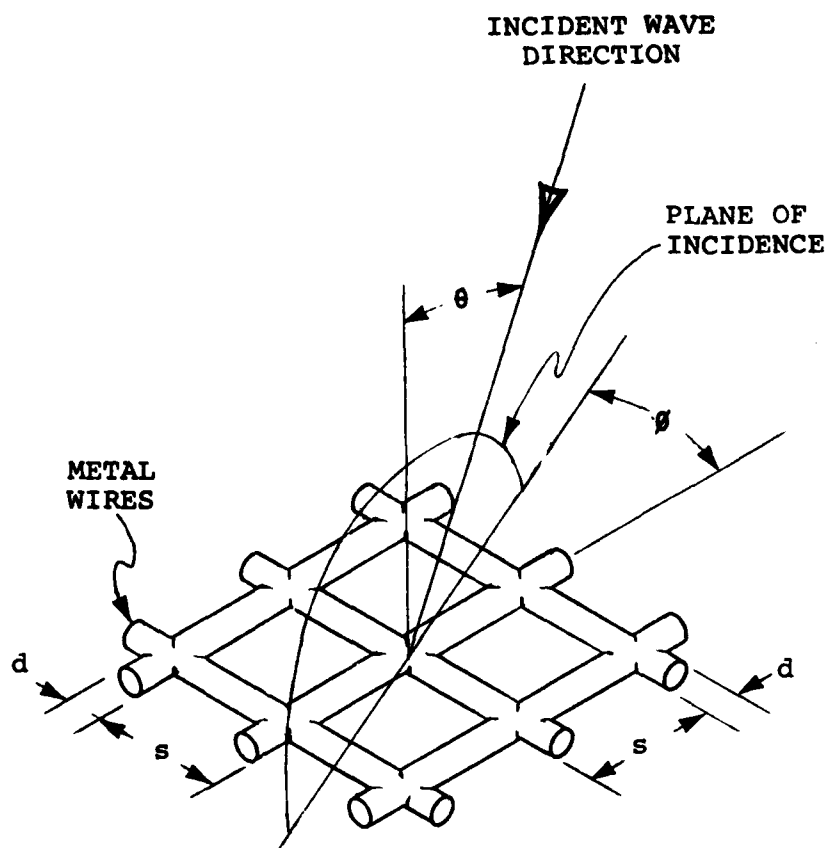
A contacting crossed grid of wires is shown in Figure 2-10. The angle of incidence  $\theta$  and the orientation of the plane of incidence  $\phi$  relative to the wires are indicated. The standard conventions for H-plane incidence and E-plane incidence are given. It is assumed that the grid is a square grid. It is also assumed that the spacing  $s$  is small compared to a wavelength, and that the diameter  $d$  of the wires is small compared to their spacing.

At broadside incidence and for angles of incidence in the H-plane this crossed grid behaves approximately the same as a parallel wire grid in which all the wires are parallel to the incident electric field. MacFarlane (Ref. 6) derived the inductive susceptance of a parallel grid of round wires for H-plane incidence. The approximate formula for inductive susceptance of the contacting crossed grid of wires for H-plane incidence is then:

$$B_H = - \frac{\lambda}{s \cos \theta \ln \left( \frac{s}{\pi d} \right)}$$

This susceptance  $B_H$  in the above formula increases with  $\theta$ . This is desirable for a spatial filter with a passband at or near broadside incidence because the grid reflection coefficients will increase with angle of incidence, yielding greater rejection at large angles of incidence. An example of the variation of rejection with angle of incidence in the H-plane for a metal grid representing one layer of a spatial filter is shown in Figure 2-11.

Ref. 6 - G. G. MacFarlane, "Surface Impedance of an Infinite Parallel-Wire Grid at Oblique Angles of Incidence", JIEE, Vol. 93, Pt. 3A, pp 1523-1527; 1946.



H-PLANE INCIDENCE: E VECTOR PERPENDICULAR  
TO PLANE OF INCIDENCE

E-PLANE INCIDENCE: E VECTOR PARALLEL TO  
PLANE OF INCIDENCE

Figure 2-10 Geometry for Contacting Crossed Grid



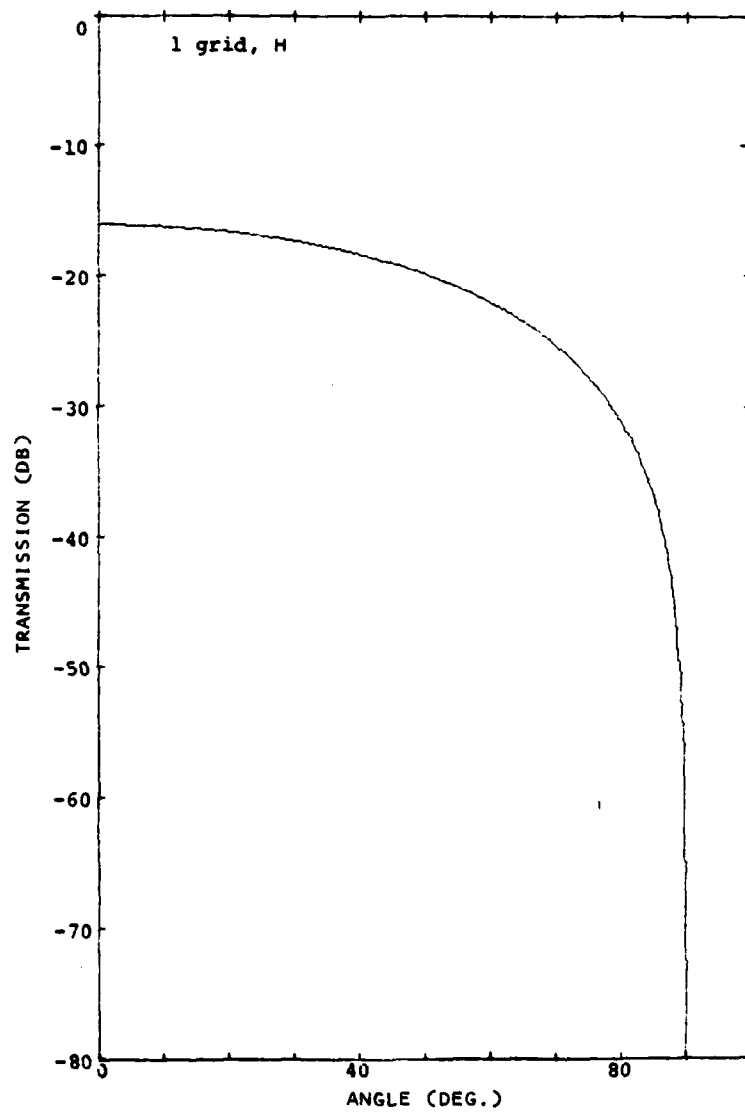


Figure 2-11 Transmission of One Metal Grid, H-Plane

Another interesting feature of this formula for  $B_H$  is the exact  $1/\cos \theta$  variation of susceptance. This results in a spatial filter that for H-plane incidence corresponds exactly to a frequency filter using shunt inductances in a transmission line. The design formulas given in Matthaei, Young, and Jones (Ref. 7), for example, will yield a Chebyshev response in which  $\cos \theta$  replaces frequency as the variable of interest. This is the basis for most of the spatial filter designs described later in this report.

For the E-plane of incidence a formula for the reflection coefficient of a contacting crossed grid of wires has been derived by Kontorovich et al (Ref. 8) and Astrakhan (Ref. 9). This relation, when converted to inductive susceptance is:

$$B_H \approx - \frac{\lambda}{s \cos \theta \ln \left( \frac{s}{\pi d} \right)} \frac{\cos^2 \theta}{1 - \frac{1}{2} \sin^2 \theta}$$

The first term is the same as the H-plane formula. The second term is an angle-dependent term which has the effect of maintaining the susceptance nearly constant from  $0^\circ$  to  $45^\circ$  (fourth-order variation with  $\theta$ ), and then reducing the susceptance to zero at  $90^\circ$ .

Ref. 7 - G. L. Matthaei, L. Young, E. M. T. Jones, "Microwave Filters, Impedance-Matching Networks, and Coupling Structures", McGraw-Hill, pp 85-101, 450-452; 1964.

Ref. 8 - M. I. Kontorovich, V. Yu Pretun'kin, N. A. Yesepkina, M. I. Astrakhan, "The Coefficient of Reflection of a Plane Electromagnetic Wave from a Plane Wire Mesh", Radio Engineering and Electronic Physics (USSR), Vol. 7, No. 2, pp 222-231; February, 1962.

Ref. 9 - M. I. Astrakhan, "Reflecting and Screening Properties of Plane Wire Grids", Radio Engineering (USSR), Vol. 23, No. 1 pp 76-83; 1968.

The reduction of the susceptance  $B_E$  to zero at  $90^\circ$  is not desirable for a spatial filter because the filter rejection will also tend to approach zero near  $90^\circ$  where substantial rejection may be desired. An example of the variation of rejection with angle of incidence in the E-plane for a metal grid representing one layer of a spatial filter is shown in Figure 2-12. Furthermore, with a small  $B_E$  near  $90^\circ$ , the filter may be susceptible to spurious passbands caused by other structures such as dielectric supporting materials. Also, for E-plane incidence there is not the exact correspondence with a frequency filter that is obtained in the H-plane. These aspects are considered in later portions of this report.

It may be noted that the formulas given for both  $B_H$  and  $B_E$  are independent of the orientation  $\phi$  of the plane of incidence relative to the wires in the contacting crossed grid. paper by Otteni (Ref. 10) states that for E-plane incidence this invariance with  $\phi$  is not exactly correct near  $\theta = 90^\circ$ . In any case, the susceptance for E-plane incidence always goes to zero at  $\theta = 90^\circ$ . For simplicity in the analysis of spatial filters using contacting crossed grids, any possible variation with  $\phi$  will not be included. However, the measurements of contacting crossed metal grids in simulators will typically be made for  $\phi = 0^\circ$  and  $45^\circ$ , thereby covering the extreme cases of any variation with  $\phi$  that may be present.

A large contacting crossed grid of wires with reliable contact (soldered junctions) is difficult to construct. Therefore, it is used in this study only as a theoretical basis for obtaining the susceptance of other, more practical grids. A contacting crossed grid of strips is relatively easy

Ref 10 - G. A. Otteni, "Plane Wave Reflection from a Rectangular-Mesh Ground Screen," IEEE Trans. AP, pp 843-851; November, 1973.

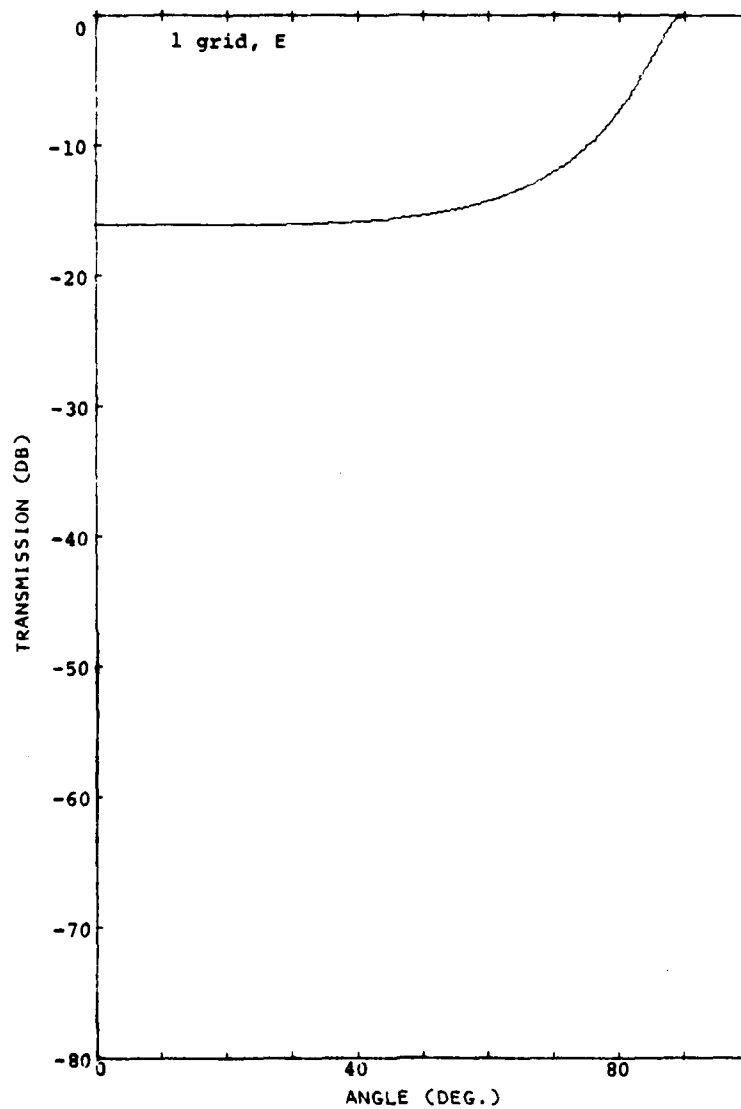


Figure 2-12 Transmission of One Metal Grid, E-Plane

to make for sizes that do not exceed the printed-circuit size capability. A contacting crossed grid of thin strips has essentially the same susceptance as the contacting crossed wires if the strip width is twice the wire diameter (Ref. 11):

$$w(\text{strip}) \approx 2d(\text{wire})$$

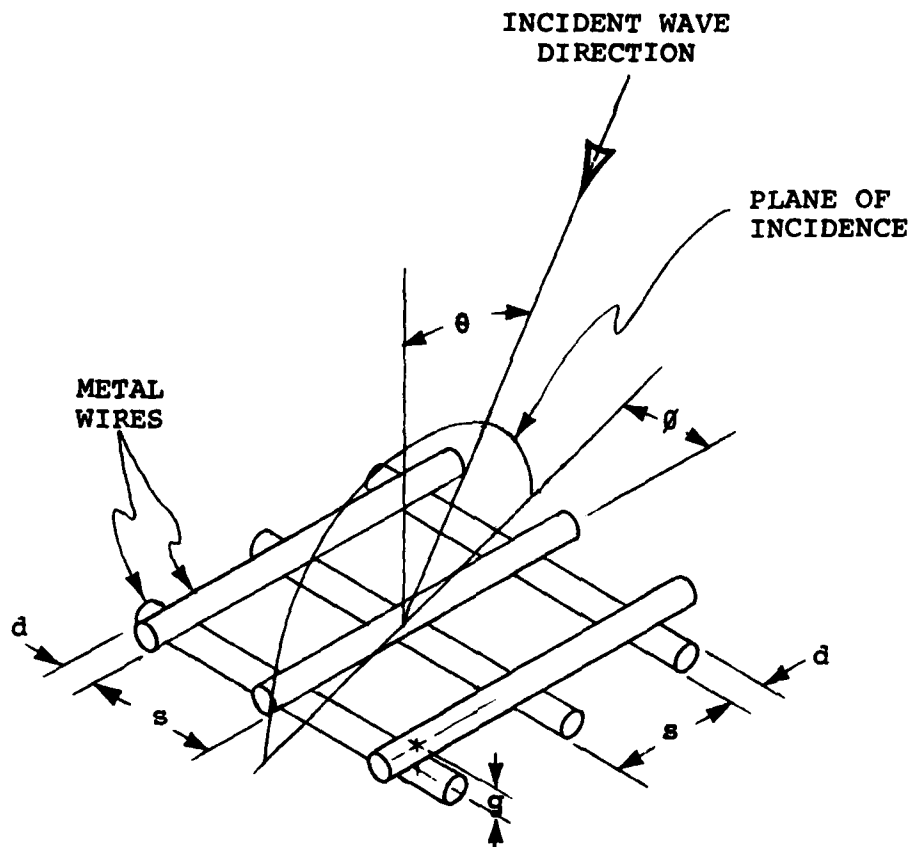
This assumes that the strip thickness is much smaller than the strip width  $w$ , and that  $w$  is much smaller than the spacing  $s$ .

Another practical form of contacting crossed metal grid is holes in a metal sheet. With round holes, simple formulas for the susceptance are not available when the holes are nearly touching and the metal sheet has finite thickness, as may be needed for a spatial filter. It is anticipated that simulator measurements of the type described later in this report would be helpful in providing the information that would be needed for the design of a spatial filter using round holes. With square holes, the simple formulas for the contacting crossed wire grid can be adapted for use (Ref. 11). Either round or square holes are expected to have a variation of susceptance with incidence angle that is identical to that of the contacting crossed wire grid in the H-plane. In the E-plane the square holes have a variation with angle that is identical to that of the contacting crossed wire grid; the round holes may be similar, if not identical.

#### Insulated Crossed Grids

An insulated crossed grid of wires is shown in Figure 2-13. The standard conventions for  $\theta$  and  $\phi$ , and for H-plane and E-plane incidence are given. A square grid is assumed,

Ref. 11 - N. Marcuvitz, "Waveguide Handbook" MIT Rad. Lab. Series, Vol. 10, McGraw-Hill, pp 284-288; 1951.



H-PLANE INCIDENCE: E VECTOR PERPENDICULAR TO PLANE OF INCIDENCE

E-PLANE INCIDENCE: E VECTOR PARALLEL TO PLANE OF INCIDENCE

Figure 2-13 Geometry for Insulated Crossed Grid

with wire spacing  $s$  small compared with a wavelength and the wire diameter  $d$  small compared with the spacing. The separation  $g$  of the crossed grids is also assumed to be small compared with the spacing and very small compared with the wavelength.

At broadside incidence and for angles of incidence in the H-plane such as insulated crossed grid behaves approximately the same as a contacting crossed grid. Thus an insulated crossed grid of wires, would have a susceptance approximately the same as the  $B_H$  given earlier for contacting crossed wires. An insulated crossed grid of strips would follow the same formula for  $B_H$  but with  $d$  replaced by  $w/2$ . For both the wires and the strips, if the separation  $g$  is not very small compared with a wavelength the reflection phase will be significantly different for the two components of polarization parallel to the two crossed sets of conductors, causing some conversion of the reflected polarization.

For the E-plane of incidence the behavior of an insulated crossed grid is more complex. An analysis of an insulated crossed grid of wires has been made by Kontorovich et al (Ref. 8), as a function of the plane of incidence  $\phi$  relative to the wires, and as a function of a parameter that is related to the impedance between the two crossed grids. When this impedance is zero, the grid behaves like a contacting crossed grid. When this impedance is substantial, as will occur with an insulated crossed grid, the grid behavior becomes highly dependent on  $\phi$  for large angles of incidence in the E-plane. For  $\phi = 45^\circ$  the grid reflection goes to zero at  $\theta = 90^\circ$ , just as with a contacting crossed grid. However, for  $\phi = 0^\circ$ , the grid reflection theoretically goes to unity at  $\theta = 90^\circ$ , as derived by Wait (Ref. 12) for a simple parallel-wire grid. In pract-

Ref. 12 - J. R. Wait, "Reflection at Arbitrary Incidence from a Parallel Wire Grid", Appl. Sci. Res., Sec. B, Vol. 4, pp 393-400; 1955.

ice this grid reflection may actually go to zero because of the finite conductivity of the wires or other reasons.

The variation with  $\phi$  for large  $\theta$ , and the possibility for a unity reflection at  $\theta = 90^\circ$  and  $\phi = 0^\circ$  is not necessarily harmful for a spatial filter because this would tend to increase the rejection in the filter stopband. However, since the reflection does go to zero at  $\theta = 90^\circ$  and  $\phi = 45^\circ$ , just as with the contacting crossed grid, the least rejection in the stopband is essentially the same as that for a contacting crossed grid in the E-plane of incidence. For simplicity in the analysis and computation of spatial filter performance characteristics given later in this report, it is therefore assumed that the relation for  $B_E$  given earlier for the contacting crossed grids of wires (or strips) also applies to the insulated crossed grids.

## 2.6 DIELECTRIC SUPPORT FOR METAL GRIDS

The metal grid spatial filter comprises several layers of metal grids separated by regions of essentially free space. For a structure that is mechanically sound, it is necessary to support the metal-grid layers with dielectric material. A representative construction is indicated in Figure 2-14. To separate the metal-grid layers a dielectric core material such as honeycomb or foam is used. To lend mechanical strength to the metal grid, it is typically bonded to or embedded in a thin dielectric skin. Both the spacers and the skins can have an effect on the performance of the spatial filter.

### Dielectric Core Effects

The dielectric core material has a dielectric constant  $k$  only slightly greater than unity. This low dielectric constant is desired in order to retain the wave angle within the spatial filter as close as possible to the angle of the wave incident on the spatial filter. The principal effect of a low- $k$  core on the passband of the spatial filter can be com-



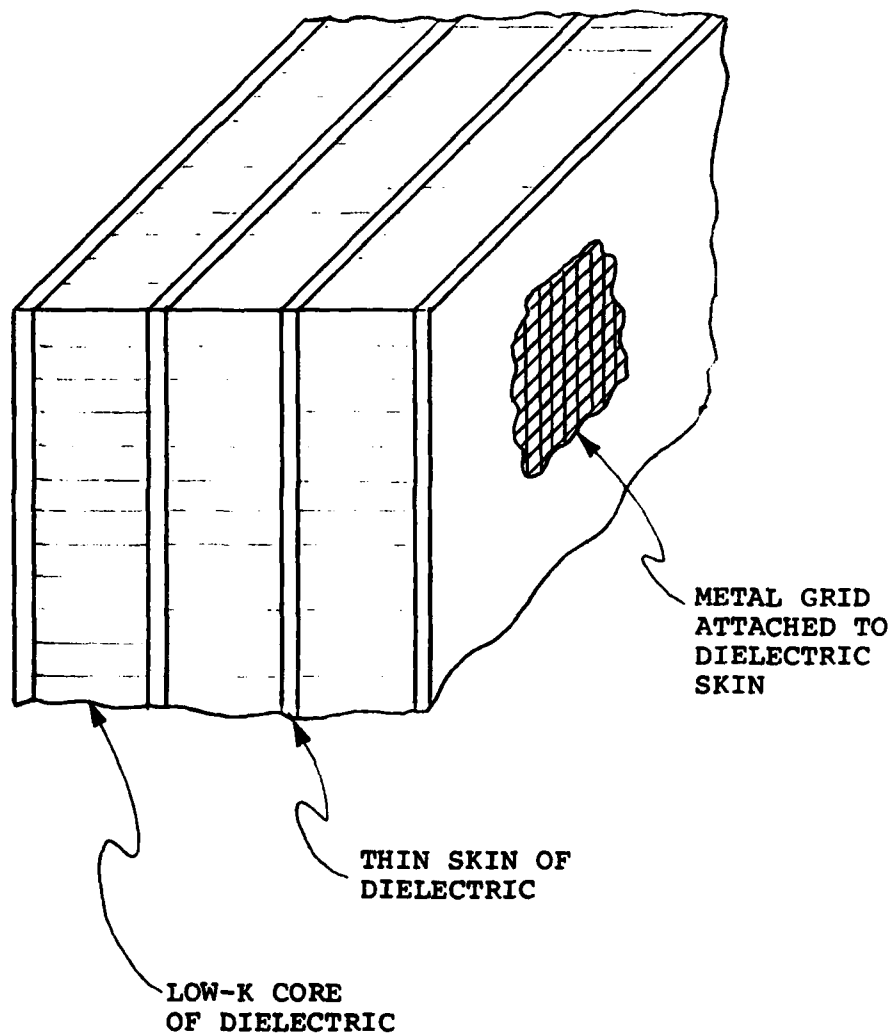


Figure 2-14 Dielectric Support Structure for  
Metal Grids in a Spatial Filter

pensated by a simple change of the separation between the metal-grid layers. The dissipative loss of the core material, while usually not substantial for ordinary radome-type applications, can be appreciable in the spatial filter because of the increased electric field in the core material caused by the resonant behavior of the spatial filter in its passband. Also, variations of the dielectric constant of the core material caused by non-uniform density or by anisotropy, although small, can contribute to a degradation of spatial-filter performance.

An additional effect of the dielectric core material is the modification of the spatial filter rejection for large angles of incidence in the E-plane. While the reflection of a crossed metal grid tends toward zero at  $\theta = 90^\circ$  in the E-plane, the reflection of a dielectric tends toward unity at  $\theta = 90^\circ$ . This is true for the low-k spacer material even though such material has a very small reflection near broadside. It happens that beyond the Brewster angle in the E-plane of incidence the reflection of the dielectric core material tends to reinforce the reflection of an inductive metal grid. This is fortunate for the rejection performance of a spatial filter because otherwise the grid and spacer reflections could cancel at some large angle of incidence in the E-plane, giving a spurious passband. Instead, the rejection of the filter is enhanced by the core material at large incidence angles in the E-plane.

An example of this effect is seen by comparing the E-plane rejection characteristic that was shown for a crossed metal grid in Figure 2-12 with the E-plane rejection characteristic shown in Figure 2-15 for the same metal grid surrounded by core material a half wavelength thick and having a dielectric constant of 1.1. The enhanced rejection at angles approaching  $90^\circ$  is evident. This result is computed assuming that there

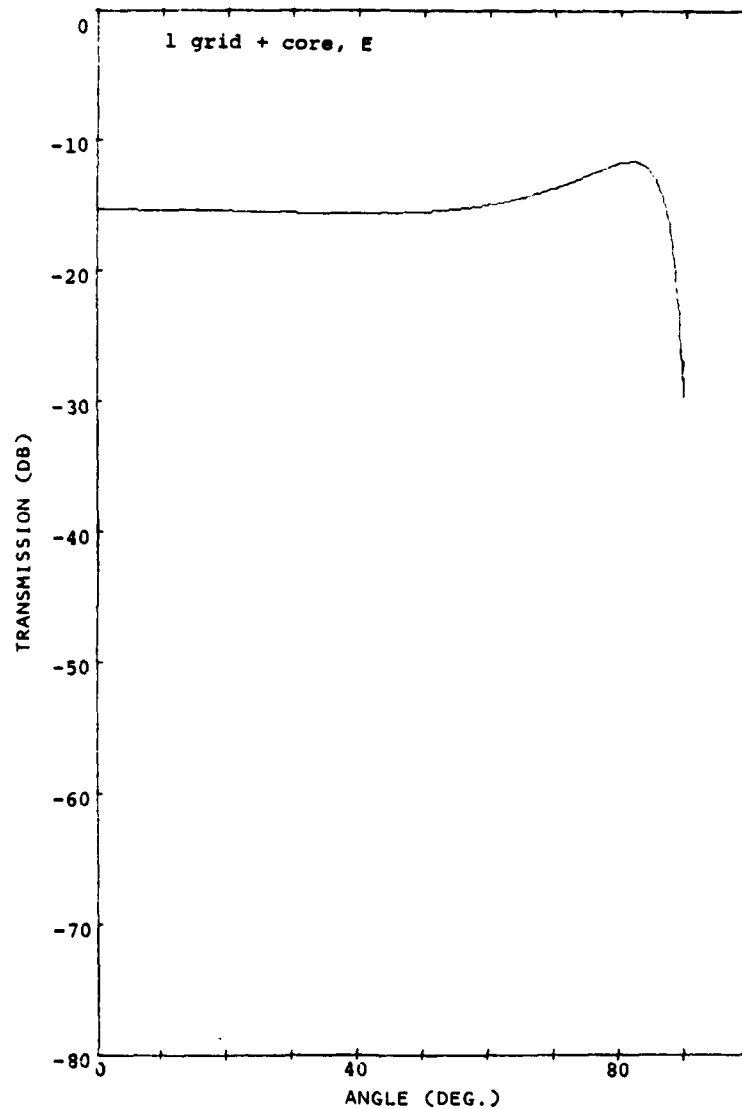


Figure 2-15 Transmission of One Metal Grid and Dielectric Core, E-Plane

is no reactive-field interactive effect between the crossed metal grid and the dielectric core material. Such an assumption is believed to be reasonable for the low-k spacer material.

In the H-plane of incidence, the reflection of dielectric material tends to subtract from the reflection of a crossed metal grid. However, the reflection of the metal grid tends toward unity at  $\theta = 90^\circ$  in the H-plane, and it predominates over the dielectric reflection. Therefore, there is no opportunity for a spurious passband in the H-plane of incidence. Also, the modification of the H-plane rejection characteristic of the metal grid by the dielectric material is not very important because the rejection provided by a crossed metal grid at large angles in the H-plane is large compared with that in the E-plane.

#### Dielectric Skin Effects

Metal grids consisting of thin strips or small-diameter wires should be bonded to or embedded in a dielectric skin in order to have mechanical integrity. Holes in a metal sheet are also likely to need a dielectric skin because of the thin metal cross-section between holes required to obtain low values of non-resonant susceptance. A typical dielectric skin is fiberglass with a dielectric constant of about 4 and a thickness of about 0.030 inches.

The basic effect of a dielectric skin on the passband of the spatial filter can be compensated approximately by a change in the susceptance of the metal grid. A thin dielectric skin behaves approximately as a capacitive susceptance with the following value at broadside incidence:

$$B_{\text{skin}} = \frac{2\pi t(k-1)}{\lambda}$$

where  $t$  is the thickness of the skin and  $k$  is its dielectric constant. The inductive susceptance of the metal grid should be increased by approximately this value in order to retain the original filter behavior at broadside incidence. The dissipative loss of the skin, in contrast to that of the core, is not enhanced by the filter resonance.

The dielectric skin also modifies the spatial filter rejection for large angles of incidence in the E-plane. As was the case with the dielectric core, at large incidence angles in the E-plane the dielectric skin increases the filter rejection. Figure 2-16 shows the computed E-plane rejection characteristic of the metal grid of Figure 2-12 embedded in a dielectric skin of  $k = 4$  and  $t = \lambda/40$ . The apparent beneficial effect of the dielectric skin at large incidence angles is evident.

The computation for Figure 2-16 is made assuming that there is no reactive-field interactive effect between the crossed metal grid and the dielectric skin material. This assumption is not expected to provide an accurate result for all incidence angles in the E-plane because the higher- $k$  skin material in close proximity to the metal grid is believed likely to modify the behavior of the grid in the E-plane of incidence. This modification could substantially reduce the rejection of the spatial filter over some angular range in the E-plane. It is also possible that the modification could result in a spurious passband at a large angle of incidence in the E-plane. Measurements of metal grids with dielectric skins in a simulator for large angles in the E-plane are described in a later section of this report.

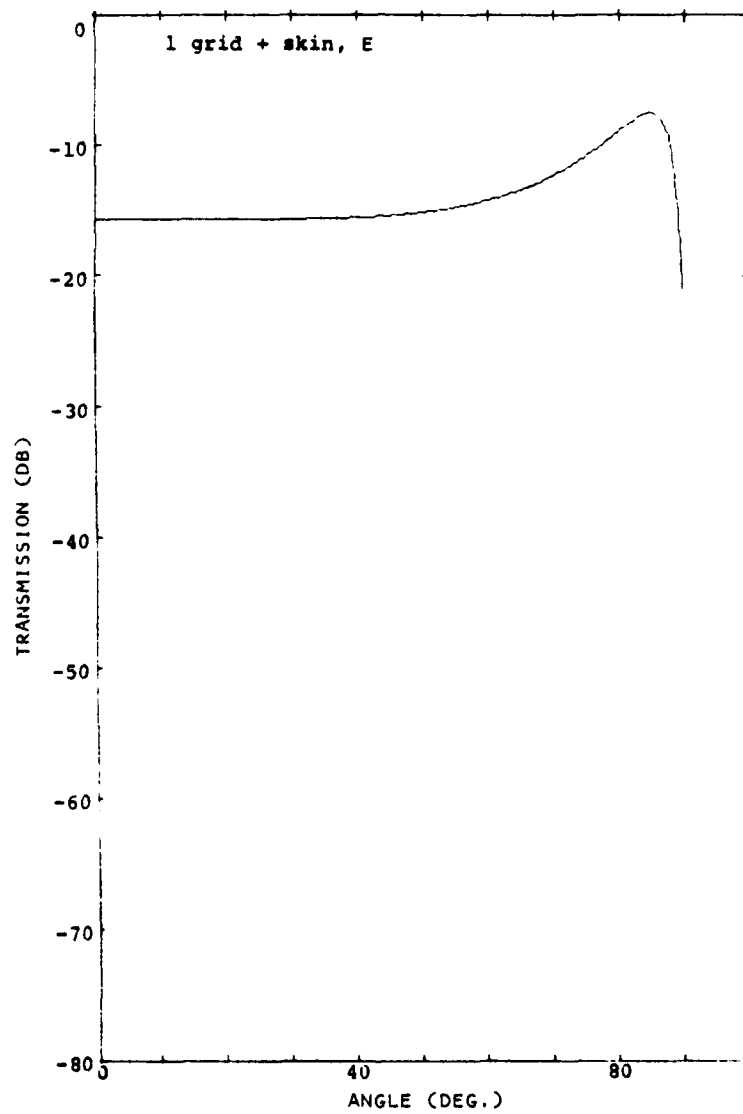


Figure 2-16 Transmission of One Metal Grid and Dielectric Skin, E-Plane

### SECTION 3

#### SPATIAL FILTER DESIGN ANALYSIS

##### 3.1 PURPOSE OF DESIGN ANALYSIS

It is the objective of this analysis to examine the basic tradeoffs between the filter parameters of passband width, passband ripple, and number of poles, and the related qualities such as stop-band rejection, cutoff slope, frequency bandwidth, and sensitivity to tolerances. For this purpose only the essential elements of the filter, and susceptances and the lengths, are considered, without the perturbing effect of the dielectric materials that would be needed in a self-supporting construction. A basic factor that limits the performance available from the spatial filter is the sensitivity to tolerances; considerable attention is given to this in the following.

##### 3.2 BASIC FILTER DESIGN

The design of the spatial filter follows conventional frequency filter methods, which are well-documented in the literature (Ref. 7). The narrowband design technique of Ref. 7 is used since it is straightforward and is adequate for the major purposes of this study. A Chebyshev equal-ripple type has been selected by reason of its characteristic sharp cutoff beyond the passband. For any desired combination of passband width, number of poles, and passband ripple, the filter element values can be determined. For speed and accuracy, a computer provides the nominal filter element values, i.e., the various lengths and susceptances in each filter.

Nominal element values have been obtained for a number of 2-, 3-, and 5-pole filters of various passband widths and ripple values. The passband widths are grouped in three representative values within a  $\pm 10^\circ$  to  $\pm 20^\circ$  range, and ripple values range upward and downward from a typical value of .01 dB transmission loss. Table 3-1 lists the various designs,

TABLE 3-1, Part 1 of 2  
FILTER IDENTIFICATION CODE

| <u>Filter Code</u> | <u>Passband Width (deg)</u> | <u>Quantity of Poles</u> | <u>Ripple (dB)</u> |
|--------------------|-----------------------------|--------------------------|--------------------|
| A20                | $\pm 11.5$                  | 2                        | .1                 |
| A21                | "                           | "                        | .01                |
| A22                | "                           | "                        | .001               |
| B20                | $\pm 14.0$                  | "                        | .1                 |
| B21                | "                           | "                        | .01                |
| B22                | "                           | "                        | .001               |
| C20                | $\pm 18.0$                  | "                        | .1                 |
| C21                | "                           | "                        | .01                |
| C22                | "                           | "                        | .001               |
| A31                | $\pm 11.5$                  | 3                        | .01                |
| A32                | "                           | "                        | .001               |
| B31                | $\pm 14.0$                  | "                        | .01                |
| B32                | "                           | "                        | .001               |
| C31                | $\pm 18.0$                  | "                        | .01                |
| C32                | "                           | "                        | .001               |
| A51                | $\pm 11.5$                  | 5                        | .01                |
| A52                | "                           | "                        | .001               |
| A54                | "                           | "                        | .00001             |
| A56                | "                           | "                        | .0000001           |
| B51                | $\pm 14.0$                  | "                        | .01                |
| B52                | "                           | "                        | .001               |
| B54                | "                           | "                        | .00001             |
| B56                | "                           | "                        | .0000001           |
| C51                | $\pm 18.0$                  | "                        | .01                |
| C52                | "                           | "                        | .001               |
| C54                | "                           | "                        | .00001             |
| C56                | "                           | "                        | .0000001           |



TABLE 3-1, Part 2 of 2  
 FILTER IDENTIFICATION CODE

| <u>Filter Code</u> | <u>Passband (deg)</u> | <u>Quantity of Poles</u> | <u>Ripple (dB)</u> |
|--------------------|-----------------------|--------------------------|--------------------|
| A31"b"             | $\pm 11.5$            | 3                        | .01                |
| B31"b"             | $\pm 14.0$            | "                        | "                  |
| C31"b"             | $\pm 18.0$            | "                        | "                  |
| A31"o"20°          | $\theta_m = 20$       | "                        | "                  |
| A31"o"30°          | $\theta_m = 30$       | "                        | "                  |
| B31"o"20°          | $\theta_m = 20$       | "                        | "                  |
| B31"o"30°          | $\theta_m = 30$       | "                        | "                  |
| C31"o"20°          | $\theta_m = 20$       | "                        | "                  |
| C31"o"30°          | $\theta_m = 30$       | "                        | "                  |

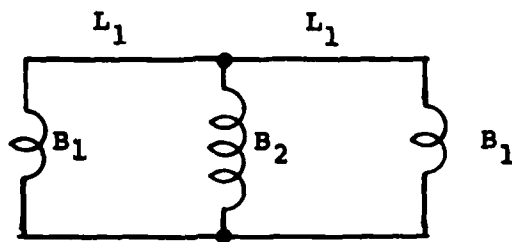
and identifies each with a code indicating the design values. The letters A, B, and C denote passband widths of  $\pm 11.5$ ,  $\pm 14$  or  $\pm 18$  degrees; the first number indicates the number of poles; and the second number counts the number of zeroes in the ripple dB value.

The element designations for the various filters are illustrated in Figure 3-1 and are tabulated in Table 3-2. In this table the lengths are given both in electrical degrees and in inches at a design frequency of 9.5 GHz (lengths in inches are needed in some tolerance studies). It can be seen from the table that the lengths approach a half wavelength as the susceptance values become large.

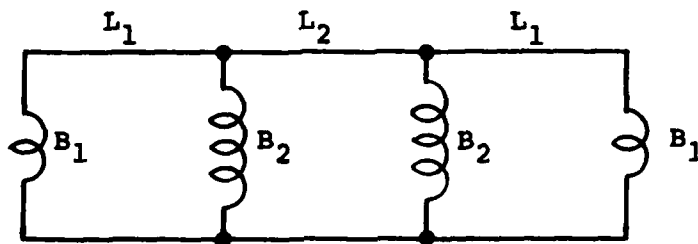
In Table 3-1 and 3-2, in addition to the element values for many filters having a frequency passband centered at broadside, the values for some broadside-biased ("b") and some off-broadside ("o") designs are listed. For the broadside-biased designs, a modification of the standard filter design was made to yield the desired response. A small adjustment of frequency was needed with the critical broadside-biased designs to obtain the desired nominal condition of zero reflection at broadside. For the off-broadside designs, the corresponding broadside-centered filter was examined at a frequency increased by the factor  $1/\cos \theta_m$  where  $\theta_m$  is the mid angle of the off-broadside passband as defined in Section 2.3.

### 3.3 NOMINAL FILTER PERFORMANCE

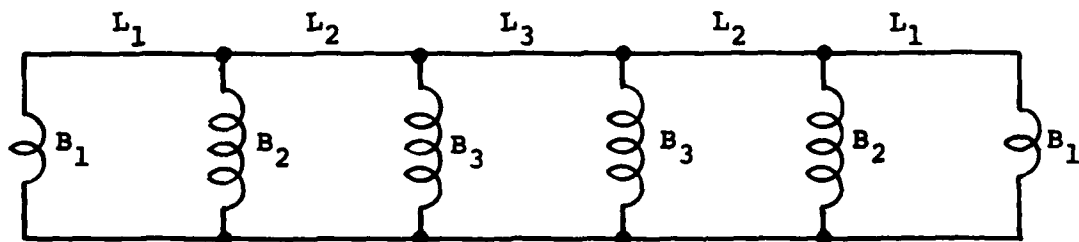
For each of the selected filter designs, performance with nominal element values has been computed and plotted. The plots include transmission loss, reflection coefficient, and insertion phase as a function of incidence angle in both the H-plane and the E-plane. In addition, computed values of cut-off slope at the -6 dB transmission point, rejection at  $25^\circ$  and  $45^\circ$  off broadside, and reflection coefficient and insertion phase at broadside (or nominal) incidence have been obtained and tabulated.



(a) Two-pole filter



(b) Three-pole filter



(c) Five-pole filter

Figure 3-1 Filter Elements for 2-, 3-, and 5-Pole Filters

TABLE 3-2, Part 1 of 2

## ELEMENT VALUES FOR BROADSIDE-CENTERED FILTERS

| FILTER<br>CODE | B <sub>1</sub> | L <sub>1</sub><br>(deg.) | @ 9.5 GHz               |                | @ 9.5 GHz                |                         | B <sub>3</sub> | L <sub>3</sub><br>(deg.) | L <sub>3</sub><br>(in.) |
|----------------|----------------|--------------------------|-------------------------|----------------|--------------------------|-------------------------|----------------|--------------------------|-------------------------|
|                |                |                          | L <sub>1</sub><br>(in.) | B <sub>2</sub> | L <sub>2</sub><br>(deg.) | L <sub>2</sub><br>(in.) |                |                          |                         |
| A20            | 3.3827         | 159.726                  | .5511                   | 11.3950        |                          |                         |                |                          |                         |
| A21            | 2.2930         | 151.067                  | .5212                   | 6.6366         |                          |                         |                |                          |                         |
| A22            | 1.4800         | 138.788                  | .4789                   | 3.6191         |                          |                         |                |                          |                         |
| B20            | 2.6730         | 154.255                  | .5322                   | 7.6312         |                          |                         |                |                          |                         |
| B21            | 1.7373         | 143.186                  | .4940                   | 4.3668         |                          |                         |                |                          |                         |
| B22            | 1.0179         | 127.598                  | .4403                   | 2.2386         |                          |                         |                |                          |                         |
| C20            | 1.9145         | 144.887                  | .4999                   | 4.4973         |                          |                         |                |                          |                         |
| C21            | 1.1234         | 129.894                  | .4482                   | 2.4232         |                          |                         |                |                          |                         |
| C22            | 0.4837         | 109.635                  | .3783                   | 0.9614         |                          |                         |                |                          |                         |
|                |                |                          |                         |                |                          |                         |                |                          |                         |
| A31            | 2.8419         | 157.817                  | .5445                   | 12.3081        | 170.770                  | .5892                   |                |                          |                         |
| A32            | 2.1531         | 151.954                  | .5243                   | 8.5252         | 166.797                  | .5755                   |                |                          |                         |
| B31            | 2.2115         | 152.127                  | .5249                   | 8.2534         | 166.378                  | .5741                   |                |                          |                         |
| B32            | 1.6152         | 144.745                  | .4994                   | 5.6687         | 160.566                  | .5540                   |                |                          |                         |
| C31            | 1.5285         | 142.562                  | .4919                   | 4.8848         | 157.734                  | .5442                   |                |                          |                         |
| C32            | 1.0172         | 132.723                  | .4579                   | 3.2621         | 148.488                  | .5123                   |                |                          |                         |
|                |                |                          |                         |                |                          |                         |                |                          |                         |
| A51            | 3.1742         | 160.261                  | .5529                   | 15.6887        | 173.850                  | .5998                   | 22.7039        | 174.966                  | .6037                   |
| A52            | 2.5924         | 156.554                  | .5402                   | 12.2909        | 172.401                  | .5948                   | 19.1715        | 174.044                  | .6005                   |
| A54            | 1.7720         | 148.333                  | .5118                   | 7.5296         | 168.150                  | .5802                   | 12.8832        | 171.176                  | .5906                   |
| A56            | 1.1574         | 138.232                  | .4769                   | 4.5793         | 161.416                  | .5569                   | 8.2829         | 166.425                  | .5742                   |
| B51            | 2.4957         | 155.280                  | .5358                   | 10.5520        | 170.912                  | .5897                   | 15.3088        | 172.557                  | .5954                   |
| B52            | 1.9968         | 150.657                  | .5198                   | 8.2417         | 168.778                  | .5823                   | 12.9150        | 171.197                  | .5907                   |
| B54            | 1.2793         | 140.370                  | .4843                   | 4.9839         | 162.554                  | .5609                   | 8.6450         | 166.974                  | .5761                   |
| B56            | 0.7241         | 127.779                  | .4409                   | 2.9270         | 152.840                  | .5273                   | 5.5022         | 160.024                  | .5521                   |
| C51            | 1.7670         | 146.932                  | .5070                   | 6.3063         | 165.085                  | .5696                   | 9.2234         | 167.765                  | .5788                   |
| C52            | 1.3463         | 140.826                  | .4859                   | 4.8775         | 161.624                  | .5577                   | 7.7581         | 165.544                  | .5712                   |
| C54            | 0.7204         | 127.250                  | .4390                   | 2.8237         | 151.692                  | .5234                   | 5.1279         | 158.693                  | .5475                   |
| C56            | 0.2101         | 111.015                  | .3830                   | 1.4548         | 136.835                  | .4721                   | 3.1561         | 147.638                  | .5094                   |

TABLE 3-2, Part 2 of 2

ELEMENT VALUES FOR BROADSIDE-BIASED (b)  
AND OFF-BROADSIDE (o) FILTERS

| FILTER<br>CODE                         | B <sub>1</sub> | L <sub>1</sub><br>(deg.) | B <sub>2</sub> | L <sub>2</sub><br>(deg.) | Opt.*<br>Freq.<br>(GHz) | PASSBAND<br>CENTER<br>$\theta_m$<br>(deg) |
|--|----------------|--------------------------|----------------|--------------------------|-------------------------|---|
| A31 "b"                                | 4.0201         | 165.942                  | 22.6105        | 176.656                  | 9.496                   | 0°  |
| B31 "b"                                | 3.1892         | 162.693                  | 15.0958        | 175.009                  | 9.491                   | 0°  |
| C31 "b"                                | 2.3050         | 157.350                  | 8.9125         | 171.642                  | 9.473                   | 0°  |
| * For zero R<br>at $\theta = \theta_m$ |                |                          |                |                          |                         |   |
| FILTER DESIGNS FOR CASE "o"            |                |                          |                |                          |                         |   |
| A31 "o"                                | SAME AS A31    |                          |                |                          | 10.11, 10.17            | 20°, 30°                                  |
| B31 "o"                                | SAME AS B31    |                          |                |                          | 10.11, 10.17            | 20°, 30°                                  |
| C31 "o"                                | SAME AS C31    |                          |                |                          | 10.11, 10.17            | 20°, 30°                                  |

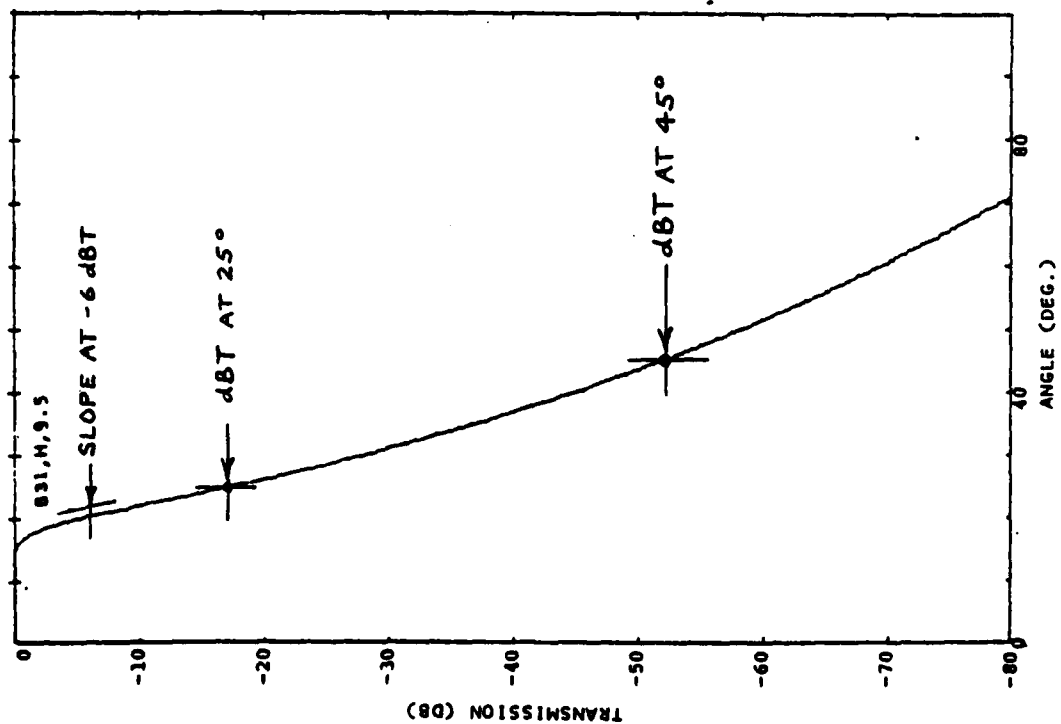
Figures 3-2 through 3-4 show the performance of a representative filter (B31), with the filter parameters and properties for evaluation indicated on the plots. The passband ripple is, by definition, the maximum transmission loss that occurs within the passband. In most cases, this loss is too small to appear on the graphs and a more critical quantity, reflection coefficient, should be observed. The passband width ( $\pm\theta_c$ ) is, by definition, determined between the outermost points at which the filter transmission loss (or reflection) equals the ripple level for that filter. The other properties for evaluation are discussed below.

Appendix A contains plots similar to those of Figures 3-2 through 3-4, for all of the spatial filters that were listed in Table 3-2. A tabulation of the computed properties of all of the filters appears here in Table 3-3.

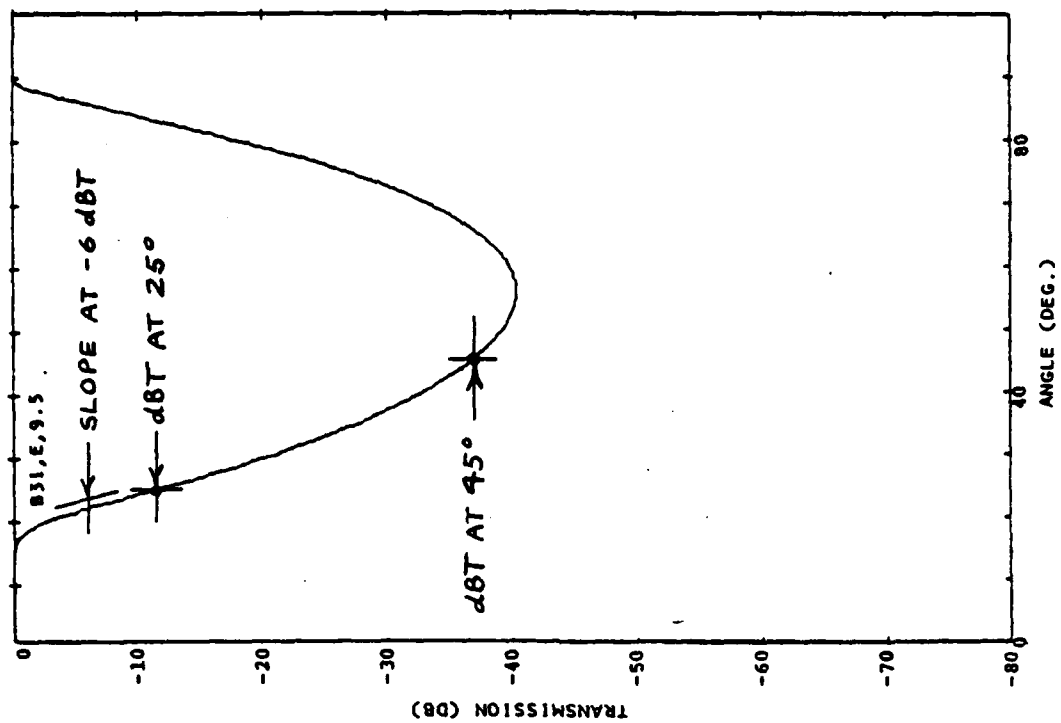
#### Evaluation of Filter Properties

Perhaps the most significant property for comparing filters is the transmission loss at angles well outside the passband, or the "rejection", expressed in dB. In this study, rejection has been evaluated at 25° and 45° off broadside. The rejection at 45° in the H-plane is used as a standard of comparison throughout this report.

Figure 3-5 shows the rejection at  $\theta = 45^\circ$  for the various filters selected for study. Several basic relationships are apparent in this plot. Rejection decreases with increased passband width for any given number of poles and ripple level. Rejection increases with an increase in ripple value, for any given number of poles and passband width. Rejection also increases with an increase in the number of poles for any given passband width and ripple level. In general, there are many combinations of passband width, number of poles and ripple level that can give a particular nominal value of rejection.



(a) H Plane



(b) E Plane

Figure 3-2 Transmission, Filter B31, H and E-Planes

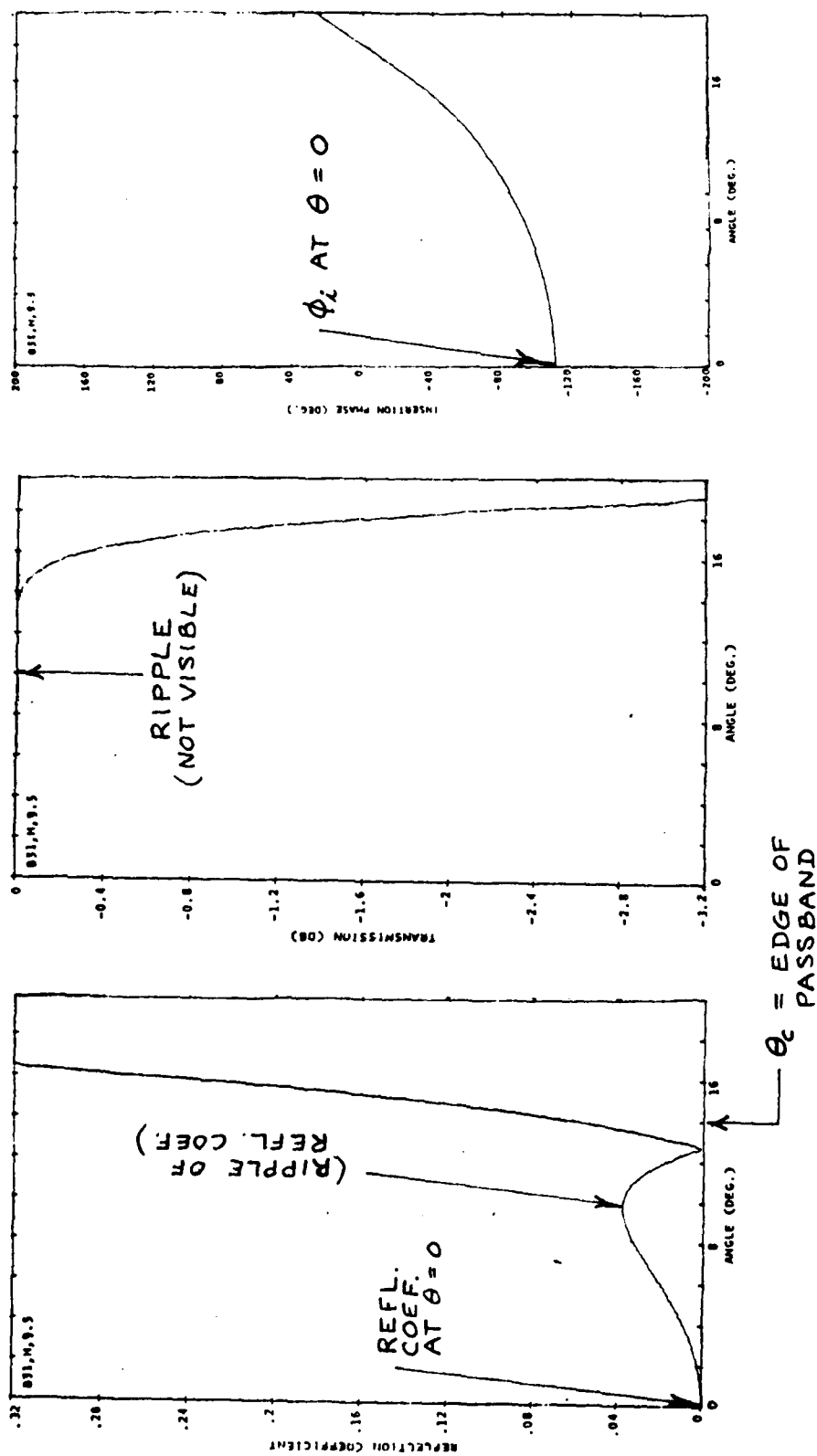


Figure 3-3 Passband Reflection and Transmission, Filter B31, H-Plane



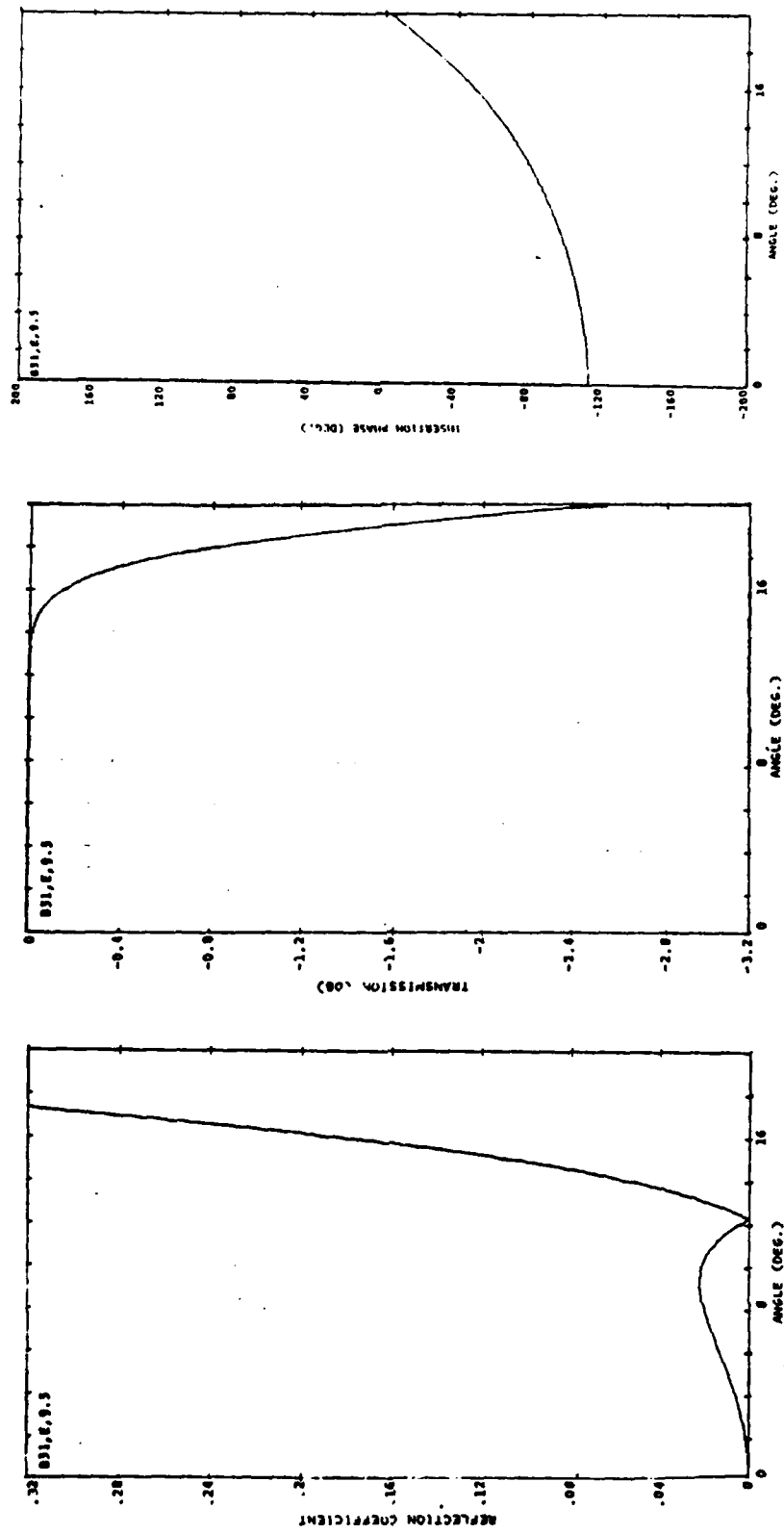


Figure 3-4 Passband Reflection and Transmission, Filter B31, E-Plane

TABLE 3-3, Part 1 of 2

## NOMINAL PERFORMANCE FOR BROADSIDE-CENTERED FILTERS

| FILTER<br>CODE | PLANE: | REJECTION<br>@ $\theta = 25^\circ$ |       | REJECTION<br>@ $\theta = 45^\circ$ |        | SLOPE<br>@ -6 dBT |          | INSERT.<br>PHASE<br>@ $\theta = 0^\circ$ | REFL.<br>COEF.<br>@ $\theta = 0^\circ$ |
|----------------|--------|------------------------------------|-------|------------------------------------|--------|-------------------|----------|--|--|
|                |        | (dBT)                              | (dBT) | (dBT)                              | (dBT)  | (dB/deg)          | (dB/deg) | (deg)                                    |  |
|                |        | H                                  | E     | H                                  | E      | H                 | E        | H;E                                      | H;E                                    |
| A20            |        | 18.14                              | 13.91 | 41.95                              | 30.51  | -1.69             | -1.42    | -161.22                                  | 0.151                                  |
| A21            |        | 8.08                               | 4.56  | 31.10                              | 19.77  | -1.25             | -0.94    | 170.96                                   | 0.048                                  |
| A22            |        | 1.44                               | 0.53  | 19.53                              | 9.13   | -0.95             | -0.53    | 134.01                                   | 0.015                                  |
| B20            |        | 11.05                              | 6.94  | 34.69                              | 23.22  | -1.42             | -1.11    | -178.37                                  | 0.151                                  |
| B21            |        | 2.76                               | 1.08  | 23.36                              | 12.42  | -1.05             | -0.67    | 147.28                                   | 0.048                                  |
| B22            |        | 0.21                               | 0.07  | 10.98                              | 3.25   | -0.77             | —        | 102.11                                   | 0.015                                  |
| C20            |        | 3.21                               | 1.14  | 25.01                              | 13.76  | -1.14             | -0.75    | 153.45                                   | 0.151                                  |
| C21            |        | 0.25                               | 0.07  | 12.69                              | 4.09   | -0.82             | -0.22    | 109.05                                   | 0.048                                  |
| C22            |        | 0.01                               | 0.00  | 1.56                               | 0.29   | -0.56             | —        | 52.81                                    | 0.015                                  |
|                |        |                                    |       |                                    |        |                   |          |  |  |
| A31            |        | 27.87                              | 22.29 | 62.65                              | 47.48  | -2.70             | -2.30    | -88.85                                   | 0.000                                  |
| A32            |        | 17.45                              | 11.92 | 51.96                              | 36.85  | -2.14             | -1.73    | -112.30                                  | 0.000                                  |
| B31            |        | 16.99                              | 11.26 | 51.81                              | 36.59  | -2.24             | -1.81    | -111.61                                  | 0.000                                  |
| B32            |        | 7.24                               | 3.26  | 40.72                              | 25.79  | -1.76             | -1.31    | -141.13                                  | 0.000                                  |
| C31            |        | 4.21                               | 1.35  | 37.38                              | 22.35  | -1.75             | -1.25    | -149.86                                  | 0.000                                  |
| C32            |        | 0.75                               | 0.22  | 25.44                              | 11.63  | -1.32             | -0.80    | 170.79                                   | 0.000                                  |
|                |        |                                    |       |                                    |        |                   |          |  |  |
| A51            |        | 68.12                              | 60.38 | 124.94                             | 102.39 | -6.85             | -6.10    | 90.77                                    | 0.000                                  |
| A52            |        | 57.82                              | 49.90 | 114.54                             | 91.95  | -5.49             | -4.81    | 74.11                                    | 0.000                                  |
| A54            |        | 37.20                              | 29.16 | 93.41                              | 70.88  | -3.90             | -3.32    | 35.49                                    | 0.000                                  |
| A56            |        | 17.39                              | 10.01 | 71.60                              | 49.56  | -2.91             | -2.35    | -14.41                                   | 0.000                                  |
| B51            |        | 50.24                              | 41.85 | 107.39                             | 84.58  | -5.72             | -4.84    | 66.03                                    | 0.000                                  |
| B52            |        | 39.85                              | 31.42 | 96.76                              | 74.00  | -4.52             | -3.80    | 44.83                                    | 0.000                                  |
| B54            |        | 19.67                              | 11.82 | 75.00                              | 52.67  | -3.16             | -2.55    | -4.76                                    | 0.000                                  |
| B56            |        | 4.23                               | 1.01  | 52.32                              | 31.47  | -2.30             | -1.72    | -69.01                                   | 0.000                                  |
| C51            |        | 26.24                              | 16.69 | 84.50                              | 61.37  | -4.40             | -3.54    | 23.07                                    | 0.000                                  |
| C52            |        | 16.35                              | 7.86  | 73.40                              | 50.61  | -3.45             | -2.71    | -5.68                                    | 0.002                                  |
| C54            |        | 2.70                               | 0.49  | 50.43                              | 29.38  | -2.32             | -1.69    | -73.79                                   | 0.000                                  |
| C56            |        | 0.12                               | 0.00  | 28.08                              | 11.35  | -1.63             | -0.96    | -160.82                                  | 0.000                                  |

TABLE 3-3, Part 2 of 2

NOMINAL PERFORMANCE FOR BROADSIDE-BIASED (b)  
AND OFF-BROADSIDE (o) FILTERS

| FILTER<br>CODE   | REJECTION<br>@ $\theta = 25^\circ$ |       | REJECTION<br>@ $\theta = 45^\circ$ |          | SLOPE<br>@ -6 dBT     |          | INSERT.<br>PHASE<br>@ $\theta = 0^\circ$<br>(deg.) | REFL.<br>COEF.<br>@ $\theta = 0^\circ$ | OPT.<br>FREQ.<br>(GHz) |
|--|------------------------------------|-------|------------------------------------|----------|-----------------------|----------|--|--|------------------------|
|  | (dBT)                              | (dBT) | (dBT)                              | (dBT)    | (dB/deg)              | (dB/deg) |  |  |                        |
| PLANE: H   | E                                  |       | H                                  | E        | H                     | E        | H;E  | H;E                                    | -                      |
| A31 "b"  | 41.77                              | 36.50 | 78.46                              | 63.40    | -4.27                 | -3.76    | -112.19  | 0.001                                  | 9.496                  |
| B31 "b"  | 29.79                              | 24.07 | 67.47                              | 52.24    | -3.54                 | -2.99    | -124.85  | 0.001                                  | 9.491                  |
| C31 "b"  | 13.14                              | 7.28  | 52.88                              | 37.43    | -2.76                 | -2.16    | -145.56  | 0.000                                  | 9.473                  |
| FILTER PERFORMANCE AT $\theta_m = 20^\circ$ ( $f_m = 10.11$ GHz) |                                    |       |                                    |          |                       |          |  |  |                        |
|  | REJECTION                          |       | SLOPES                             |          | INSERTION PHASE       |          | REFL. COEFFICIENT                                  |  |                        |
|  | @ $\theta = 45^\circ$              |       | @ -6 dBT                           |          | @ $\theta = \theta_m$ |          | @ $\theta = \theta_m$                              |  | @ $\theta = 0^\circ$   |
|  | (dBT)                              | (dBT) | (dB/deg)                           | (dB/deg) | (deg)                 | (deg)    |  |  |                        |
| PLANE: H   | E                                  |       | H                                  | E        | H                     | E        | H  | E                                      | H;E                    |
| A31 "o"  | 57.28                              | 41.39 | 1.44,                              | 1.39,    | -89.                  | -105.    | 0.000  | 0.100                                  | .976                   |
|  |                                    |       | -4.30                              | -3.17    |                       |          |  |  |                        |
| B31 "o"  | 46.45                              | 30.38 | -                                  | -        | -112.                 | -126.    | 0.001  | 0.063                                  | .785                   |
|  |                                    |       | -3.25                              | -2.27    |                       |          |  |  |                        |
| C31 "o"  | 32.08                              | 16.05 | -                                  | -        | -150.                 | -162.    | 0.000  | 0.027                                  | .222                   |
|  |                                    |       | -2.27                              | -1.41    |                       |          |  |  |                        |
| FILTER PERFORMANCE AT $\theta_m = 30^\circ$ ( $f_m = 10.97$ GHz) |                                    |       |                                    |          |                       |          |  |  |                        |
| A31 "o"  | 47.95                              | 30.48 | 3.61,                              | 3.20,    | -87.                  | -127.    | 0.000  | 0.166                                  | 1.000                  |
|  |                                    |       | -5.89                              | -3.56    |                       |          |  |  |                        |
| B31 "o"  | 37.15                              | 19.23 | 2.01,                              | 1.81,    | -110.                 | -144.    | 0.000  | 0.033                                  | .997                   |
|  |                                    |       | -4.34                              | -2.50    |                       |          |  |  |                        |
| C31 "o"  | 22.82                              | 5.67  | 2.31,                              | 2.31,    | -149.                 | -177.    | 0.000  | 0.038                                  | .945                   |
|  |                                    |       | -2.88                              | -1.46    |                       |          |  |  |                        |

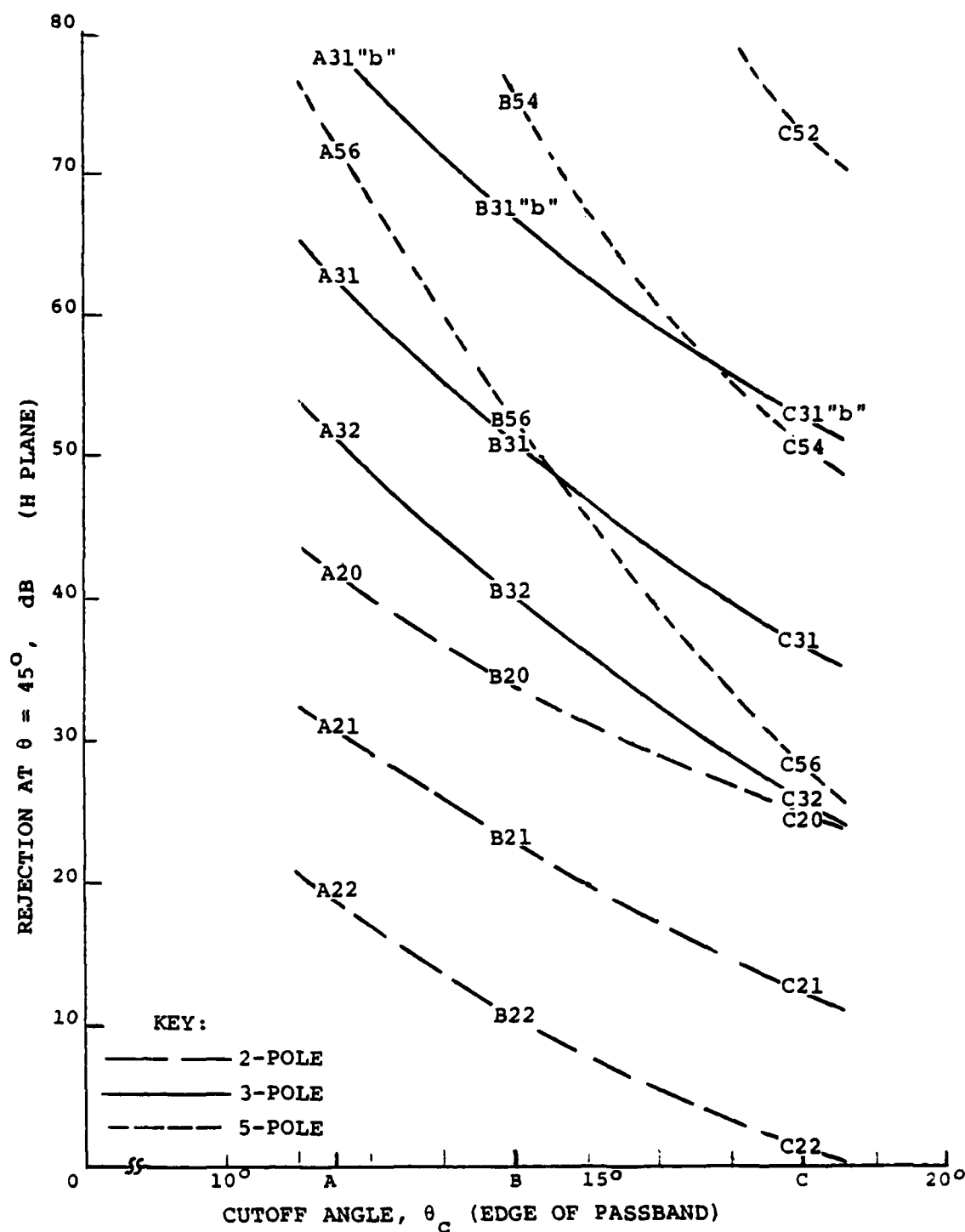


Figure 3-5 Rejection for Filters with Various Parameters

Cutoff slope is the rate of change of filter transmission near the edge of the passband. It is evaluated here as the slope in dB/degree of the transmission loss vs.  $\theta$  curve at the -6 dB point. Figure 3-6 shows a correlation between the slope and the rejection at 45°.

Another interesting correlation is shown in Figure 3-7, relating the sum of all the susceptive (B) elements of a filter to its rejection at 45°. For a given quantity of poles, a single curve relates the rejection to the total B, regardless of passband width or ripple level. More poles tend to give greater rejection for a given total B, particularly for filters with large rejection.

#### 3.4 FILTER ELEMENT TOLERANCES

For all the filter designs considered, the variation in reflection and insertion phase with percentage changes in element values have been computed at broadside (or nominal) incidence. The results have been expressed as "standard tolerances", or the percentage change in all susceptances or all lengths causing either 5° change in insertion phase or 0.2 change in reflection coefficient of the filter. The 5°  $\Delta\phi_i$  and 0.2  $\Delta R$  have been arbitrarily chosen as standard allowable errors of filter performance at broadside. In this way, a common "medium of exchange" that can be related to mechanical or material-property tolerances in practical filters has been established.

The significance of the properties considered lies in the application of the spatial filter in passing the main beam of a reflector antenna while reducing the sidelobe radiation that occurs in the stopband of the filter. The filter reflection at the mainbeam incidence angle (broadside) usually passes directly back into the antenna, and therefore must be limited. The filter insertion phase at broadside, if not uniform over the entire area of the antenna aperture, will perturb the aperture illumination and generate sidelobes in the radiation pattern of

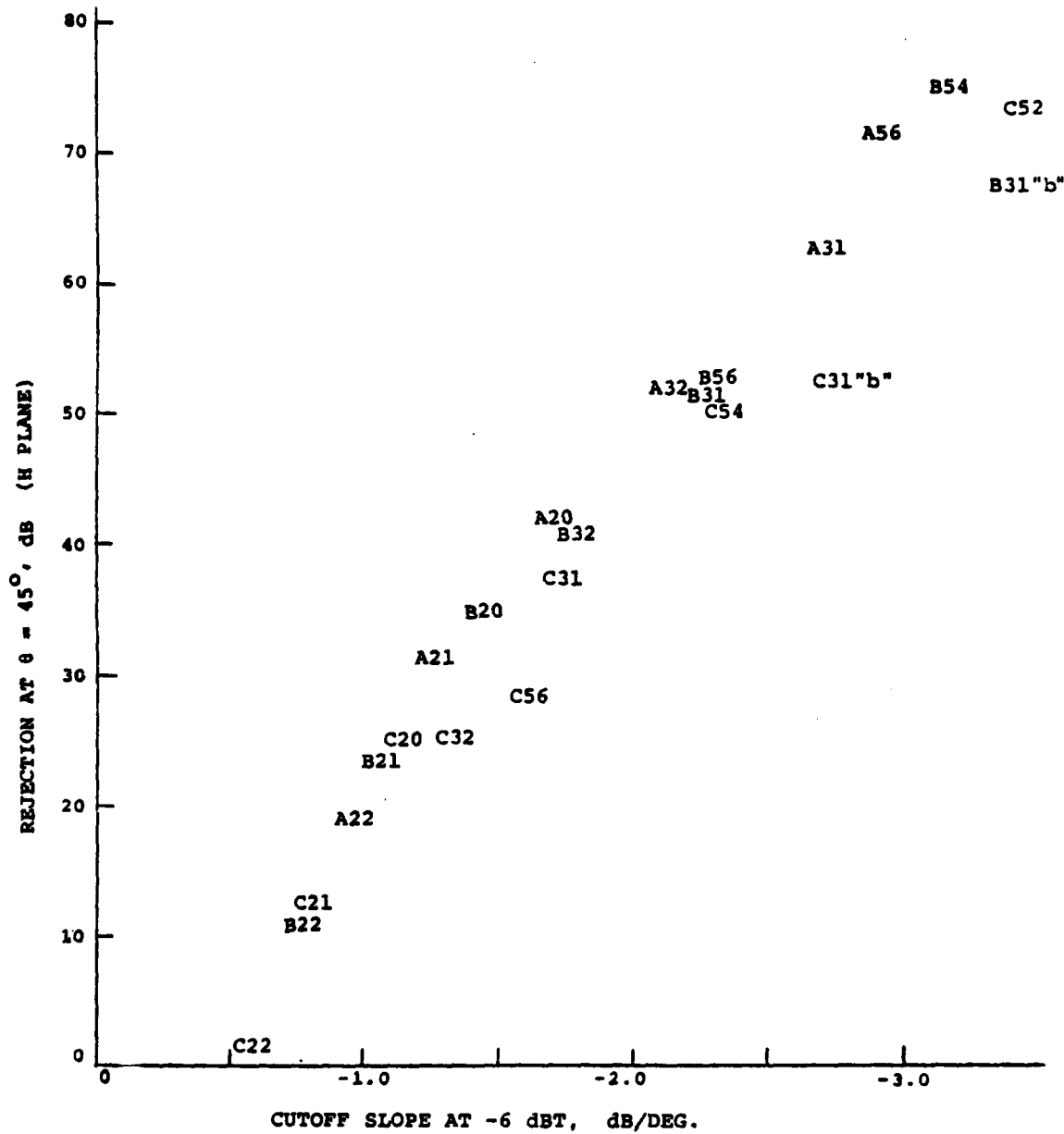


Figure 3-6 Rejection vs. Cutoff Slope for Various Filters

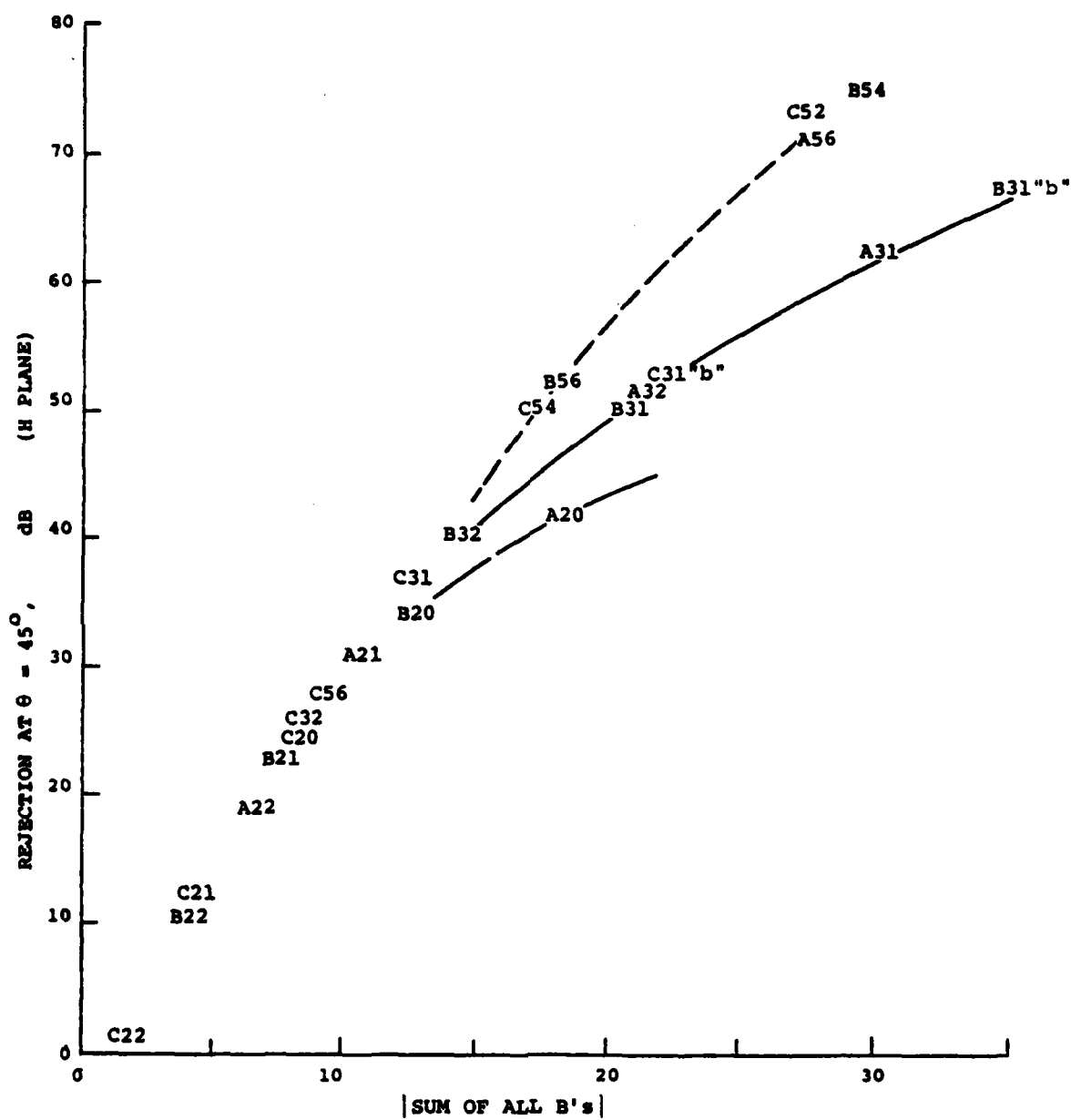


Figure 3-7 Rejection vs. Susceptance Sum for Various Filters

the antenna/filter combination.

Computation of the "standard tolerance" based on insertion phase is illustrated in Figure 3-8. Filter performance with a length increased 1% was computed, and the change in insertion phase from the nominal-length performance was calculated (2.7 degrees in the example illustrated). Next, the performance with a length increased 3% was compared with nominal; the insertion-phase change at broadside incidence was again calculated (8.3 degrees). A simple linear interpolation yields 1.8% as the "standard tolerance" on length for this example, based on 5° insertion phase. Standard tolerances based on reflection were determined in a similar manner.

#### Single-Element Deviations

The most critical length in a Chebyshev filter is the center length because this length corresponds to the highest Q resonator. Figure 3-9 shows the percent standard tolerance on one center length, based on 5°  $\Delta\phi_i$ , plotted vs. the nominal rejection at 45° in the H-plane for various filters. A clear trend of tighter tolerances required for greater rejection is evident, regardless of passband width or ripple level. Increasing the number of poles yields greater rejection for a given tolerance in most cases.

A similar presentation is given in Figure 3-10 for the percent standard tolerance on one center length, based on 0.2  $\Delta R$ . Again, a clear trend of tighter tolerances required for greater rejection is evident, as well as a greater rejection-tolerance product with increasing number of poles. For any particular filter the tolerances based on 0.2  $\Delta R$  are looser than the tolerances based on 5°  $\Delta\phi_i$ .

The tolerances on susceptance have trends similar to those given above when the case of susceptance at the edge of the filter is considered. Figure 3-11 shows the percent standard tolerance on one edge susceptance, based on 5°  $\Delta\phi_i$ , plotted vs.



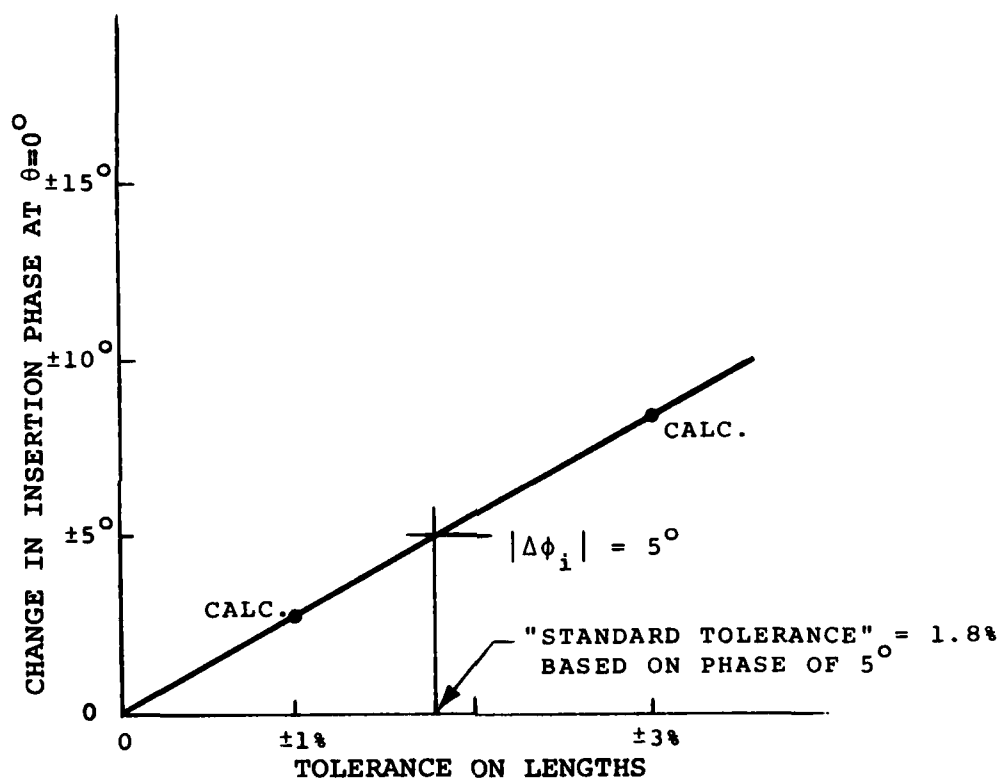


Figure 3-8 Method for Determination of Tolerance

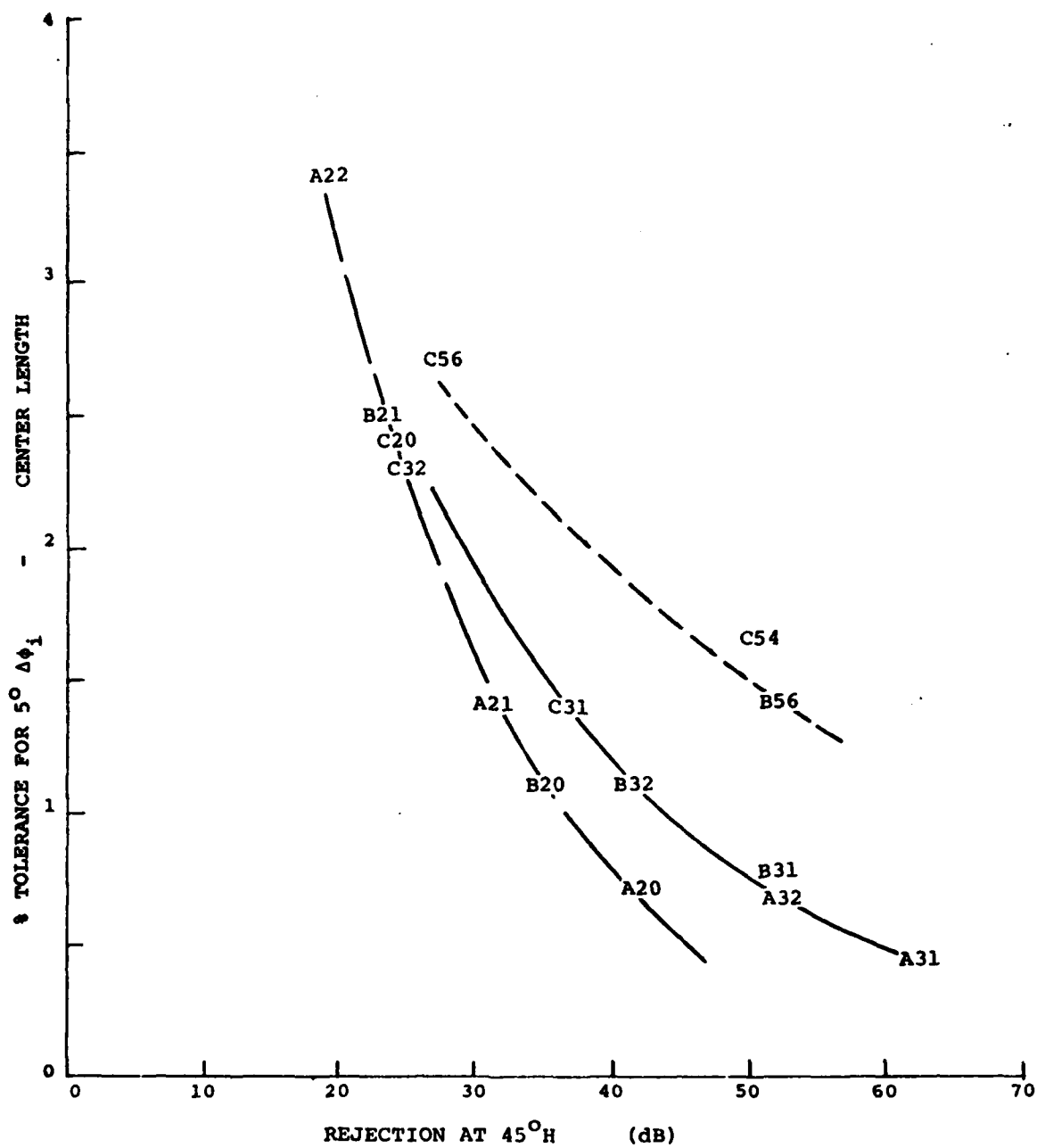


Figure 3-9 Tolerance on Center Length vs. Rejection,  
for 5° Δφ<sub>i</sub> Allowable

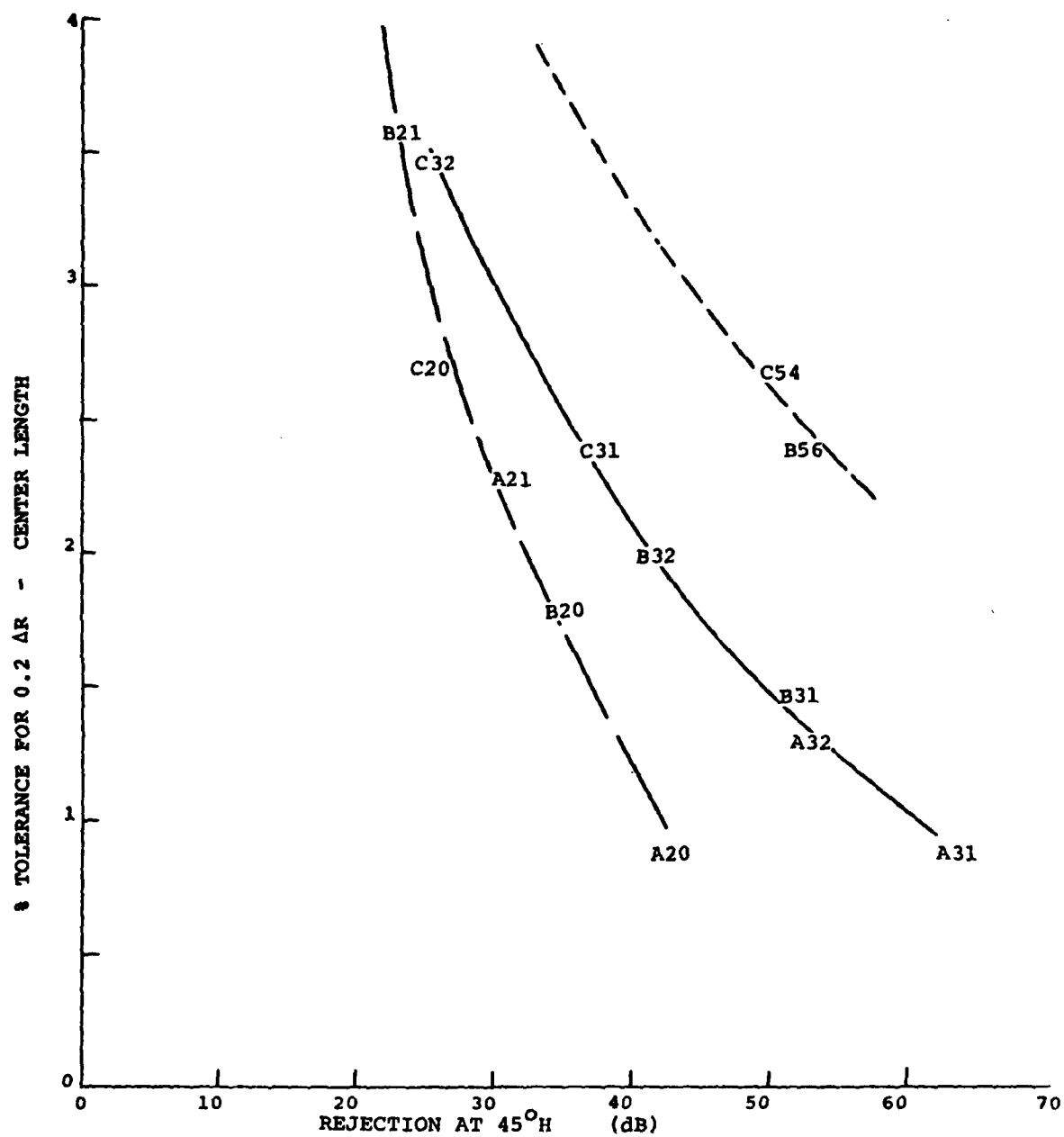


Figure 3-10 Tolerance on Center Length vs. Rejection,  
for 0.2 ΔR Allowable

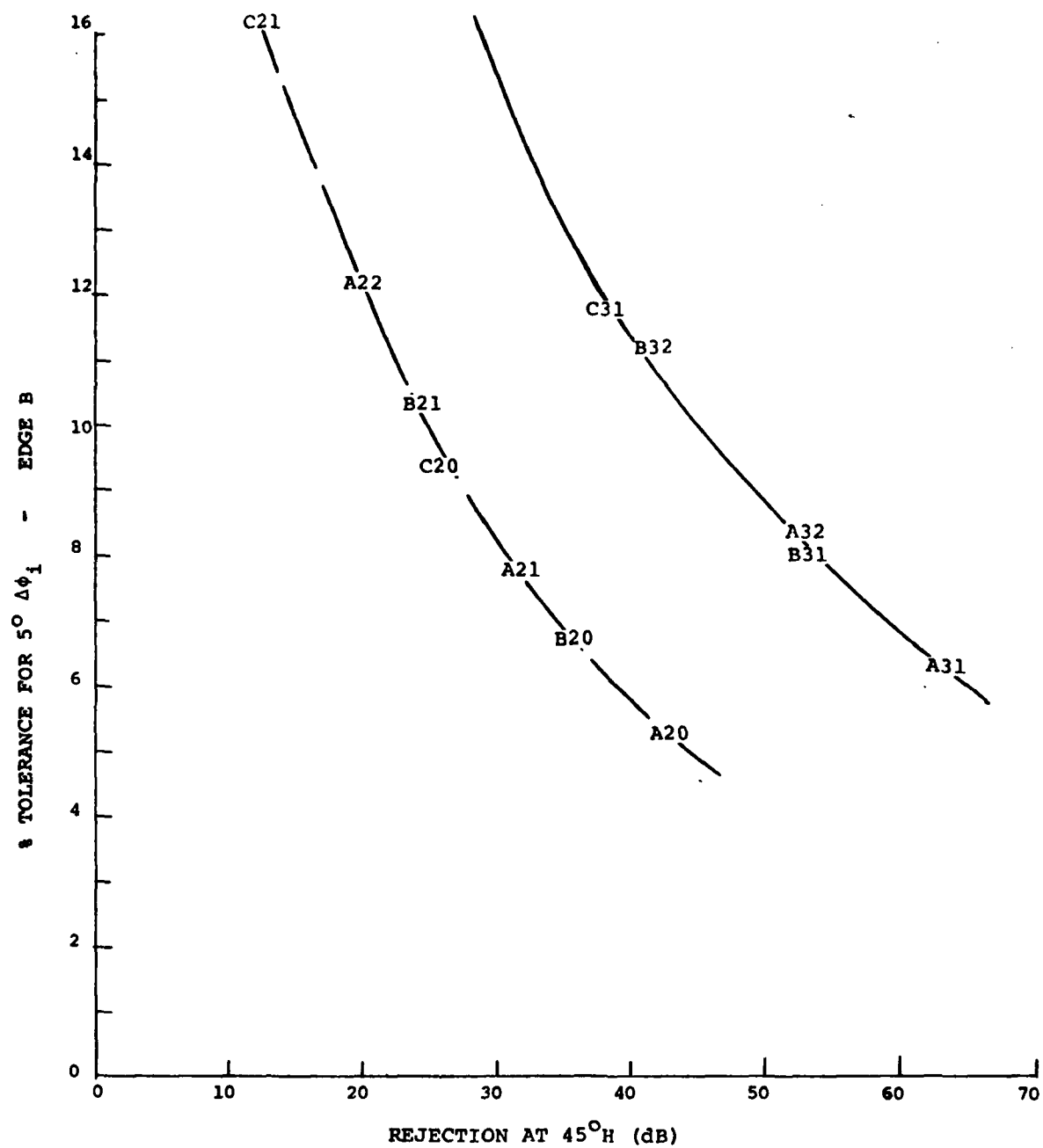


Figure 3-11 Tolerance on Edge Susceptance vs. Rejection,  
for 5° Δφ<sub>i</sub> Allowable

the rejection at  $45^\circ$ . Figure 3-12 shows the tolerance based on  $0.2 \Delta R$ . It is evident that on a percentage basis, these edge susceptance tolerances are substantially looser than the center length tolerance. Center susceptance tolerances, not shown here, do not have a clear trend of tighter tolerances with increasing rejection. Instead, the center susceptance tolerances are typically 8 to 10% based on  $5^\circ \Delta \phi_i$ , and are typically 20% or more based on  $0.2 \Delta R$ .

#### All-Element Cumulative Deviations

The "standard tolerances" discussed so far have assumed that only one length or one susceptance in the filter deviates from the nominal value. This assumption is obviously optimistic. Another assumption that can be made is that all the lengths or all the susceptances deviate in such a way as to create the greatest effect. This assumption is used in the following.

For the length tolerances based on  $\Delta \phi_i$ , the greatest deviation of  $\phi_i$  occurs when all the length deviations have the same sign. Figure 3-13 shows this case, based on a  $5^\circ \Delta \phi_i$ . As expected, the allowable tolerance on length is tighter for this worst-case assumption than it is when only one length deviates, as may be seen by comparison with Figure 3-9.

For the length tolerances based on  $\Delta R$ , the greatest deviation of  $R$  occurs when successive length deviations have alternating signs. Figure 3-14 shows this case, based on a  $0.2 \Delta R$ . Again, the allowable tolerance on length is tighter for this worst-case assumption than it is when only one length deviates, as may be seen by comparison with Figure 3-10.

For the susceptance tolerances based on  $\Delta \phi_i$ , the greatest deviation of  $\phi_i$  appears to occur when all the susceptance deviations have the same sign. For the susceptance tolerances based on  $\Delta R$ , the greatest deviation of  $R$  is expected to occur when successive susceptance deviations have alternating signs.

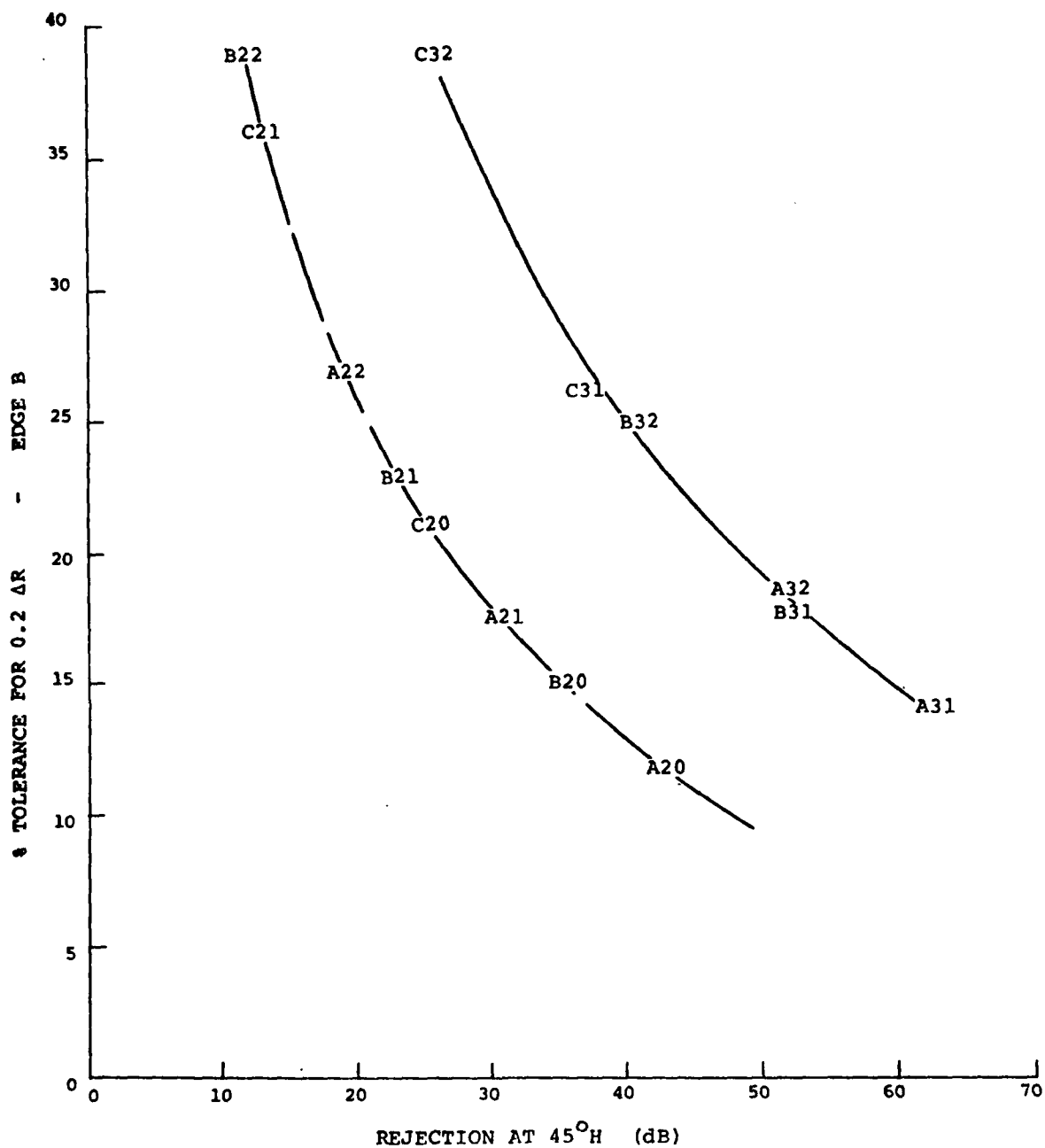


Figure 3-12 Tolerance on Edge Susceptance vs. Rejection, for 0.2 ΔR Allowable

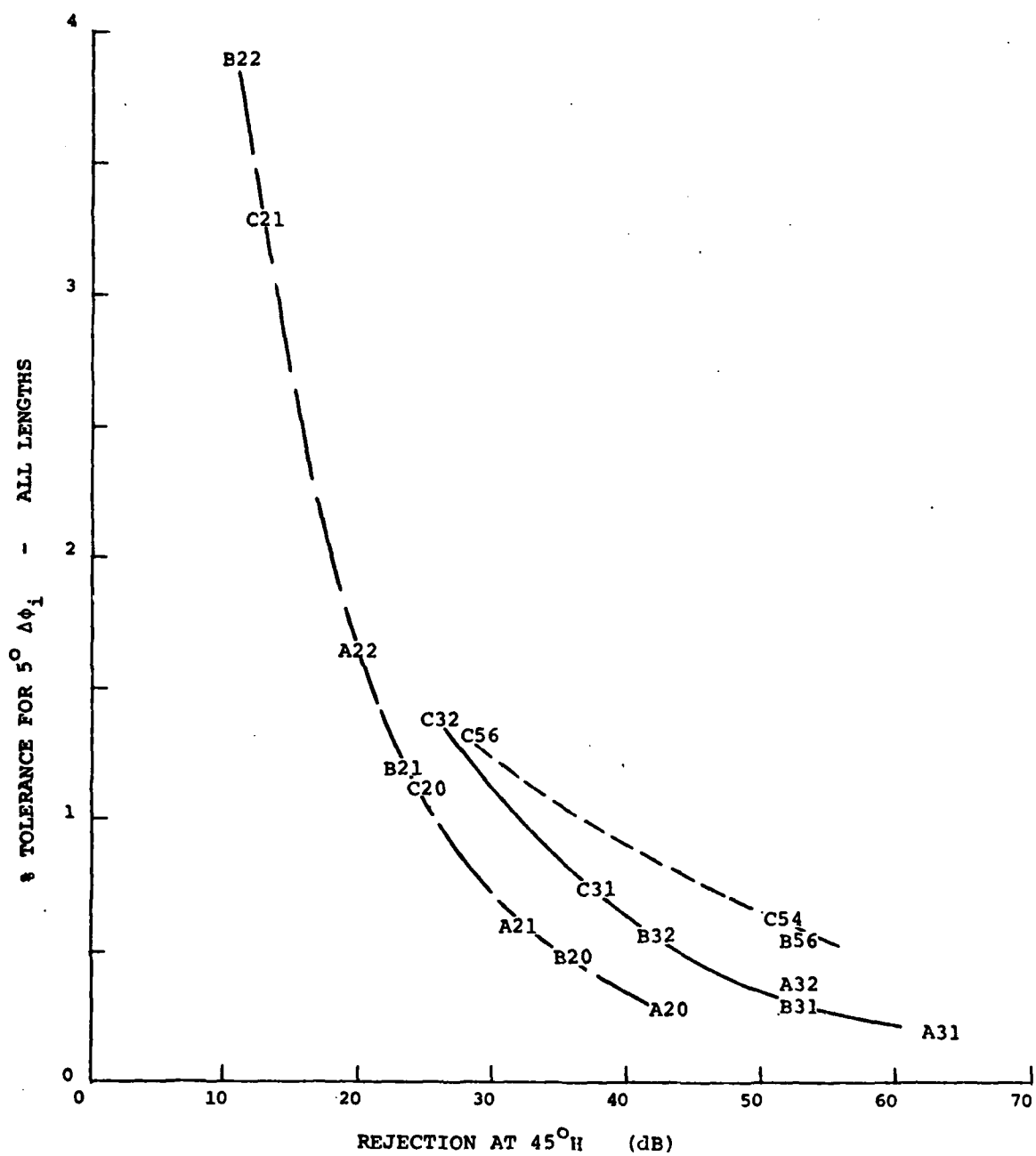


Figure 3-13 Tolerance on All Lengths Cumulative vs. Rejection for 5° Δφ₁ Allowable

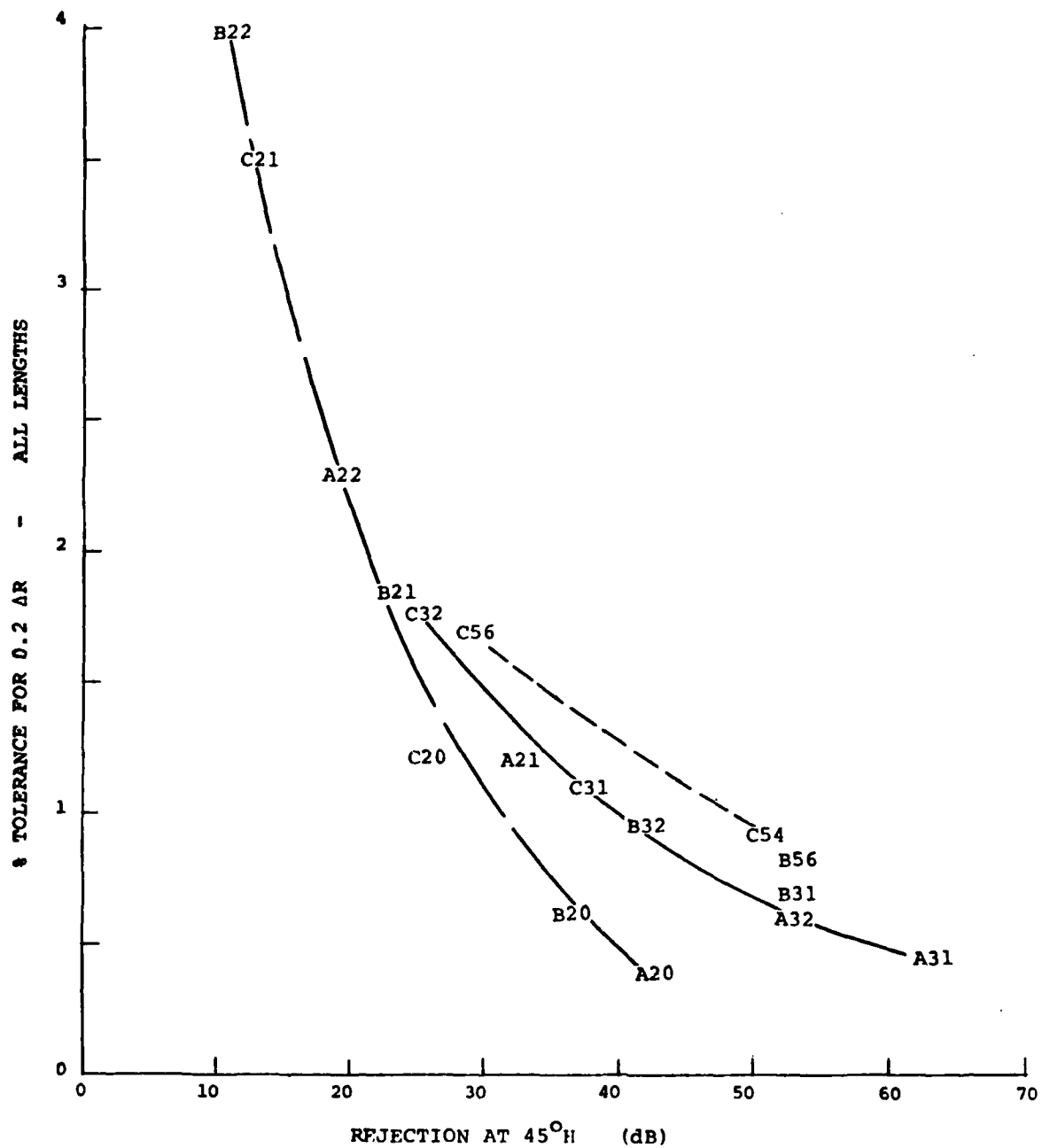


Figure 3-14 Tolerance on All Lengths Cumulative vs. Rejection, for 0.2 AR Allowable



Neither of these cases is presented here; both will require tighter tolerances than the corresponding cases for only one deviation.

#### Discussion

The assumption that all the length deviations or susceptance deviations in a multi-layer spatial filter will occur in the worst-case cumulative manner is likely to be a pessimistic one. In designing a spatial filter, a tolerance assumption should be made that is intermediate between the optimistic single-deviation case and the pessimistic all-deviation cumulative case. Since the different layers in a spatial filter have different tolerance sensitivities, the single-deviation approach applied to each successive layer yields a comprehensive view of the overall tolerance situation. Such a view should ultimately include the actual construction techniques and their errors as they relate to length and susceptance tolerances.

With the single-deviation results, it was noted that an increase in the number of poles yields an increase in the tolerance-rejection product, which is desirable. It is interesting that with the all-element cumulative deviations this effect still occurs for the length tolerances, even though there are more lengths in a many-pole filter. Thus it appears to be generally true that, at least for the larger values of rejection, an increase in the number of poles will permit an increase in the tolerance-rejection product. Of course an increase in the number of poles requires a spatial filter with more layers, which increases its complexity, weight and cost.

The assumption of  $5^\circ \Delta\phi_i$  and  $0.2 \Delta R$  that was used for the preceding tolerance analysis was an arbitrary choice. With a greater value permitted for  $\Delta\phi_i$ , either the tolerances could be loosened or the filter could be designed for greater rejection in its stopband. However, a greater value of  $\Delta\phi_i$  would result in higher sidelobes generated by filter non-uniformities.

Similarly, with a greater value permitted for  $\Delta R$ , tolerances could be loosened or rejection could be increased. However, this may result in an increased antenna VSWR; also the filter/antenna reflection interaction may cause some increase of sidelobes within the filter angular passband. For each specific application for a spatial filter, these effects should be considered when selecting an allowable value for  $\Delta\phi_i$  and  $\Delta R$ . The results presented here can be simply scaled if greater or lesser values for  $\Delta\phi_i$  or  $\Delta R$  are selected for a particular application.

The relationship between filter tolerances and obtainable stopband rejection that has been presented in this section is of fundamental importance in the design of spatial filters and in their use for controlling antenna sidelobes. A spatial filter designed for greater stopband rejection can theoretically reduce antenna sidelobes further, but in practice this may result in an increase of sidelobes. For each specific application there is probably an optimum value of stopband rejection that, when the effect of tolerances is included, will yield the lowest antenna/filter sidelobes.

### 3.5 FREQUENCY BANDWIDTH

For some of the filters, computer plots were generated with frequency changed incrementally until each edge of the passband had moved in the H-plane to the nominal design angle ( $0^\circ$  or  $\theta_m$ ) of the filter. The results of this exercise are given in Table 3-4.

For the three broadside-centered filters (A31, B31, C31) the resulting bandwidths (4.0%, 5.8%, 9.2%) are close to the bandwidths that can be calculated by the simple formulas in Section 2.3. This is also the case for the six off-broadside ("o") filters.

TABLE 3-4  
FREQUENCY BANDWIDTH

| FILTER CODE | NOMINAL $\theta_m$ (deg.) | PASSBAND EDGE ON PLOT (deg.) | RELATIVE FREQ. CHANGE FOR EDGE AT $\theta_m$ | BANDWIDTH $\Delta f/f_m$ (%) |
|-------------|---------------------------|------------------------------|--|------------------------------|
| A 31        | 0                         | 11.4                         | $\pm .020$                                   | 4.0                          |
| A 31 "b"    | 0                         | 11.4                         | $+ .0017 - .020$                             | 0.34                         |
| A 31 "o"    | 20                        | 16.6, 23.0                   | $\pm .020$                                   | 4.0                          |
| A 31 "o"    | 30                        | 27.9, 31.8                   | $\pm .020$                                   | 4.0                          |
| B 31        | 0                         | 13.8                         | $\pm .029$                                   | 5.8                          |
| B 31 "b"    | 0                         | 13.8                         | $+ .0024 - .029$                             | 0.48                         |
| B 31 "o"    | 20                        | 14.9, 24.2                   | $\pm .029$                                   | 5.8                          |
| B 31 "o"    | 30                        | 27.0, 32.7                   | $\pm .029$                                   | 5.8                          |
| C 31        | 0                         | 17.2                         | $\pm .046$                                   | 9.2                          |
| C 31 "b"    | 0                         | 17.5                         | $+ .0049 - .048$                             | 0.98                         |
| C 31 "o"    | 20                        | 11.0, 26.1                   | $\pm .046$                                   | 9.2                          |
| C 31 "o"    | 30                        | 25.2, 34.1                   | $\pm .046$                                   | 9.2                          |

For the three broadside-biased ("b") filters the resulting bandwidths are relatively narrow. This is expected, in accordance with the discussion given in Section 2.3. It is believed that a broadside-centered filter is generally preferable to a broadside-biased filter, since the centered filter can provide the same passband width and stopband rejection with a much wider frequency bandwidth.

### 3.6 AVAILABLE REJECTION VS. FREQUENCY

In Section 3.4, the allowable percent tolerances on lengths and susceptances were presented vs. spatial filter rejection at  $45^\circ$ , based on an allowable  $\Delta\phi_i$  of  $5^\circ$  and  $\Delta R$  of 0.2. In the following example, that tolerance information is applied to yield a significant relation between the frequency of operation and the rejection that is available from an allowable filter.

The tolerances on the length dimensions are critical ones in a spatial filter. These tolerances were considered on a percentage basis in Section 3.4. However, the actual construction of a spatial filter would be likely to employ core material such as honeycomb as the principal means for controlling the length dimensions, and these materials typically can be made with length tolerances that are specified directly rather than as a percent of their length. For example, assume that a 0.010 inch length tolerance is available, independent of the actual length. For a length of about  $\lambda/2$ , this corresponds to about 1.8% at 10 GHz (X-band) and to about 0.6% at 3 GHz (S-band). As a result, a filter that gives no more than the allowable  $5^\circ \Delta\phi_i$  or 0.2  $\Delta R$  can be designed to provide considerably greater rejection at S-band than at X-band.

Figure 3-15 shows curves of the rejection at  $45^\circ$  that is available vs. the frequency of operation of a 3-pole spatial filter, assuming particular values for the center-length tolerance in inches, and using certain values of allowable  $\Delta\phi_i$  as

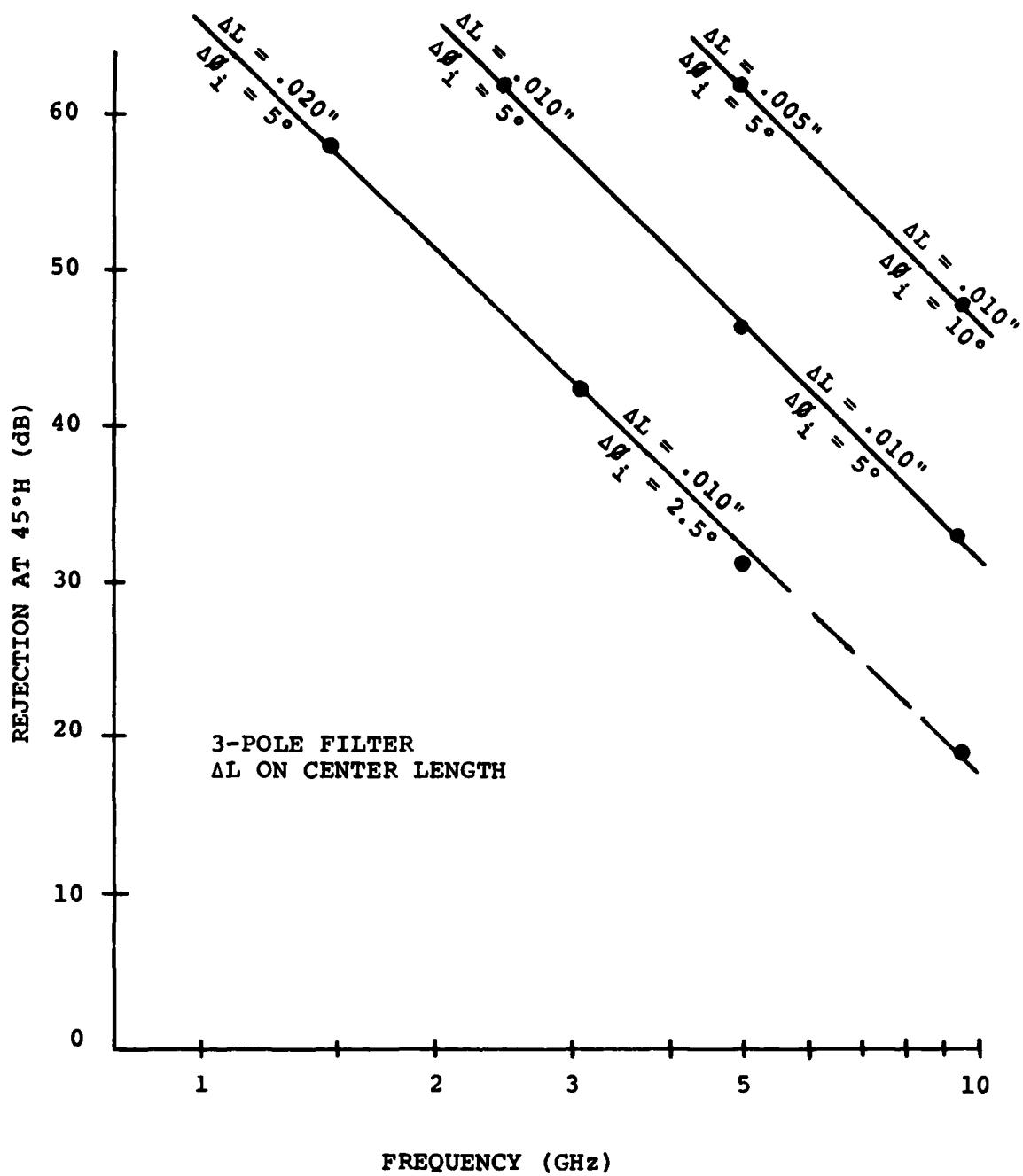


Figure 3-15 Available Rejection vs. Frequency

the basis. These curves were obtained from the curves of Figure 3-9 as indicated above. For a 0.010 inch tolerance on the center length and a  $5^\circ$  allowable  $\Delta\phi_i$ , the available rejection at  $45^\circ$  is about 31 dB at X-band and about 57 dB at S-band.

The curves of Figure 3-15 are for a 3-pole filter. For a greater number of poles, the effect of frequency of operation is still greater. It should also be recognized that the curves of Figure 3-15 represent one family in which only the center length has a tolerance and only  $\Delta\phi_i$  is considered. There are other cases that can be considered, as outlined in Section 3.4. However, in most cases a similar trend of more available rejection for lower frequencies of operation will occur.

It is interesting to note that over the range of values plotted in Figure 3-15, the curves of dB rejection vs. log frequency are substantially linear and parallel. Over this range a 3-pole filter at  $45^\circ$  yields about 15 dB less available rejection per octave of frequency.

## SECTION 4

### SIMULATOR TESTS OF METAL GRIDS

#### 4.1 PURPOSE OF SIMULATOR TESTS

A simulator is a waveguide in which small samples of metal grids can be measured, yielding results corresponding to large (infinite) metal grid areas. Two simulators have been employed in this program. One simulator provides a range of incidence angles near grazing in the E-plane of incidence. The other provides incidence angles near broadside in the H-plane of incidence.

As discussed earlier in this report, crossed inductive metal grids have a susceptance that goes to zero at grazing incidence ( $\theta = 90^\circ$ ) in the E-plane of incidence. This will cause the rejection of a metal-grid spatial filter to become weak at angles near grazing in the E-plane. It also makes the filter susceptible to possible spurious passbands caused by dielectric skin material used for supporting the metal grids.

A calculation using a simplified analysis that is known to be inexact indicates that the dielectric skin may actually enhance the rejection of a metal grid near grazing in the E-plane. However, another viewpoint indicates that a dielectric skin will reduce the susceptance of a metal grid at large incidence angles in the E-plane, thereby increasing the possibility of a spurious passband. It is a purpose of the near-grazing E-plane simulator to determine the effect on E-plane behavior of adding dielectric skin material to metal grids. An additional purpose is to check the accuracy of the basic formula for susceptance of inductive crossed metal grids at angles near grazing in the E-plane, for various configurations of metal grids.

The other simulator is a relatively simple one that provides angles of incidence near broadside. It is important that the metal-grid susceptance be accurately and positively known near broadside because the critical passband of a spatial filter is at or near broadside. Some metal-grid configurations such as nearly-touching round holes do not have a simple formula for susceptance and may be more easily determined by a simulator measurement. Also, the effect of dielectric on this and other metal grids near broadside can be measured directly in the simulator, to check or supplement theoretical results. Additionally, the near-broadside simulator provides a point of reference for comparison with the results obtained from the near-grazing E-plane simulator.

#### 4.2 NEAR GRAZING SIMULATOR TESTS

To simulate plane-wave incidence angles in the E-plane of incidence, a waveguide operating in a TM mode is used (Ref. 13, 14, 15). The angle of incidence ( $\theta$ ) is related to the waveguide mode parameters by the following:

$$\sin \theta = \frac{\lambda}{\lambda_c} \quad \cos \theta = \frac{\lambda}{\lambda_g}$$

where the constant  $\lambda_c$  is the cutoff wavelength of the mode in its waveguide, and  $\lambda_g$  is the guide wavelength of this mode. To obtain angles of incidence near  $90^\circ$  the simulator waveguide must be operated at a wavelength close to the cutoff wavelength, and the guide wavelength of the mode in the waveguide must be much longer than the free-space wavelength.

Ref. 13 - P. W. Hannan and M. A. Balfour, "Simulation of a Phased Array in Waveguide", IEEE Trans. AP, pp 342-353; May, 1965

Ref. 14 - P. W. Hannan, "Discovery of an Array Surface Wave in a Simulator", IEEE Trans. AP, pp 574-576; July, 1967

Ref. 15 - H. A. Wheeler, "A Survey of the Simulator Technique for Designing a Radiating Element in a Phased Array", Phased Array Antenna Symposium, Artech House, pp 132-148; 1970



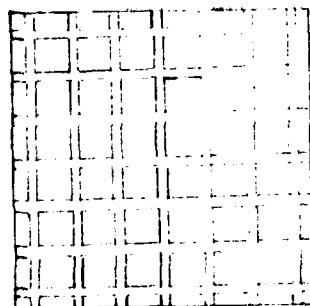
The angle of incidence in the waveguide can be changed by changing the wavelength (frequency). Only a relatively small change of frequency is needed when  $\theta$  is near  $90^\circ$ . Thus the simulator can cover a range of incidence angles near grazing incidence.

A square waveguide cross section has been chosen for the simulator. A contacting crossed metal grid having a square grid is placed in this waveguide in either of two orientations, as shown in Figure 4-1. In both cases the small grid sample is perfectly imaged into an infinite grid by the waveguide walls.

With an insulated crossed grid in which one set of parallel conductors is separated from the other, only the first of the two grid orientations (the perpendicular orientation) in the square waveguide provides perfect imaging. In the other orientation (the oblique orientation) the imaged conductors form zigzag lines rather than straight lines. Some measurements were made with insulated grids in the oblique orientation but those measurements should not be considered to be absolutely reliable.

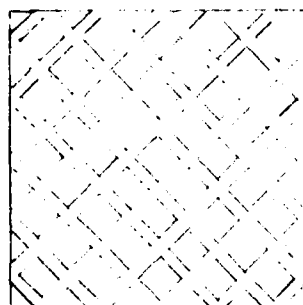
The lowest-order TM mode, the TM-11 mode, is used in the square waveguide. In this case the plane of incidence of a plane-wave component of the waveguide mode lies across the diagonal of the square (Ref. 13). Thus the perpendicular orientation corresponds to  $\theta = \pm 45^\circ$ , and the oblique orientation corresponds to  $\theta = 0^\circ, 90^\circ$ .

The TM-11 mode in square waveguide is excited in a pure form by a transition from coaxial line. For operation over a frequency range, the transition waveguide must not be close to cutoff, and its cross section must be larger than the grid sample cross section. Therefore, a taper is used between the square transition and the square sample. Because of the large  $\lambda_g$  the length of this taper is made many free-space wavelengths ( $25 \lambda$ ) long.



PERPENDICULAR  
ORIENTATION

$$\phi = \pm 45^{\circ}$$



OBLIQUE  
ORIENTATION

$$\phi = 0^{\circ}, 90^{\circ}$$

Figure 4-1 Sample Orientations for Near-Grazing Simulator

The frequency band of this simulator has been chosen to be at C-band (about 5 GHz). This is a compromise between a higher frequency where construction of tiny grids with close tolerances and problems of electrical contact would be difficult, and a lower frequency where the physical length of a taper would be cumbersome. At this frequency a taper is 5 feet long and each grid sample is in a square waveguide 1.7 x 1.7 inches. As indicated in Figure 4-2, there are two tapers and two transitions, one on each side of the grid sample. The overall length of this simulator system is about 10 feet.

Twenty-six frequencies are used to obtain incidence angles from  $60^\circ$  to  $84^\circ$  in  $1^\circ$  steps. At  $84^\circ$  the frequency is only 1.005 times the cutoff frequency of the sample waveguide. Because of this, construction of the tapers and the sample waveguide is held to close tolerances.

Operation of the simulator involves the measurement of transmission loss through a grid sample. To minimize errors, the residual mismatch of each taper and transition is tuned out with a calibrated slide-screw tuner at each frequency. A well-matched generator and detector system is also provided. The use of twenty-six closely-spaced frequencies provides a degree of redundancy that permits some averaging of residual system errors and operator errors when the measured data is plotted on graphs. Figure 4-3 shows a photograph of the near-grazing simulator system.

#### Contacting Strip Results

Figure 4-4 shows the two samples representing a contacting crossed grid of thin metal strips. These samples were 0.040 inch wide copper strips printed on a thin (0.005 inch) teflon substrate for support.

Figure 4-5 shows the data points measured with the near-grazing simulator. Also shown are curves calculated from the strip grid dimensions using the susceptance formulas for E-

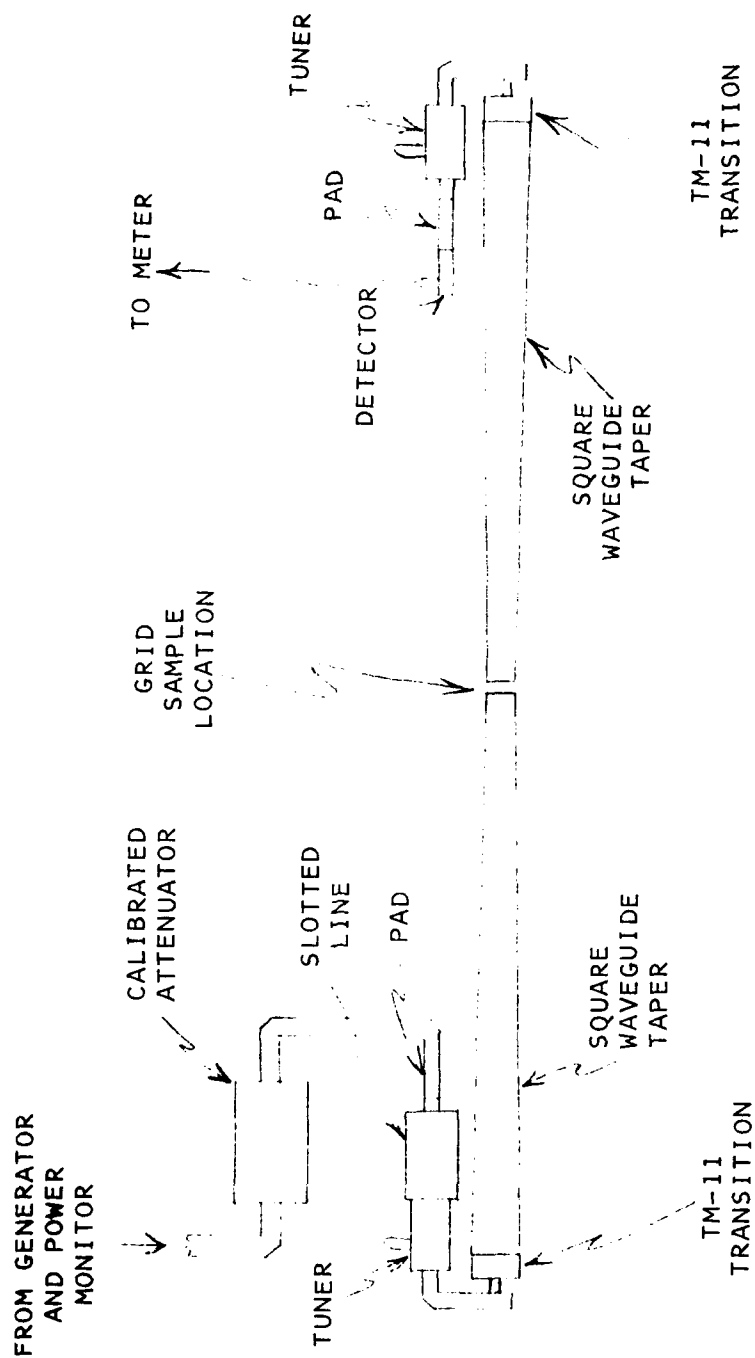


Figure 4-2 Diagram for Near-Grazing Simulator

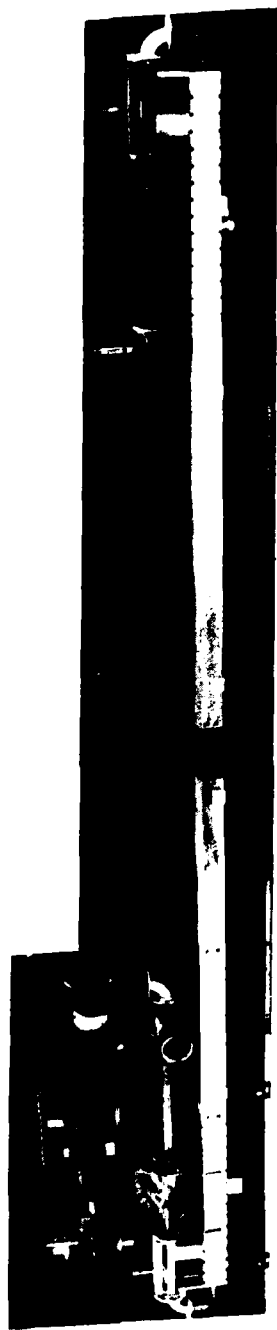


Figure 4-3 Near-Grazing Simulator

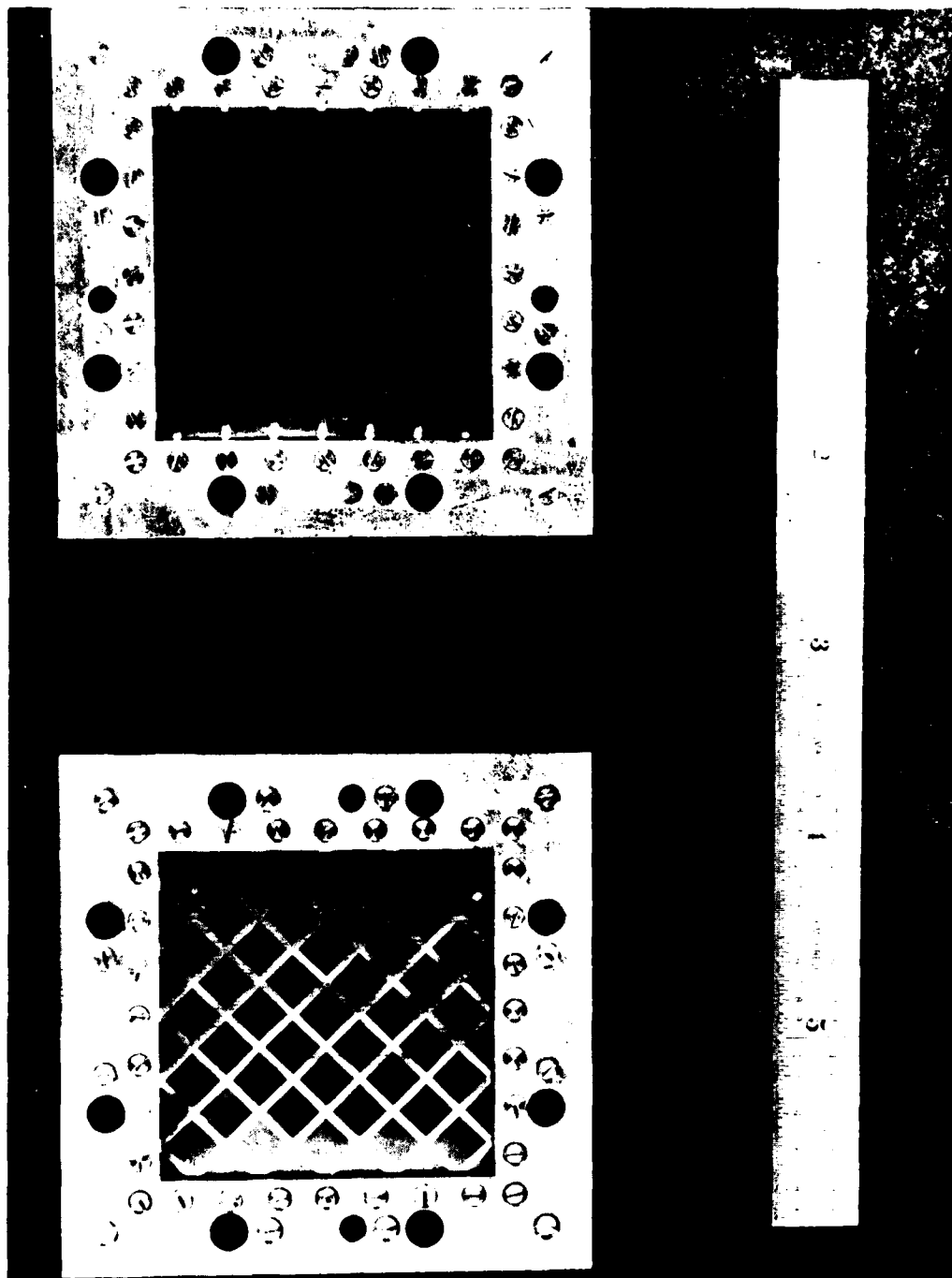


Figure 4-4 Contacting Crossed Strip Samples for Near-Grazing Simulator

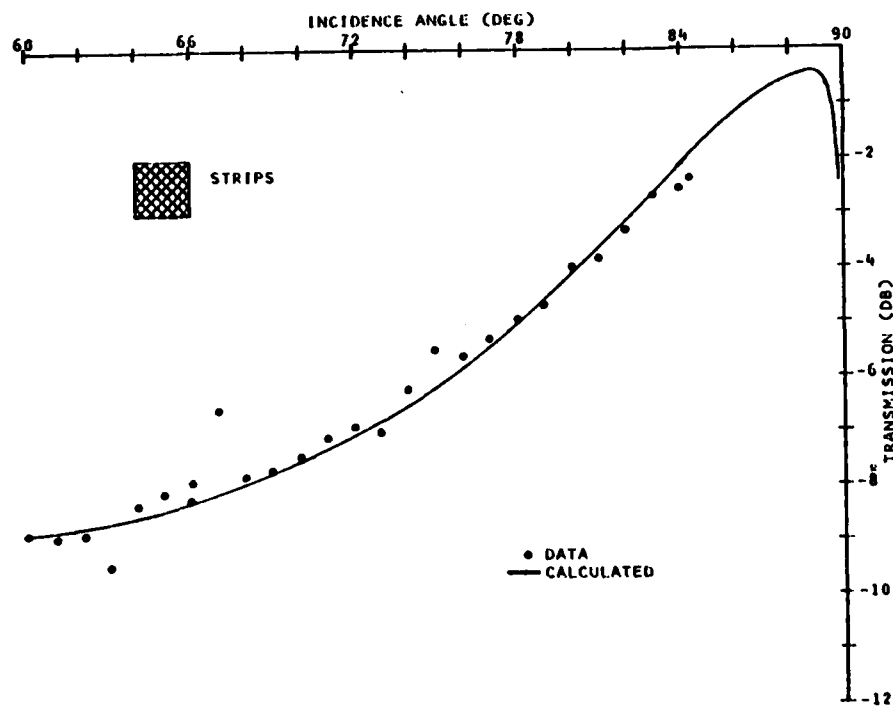
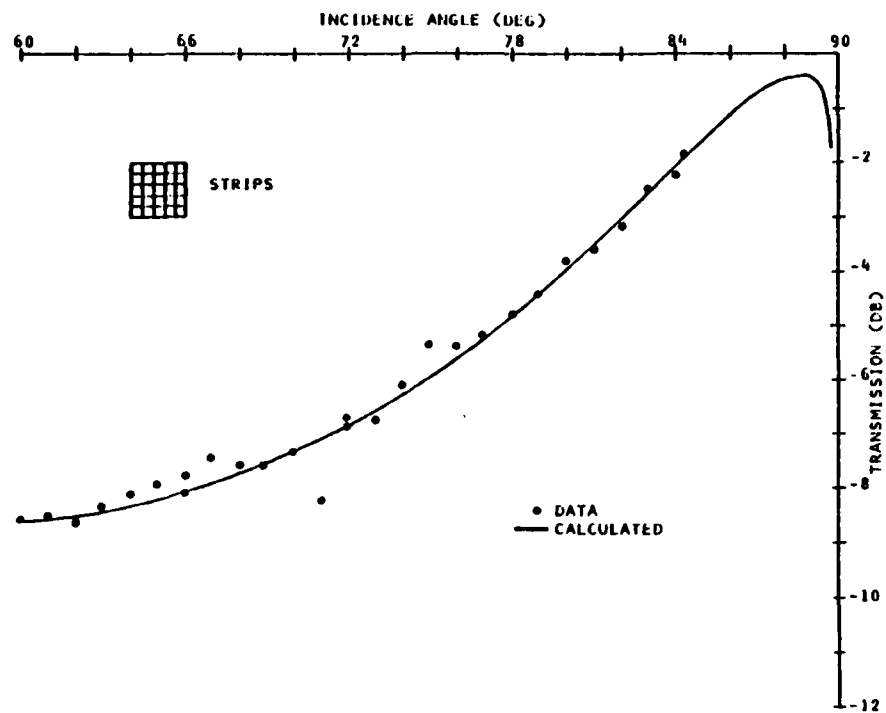


Figure 4-5 Data for Contacting Crossed Strip Samples Near Grazing

plane incidence given in Section 2.5. Included in the calculation is the minor effect of the very thin substrate, which shows up as a bend in the curve between  $88^\circ$  and  $90^\circ$ , and which is of no significance in these measurements. The agreement between the measured data and the calculated curve is evident.

Figure 4-6 shows the data points measured for these strip samples encased in a sheet of dielectric about  $1/16$  inch thick, having a dielectric constant of about 3.5. Also shown are curves calculated on the assumption that this dielectric has no reactive-field interaction effect on the grid susceptance, but merely contributes its own independent reflection effect. There is a clear displacement of the measured data from the calculated curves. It is our conclusion that the assumption of no interaction in the calculation is not an accurate one for large angles of incidence in the E-plane of incidence.

Figure 4-7 compares the measured data for the strip samples encased in dielectric with the data for the strip samples alone. It is seen that at incidence angles greater than about  $80^\circ$  the dielectric causes a decrease in the transmission; the effect appears to become greater as  $\theta$  approaches  $90^\circ$ . This is a characteristic of the simple independent effect of the dielectric skin. At incidence angles less than about  $80^\circ$  the dielectric causes an increase in the transmission. This is indicative of the interaction effect of the dielectric on the grid susceptance. The increase of transmission is undesirable because it will result in a spatial filter having less stopband rejection in the E-plane of incidence. However, there is no indication of a spurious passband in this measured data.

#### Round Hole Results

Figure 4-8 shows one sample of a contacting crossed grid of round holes in a metal sheet. The metal sheet is  $1/16$  inch thick aluminum, and the holes are  $13/32$  inch in diameter with a



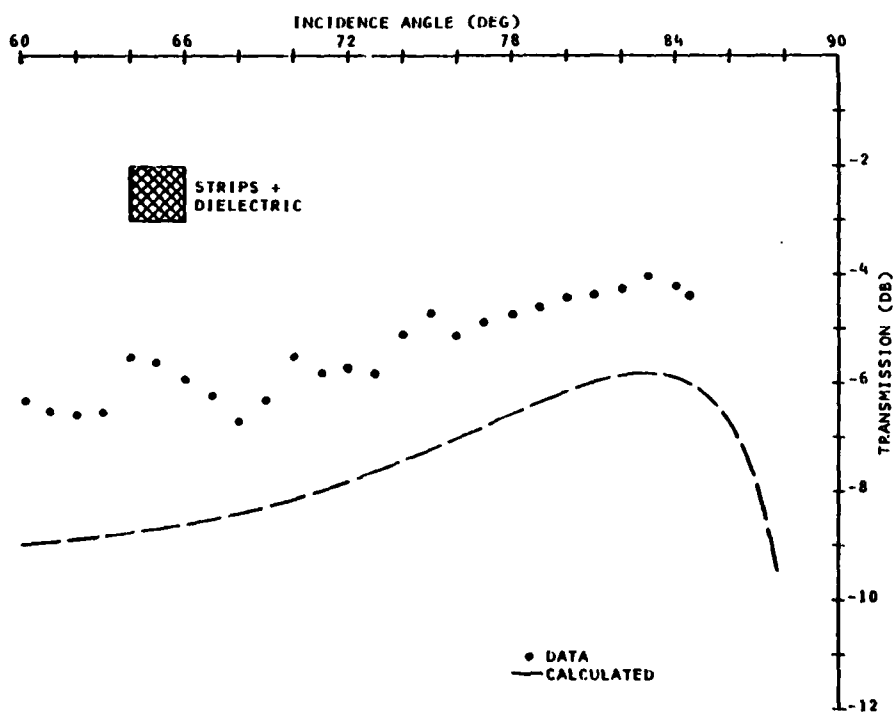
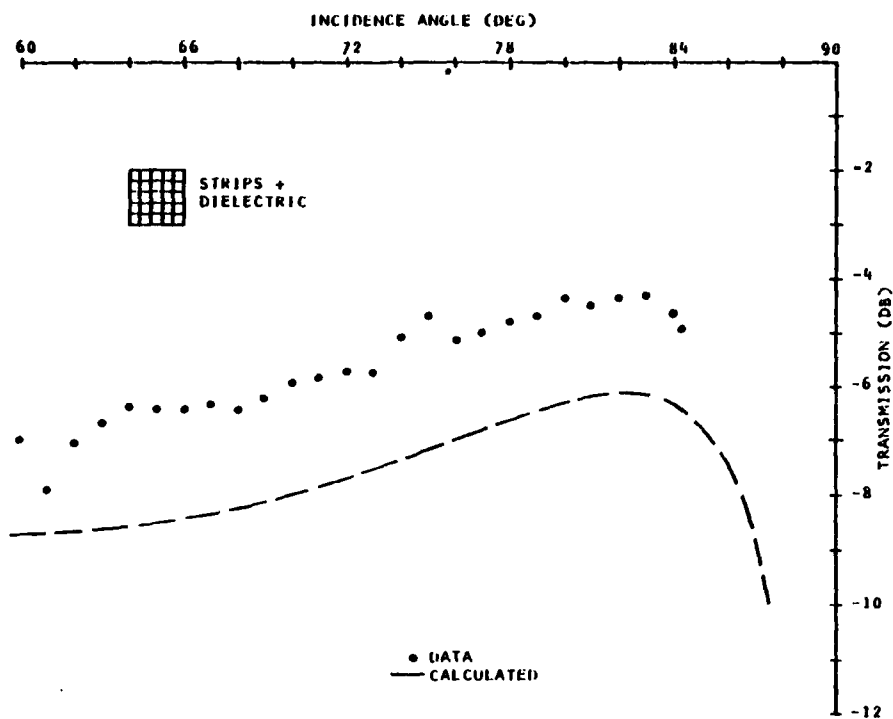


Figure 4-6 Data for Contacting Crossed Strips with Dielectric Near Grazing

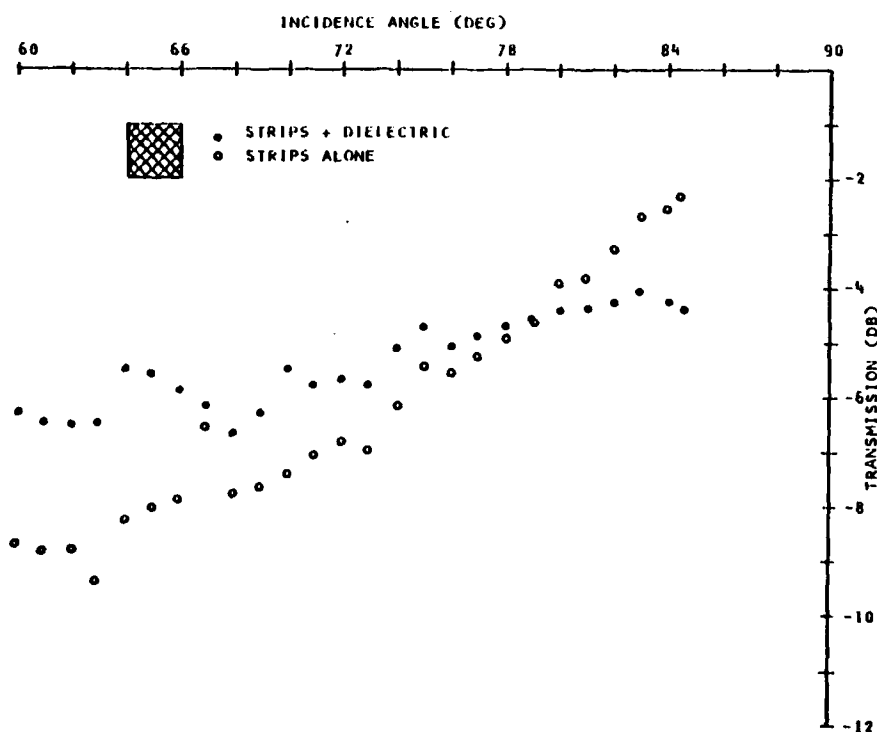
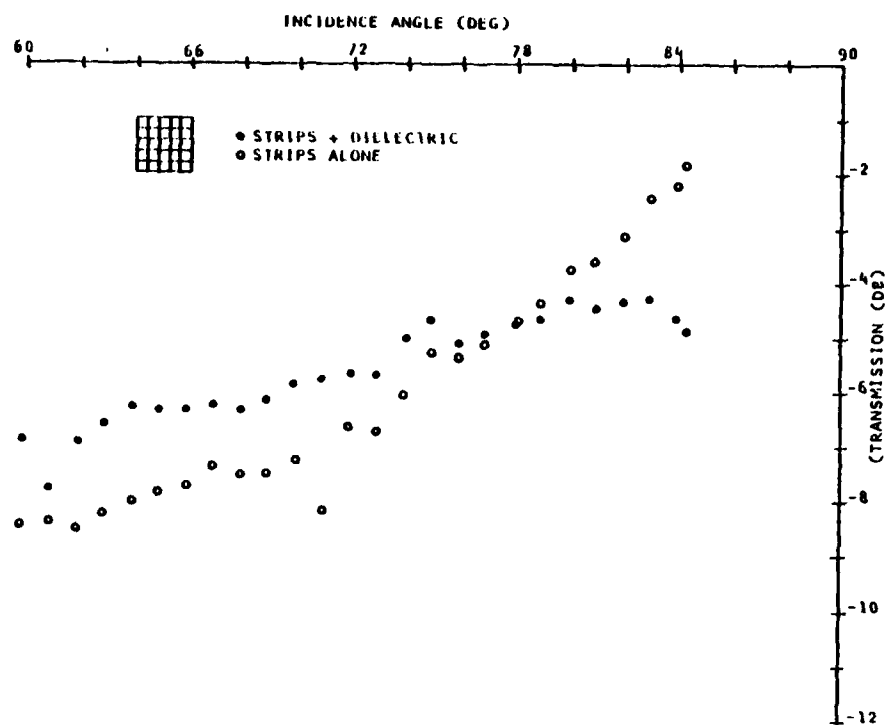


Figure 4-7 Data Comparison for Strips With and Without Dielectric Near Grazing

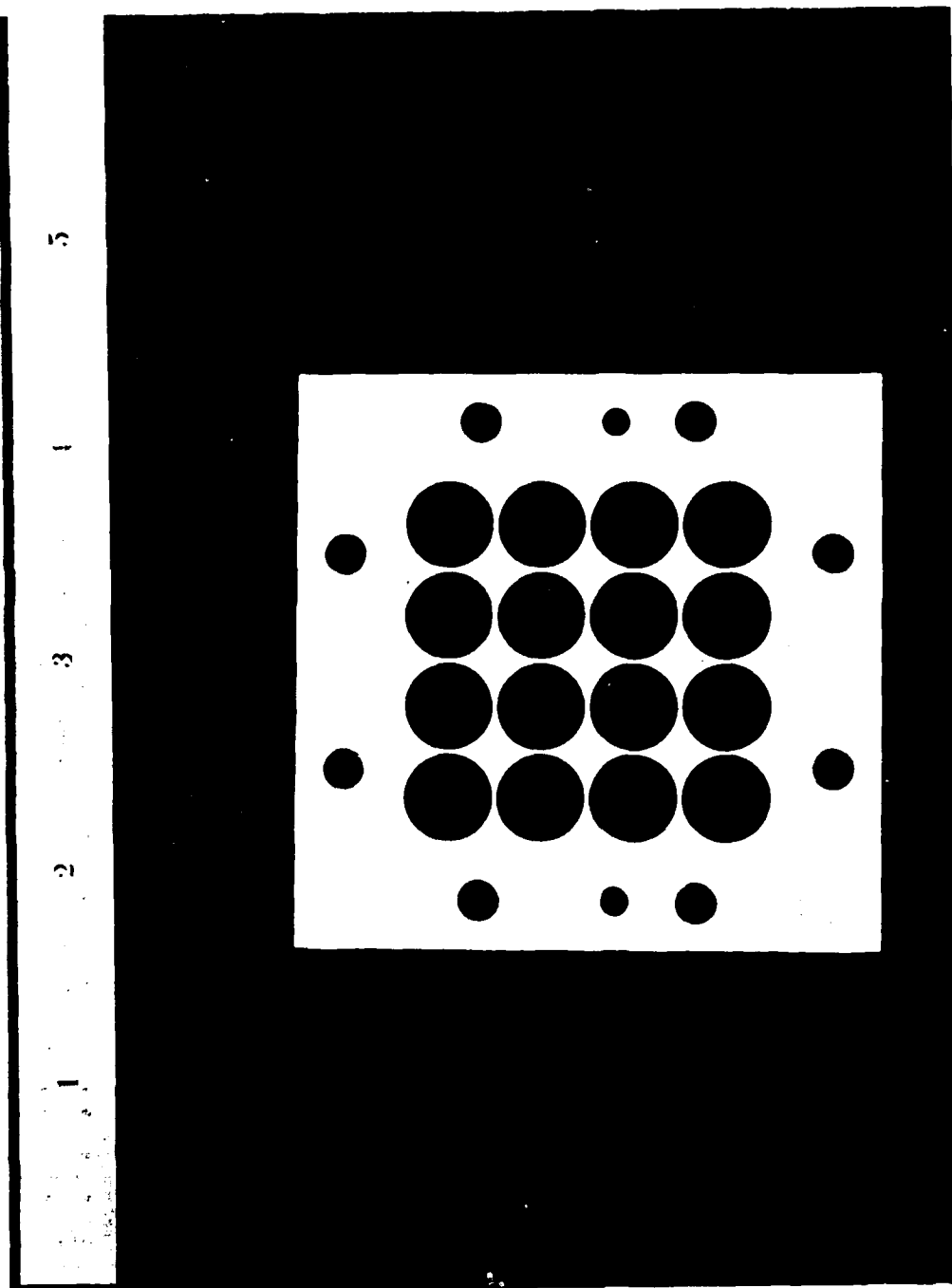


Figure 4-8 Round Hole Sample for Near-Grazing Simulator

0.020 inch web of metal between the holes. Only the perpendicular grid orientation was constructed with these holes.

Figure 4-9 shows the data points measured with the near-grazing simulator. With these almost-touching holes a simple formula for susceptance is not available, so a theoretical curve is not calculated. However, a curve is shown that is set to coincide with the measured point at  $60^\circ$ , and that has the variation with incidence angle resulting from the formula for E-plane incidence in Section 2.5. The trend of the data points is very similar to that of the curve.

Figure 4-10 shows data points measured for these round holes in which dielectric with a  $k$  of about 3.5 fills the holes and forms a sheet  $1/32$  inch thick on one side of the metal sheet. Also shown for comparison are the data points for the sample without dielectric. The same kind of result is seen that was observed when substantial dielectric was added to the strips. Again, the transmission is increased by the dielectric at angles less than about  $80^\circ$ , but there is no evidence of a spurious passband.

#### Insulated Wire Results

Figure 4-11 shows the two samples representing an insulated crossed grid of wires. In these samples the wires are gold-plated steel rod 0.020 inches in diameter. The separation ( $g$ ) between centerlines of the crossed sets of parallel wires is 0.030 inches, giving a minimum air space of 0.010 inches at the crossing points. As mentioned earlier, the oblique orientation case does not provide perfect imaging and the measurements of this case should not be regarded as absolutely reliable.

Figure 4-12 shows the data points measured for these insulated crossed wire grid samples in the near-grazing simulator. Also shown are curves calculated from the grid dimensions using the susceptance formula for E-plane incidence given in Section

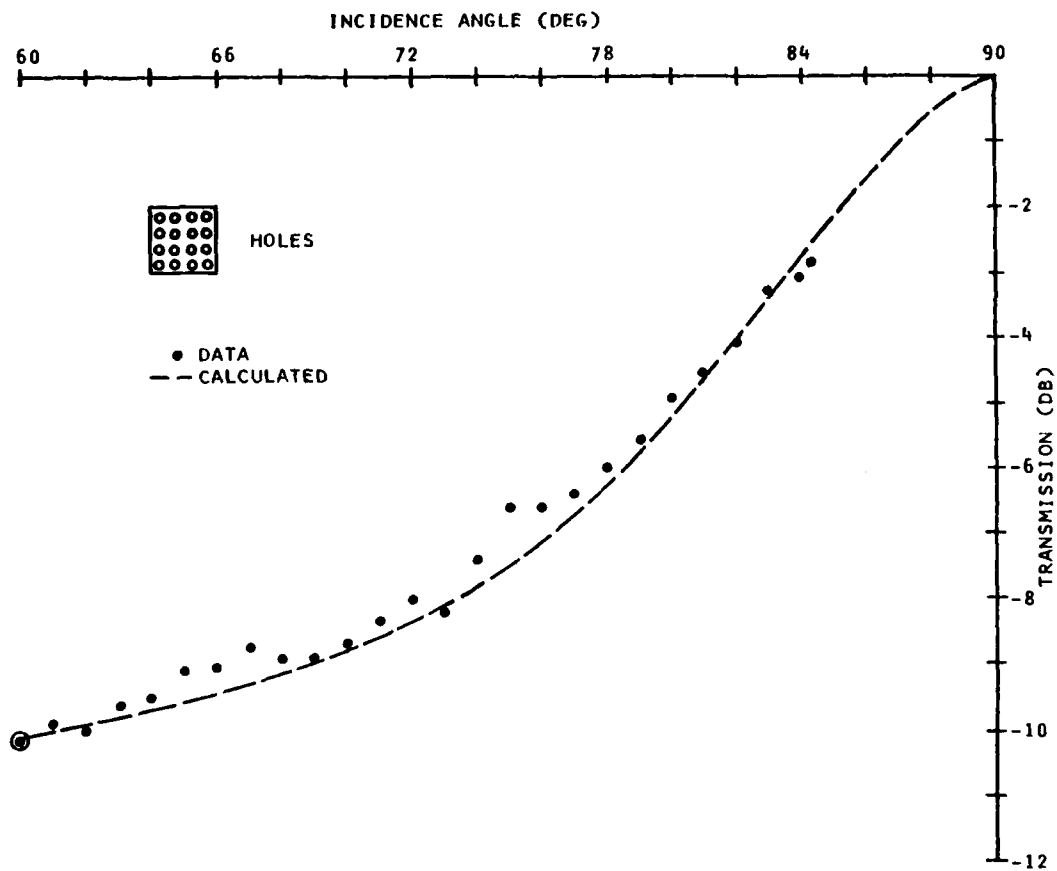


Figure 4-9 Data for Round Holes Near Grazing

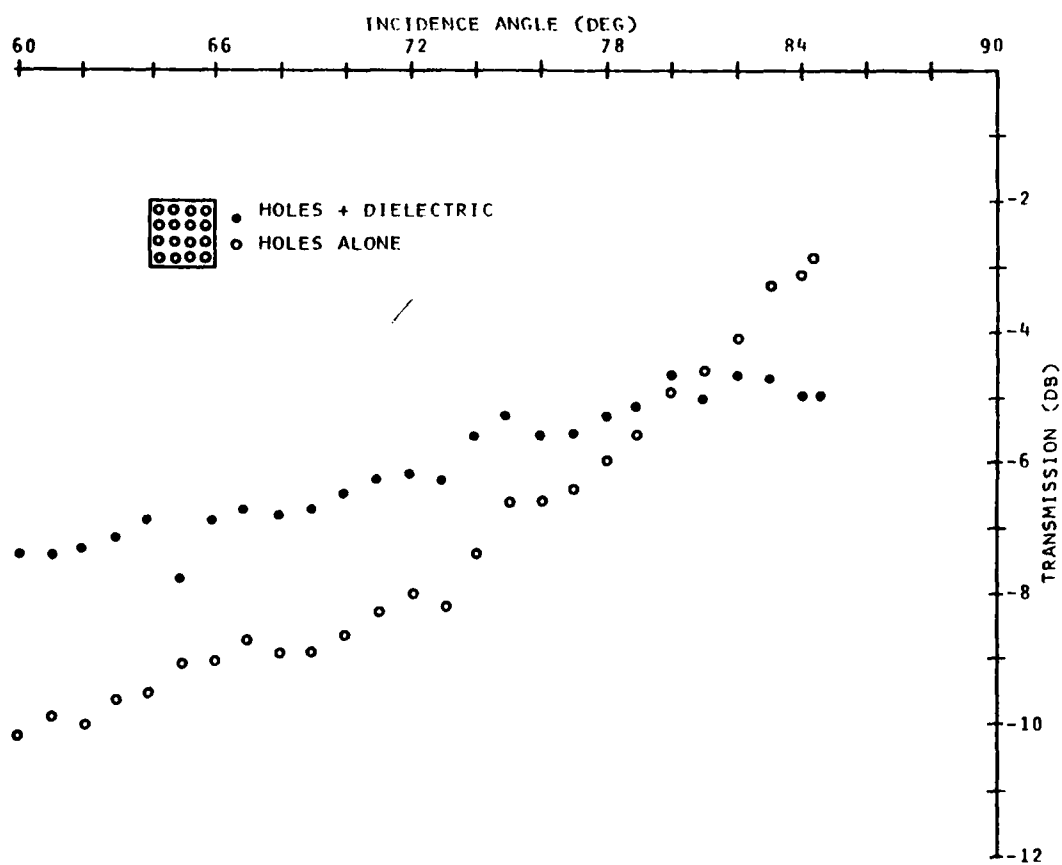


Figure 4-10 Data for Round Holes With and Without Dielectric Near Grazing

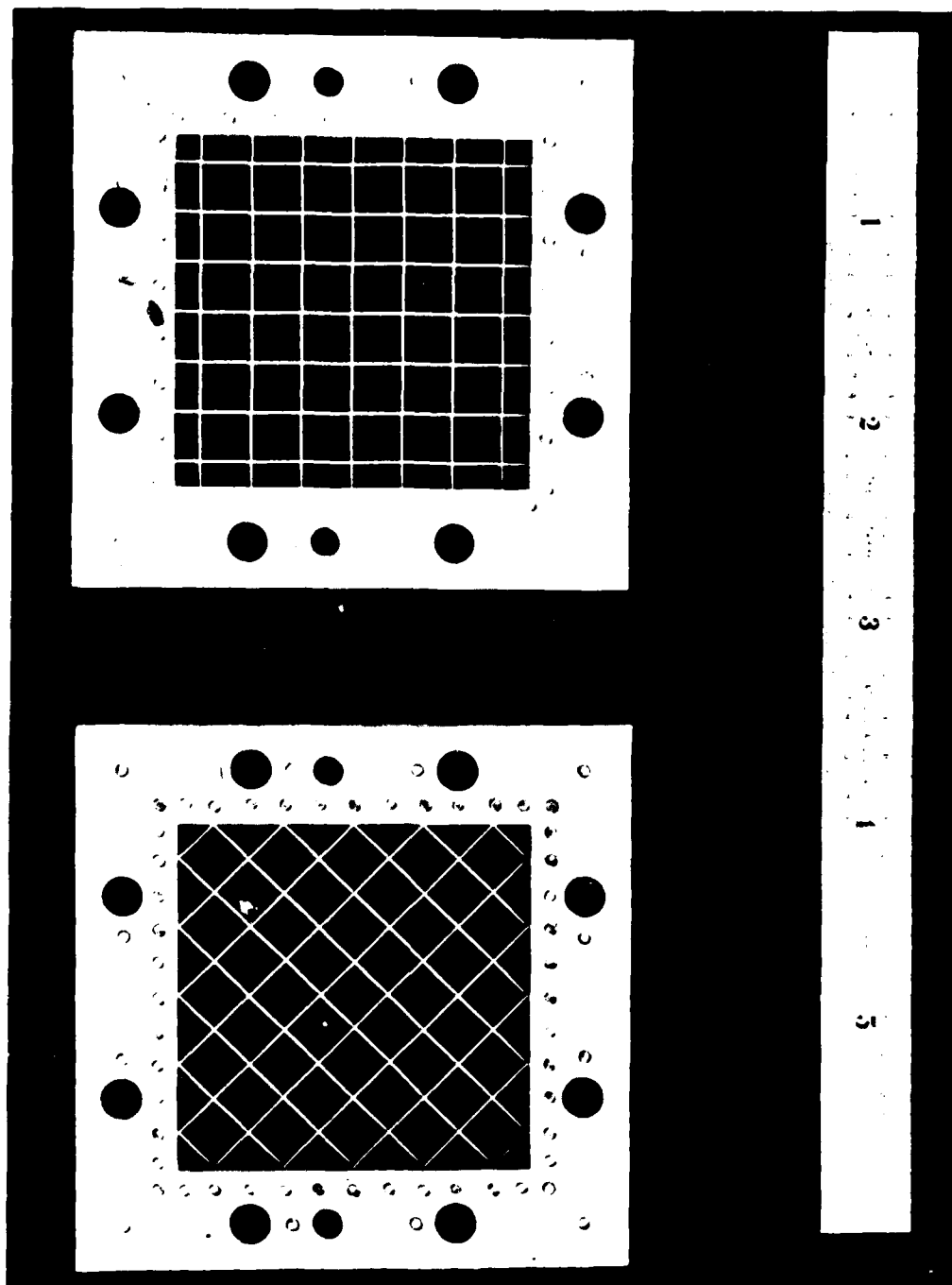


Figure 4-11 Insulated Crossed Wire Samples for Near-Grazing Simulator

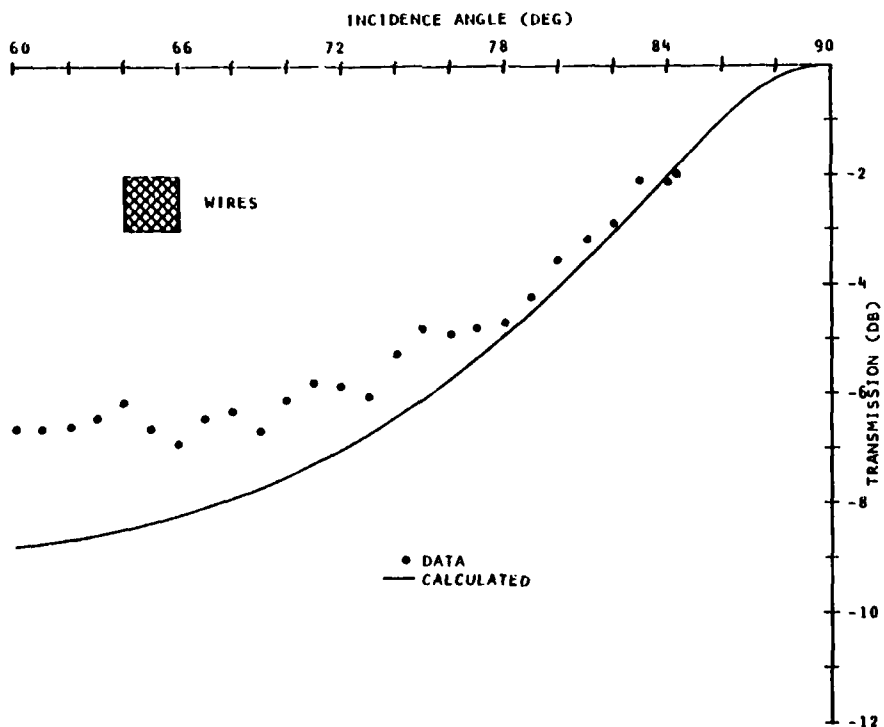
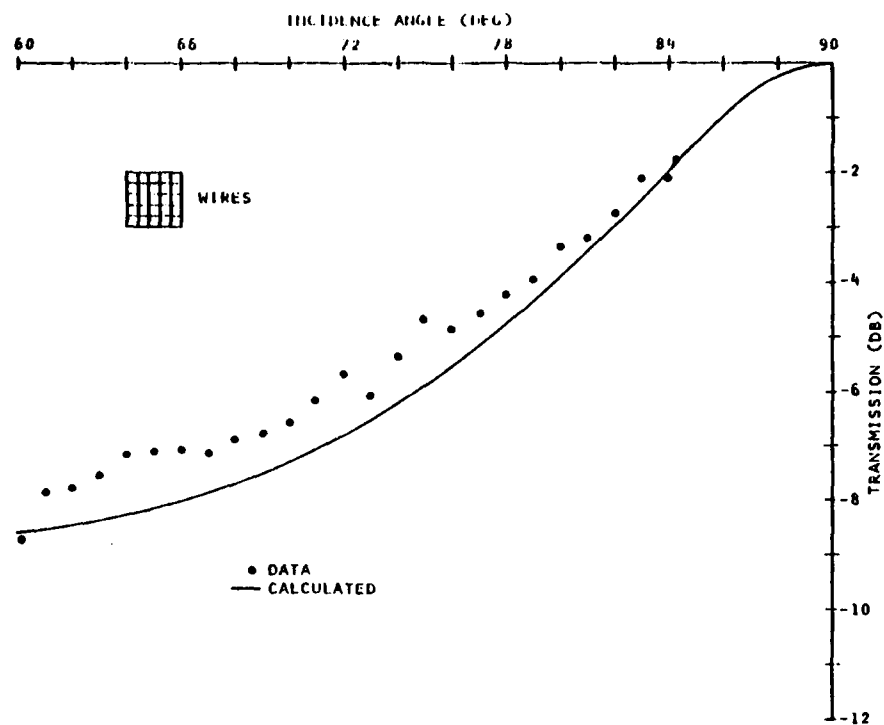


Figure 4-12 Data for Insulated Crossed Wire Samples Near Grazing



2.5. Although the trend of the data is similar to that of the calculated curves, the data gives greater transmission than the calculation, particularly at incidence angles near  $60^\circ$ .

It was considered possible that this deviation was caused by either poor contact between the wires and the simulator waveguide, or by imperfect gold plating of the steel rods. Further experiments were made which indicated that neither of these possibilities were likely to be the cause of the deviations. It is also noted that the deviation for the oblique orientation is greater; this may be a result of the imperfect imaging. However, a deviation also exists for the perpendicular orientation, where the imaging is perfect. On the basis of the measurements made, it appears that the transmission with insulated crossed wires is indeed greater than that calculated from the available formulas for E-plane incidence.

Figure 4-13 shows the data for these insulated wire samples encased in a sheet of dielectric about 1/10 inch thick and having a  $k$  of about 3.5. (The dielectric used for these samples as well as all the other samples is a potting resin, which is poured into the grid sample and then solidifies. This yields a dielectric which completely fills the available space, and best represents the fiberglass skin that would most likely be used to support the wires or other grids.) Also shown are curves calculated on the assumption that this dielectric has no reactive-field interaction effect on the grid susceptance. As with the previous grid samples, there is a clear displacement between the measurements and the calculation, indicating that the assumption of no interaction is not an accurate one in the E-plane of incidence.

Figure 4-14 compares the measured data for the wire samples encased in dielectric with the data for the wire samples alone. The effect of the dielectric is similar to

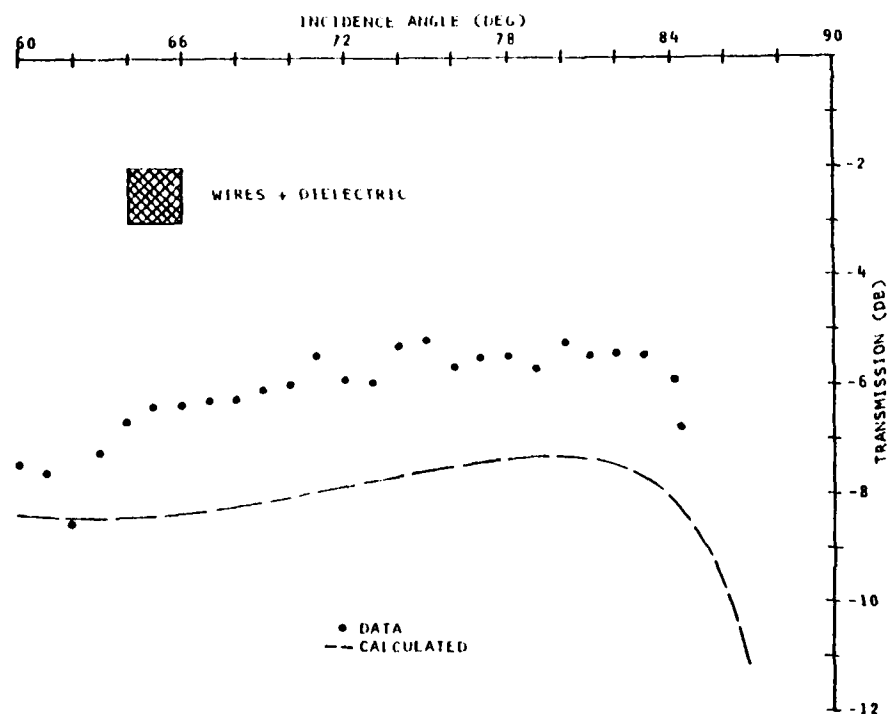
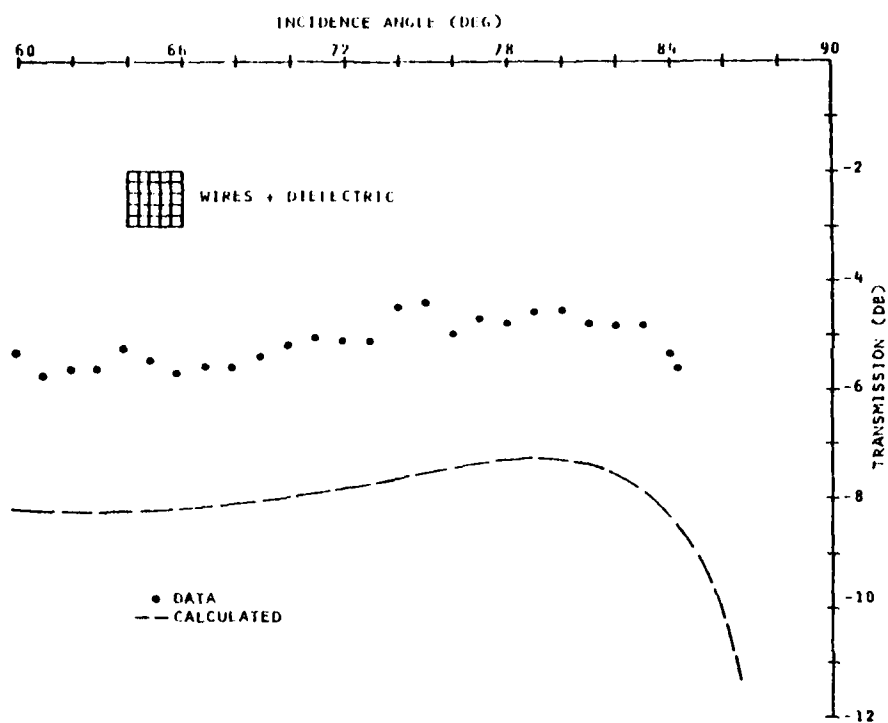


Figure 4-13 Data for Insulated Crossed Wires with Dielectric Near Grazing

AD-A089 792

HAZELTINE CORP GREENLAWN NY

F/6 9/1

METAL-GRID SPATIAL FILTER. VOLUME I.(U)

JUL 80 P W HANNAN, P L BURGHYER

F19628-78-C-0152

UNCLASSIFIED

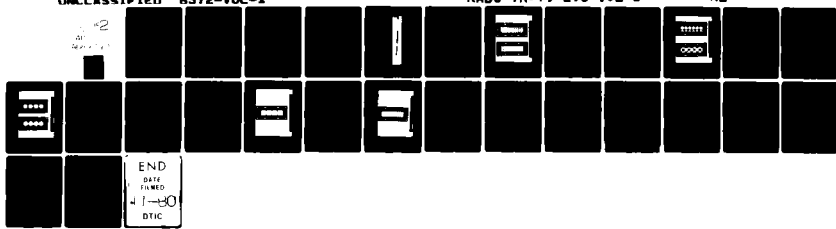
6372-VOL-1

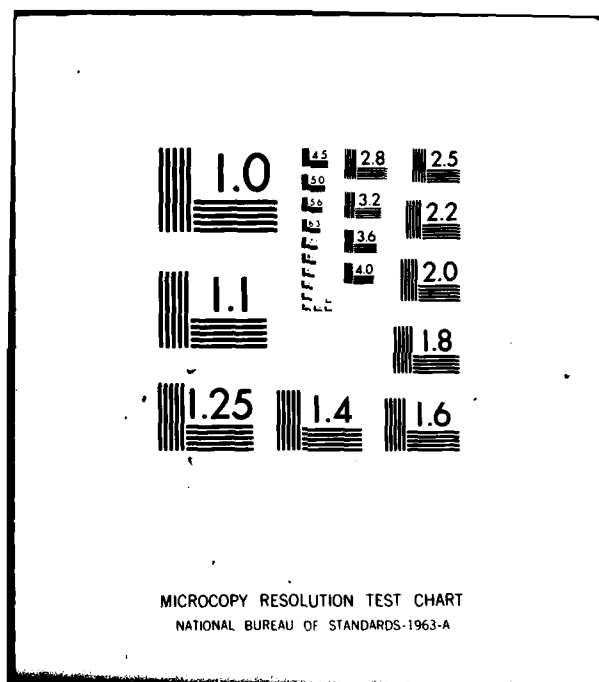
RADC-TR-79-295-VOL-1

NL

#2

AD-A089 792





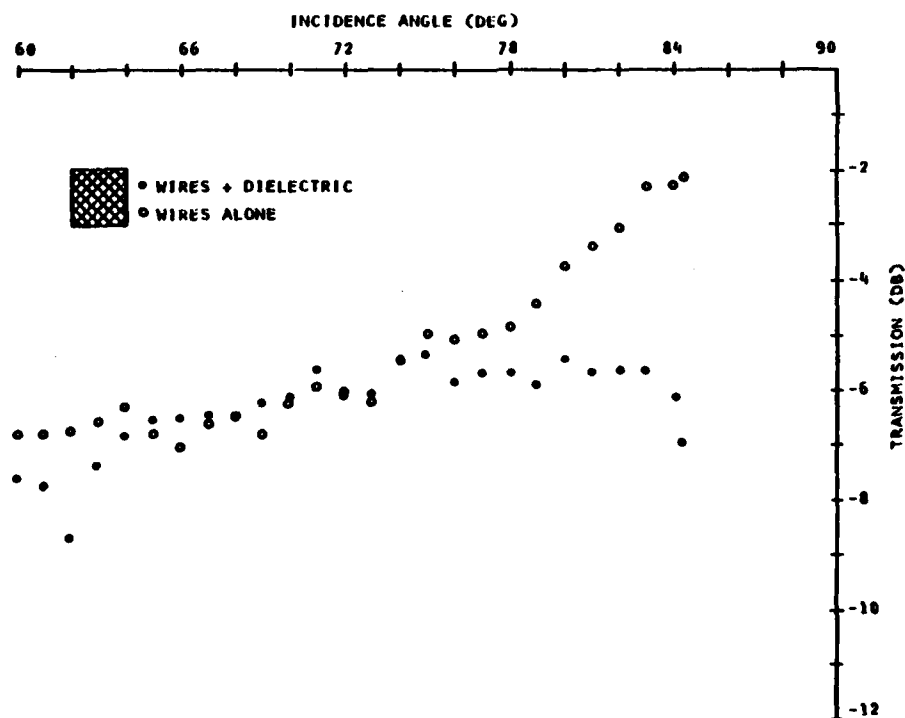
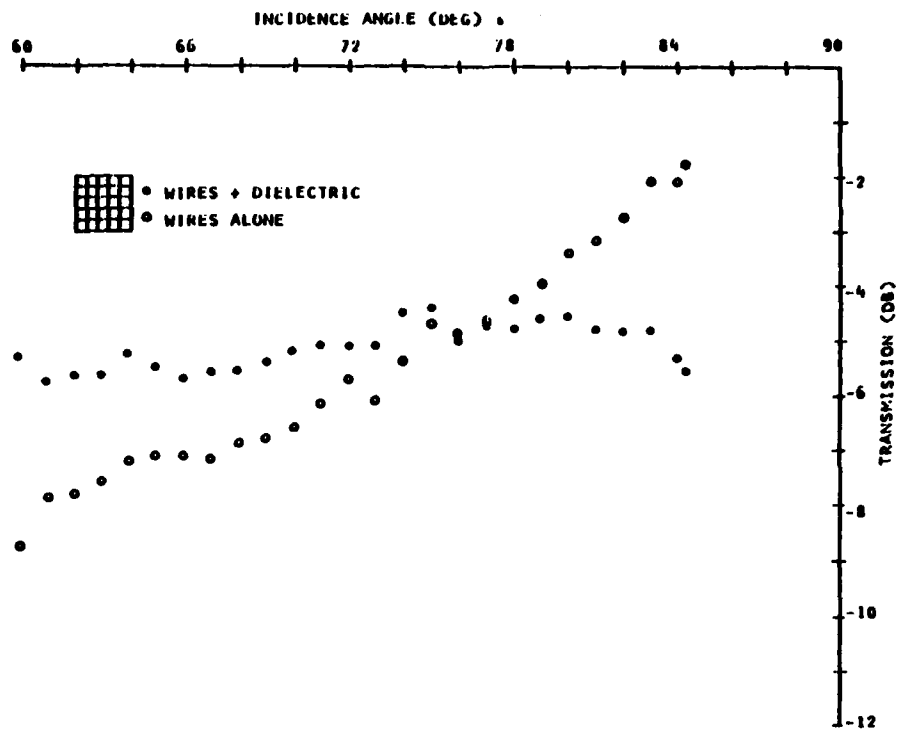


Figure 4-14 Data Comparison for Wires With and Without Dielectric Near Grazing

that seen earlier for the other samples. The "crossover" angle in this case is between  $65^\circ$  and  $75^\circ$  as compared with the previous cases where it is about  $80^\circ$ . This may be a result of the relatively thick dielectric used in this case, or it may be an effect that occurs with an insulated crossed grid. Again, there is no evidence of a spurious passband.

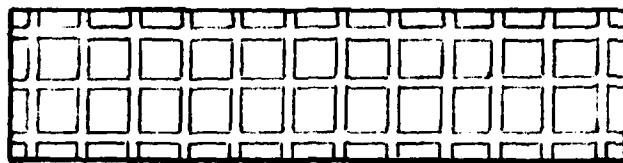
#### 4.3 NEAR BROADSIDE SIMULATOR TESTS

The near-broadside simulator uses the dominant TE-11 mode in a wide rectangular waveguide. The width of the waveguide is 3.5 inches, instead of the normal 1.8 inches at C-band, in order to obtain an angle of incidence that is fairly near broadside. At 5.0 GHz the incidence angle is about  $20^\circ$ . Since the simulator operates with a TE mode it yields incidence in the H-plane.

The rectangular cross section of the near-broadside simulator is shown in Figure 4-15 for the two grid sample orientations that are used. With a contacting crossed grid, both sample orientations are perfectly imaged by the waveguide. With an insulated crossed grid having one set of parallel conductors separated from the other, the oblique orientation yields zigzag lines rather than straight lines. In this simulator the perpendicular orientation corresponds to  $\theta = 0^\circ, 90^\circ$ , while the oblique orientation corresponds to  $\theta = \pm 45^\circ$ .

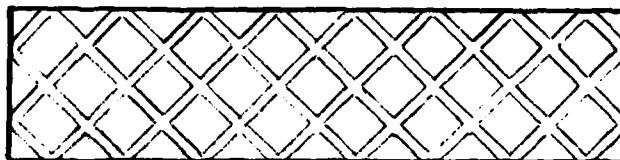
The wide simulator waveguide is connected to the generator and the detector by tapers each about 20 inches long. No mode transition is used, and tuners are not needed. The arrangement of this simulator system is indicated in Figure 4-16 and is seen in the photograph of Figure 4-17.

Since the purpose of the near-broadside simulator is to measure the grid at a single angle of incidence near broadside, only one measurement frequency is theoretically needed. However, in order to benefit from the averaging of errors and to obtain some data on the grid behavior vs. frequency, seven frequencies are typically used in the measurement.



PERPENDICULAR ORIENTATION

$$\phi = 0^{\circ}, 90^{\circ}$$



OBLIQUE ORIENTATION

$$\phi = \pm 45^{\circ}$$

Figure 4-15 Sample Orientations for Near-Broadside Simulator

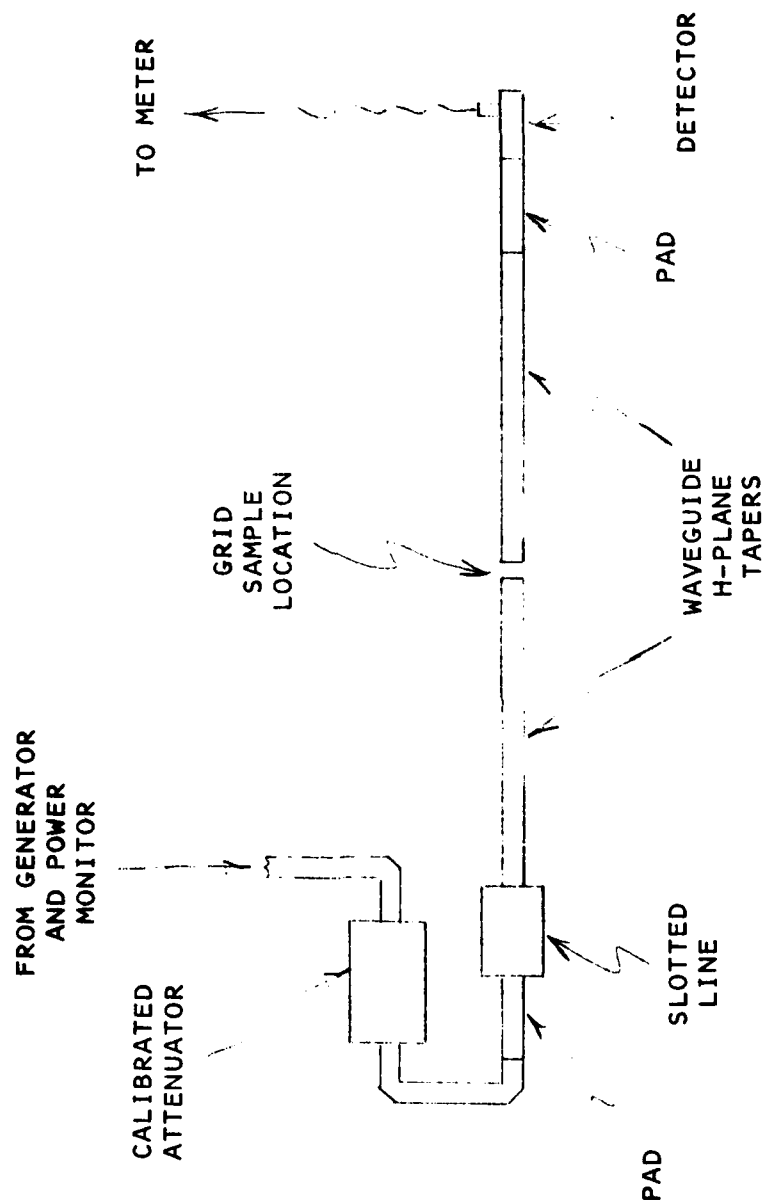


Figure 4-16 Diagram of Near-Broadside Simulator



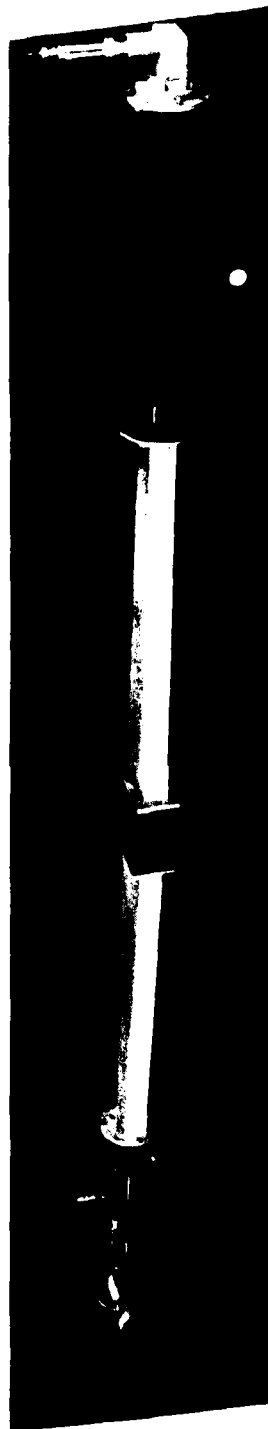


Figure 4-17 Near-Broadside Simulator

#### Contacting Strip Results

Figure 4-18 shows the two samples representing a contacting crossed grid of thin metal strips. As before, the samples were 0.040 inch wide copper strips printed on a thin (0.005 inch) substrate of teflon.

Figure 4-19 shows the data points measured with the near-broadside simulator. Also shown are curves calculated from the strip grid dimensions using the formulas for H-plane incidence given in Section 2.5. It is seen that the average of the measured data gives about 0.4 dB less transmission than the calculated curves. This corresponds to an error in susceptance of about 5%.

Part of this error is probably caused by measurement errors. However, part is believed to be caused by the magnetic-field blocking effect of the crossed grid of strips, which is not included in the simple formula. A measurement was made of a parallel (not crossed) strip grid in the perpendicular orientation; such a grid does not have the magnetic-field blocking effect of the crossed grid. The results indicated that about half of the 0.4 dB deviation could be ascribed to this effect.

Figure 4-20 shows the data points measured for these strip samples encased in a sheet of dielectric about 1/16 inch thick having a  $k$  of about 3.5. Also shown are calculated curves based on the approximate formula for capacitive susceptance of a thin dielectric sheet. The measured data agrees reasonably well with the simple calculation, as expected.

#### Round and Square Hole Results

Figure 4-21 shows two samples representing a contacting crossed grid of round holes in a metal sheet. Figure 4-22 shows the data points measured for these holes. Since the holes were fairly close to touching (1/16 inch web), a simple formula for their susceptance is not available; therefore, no

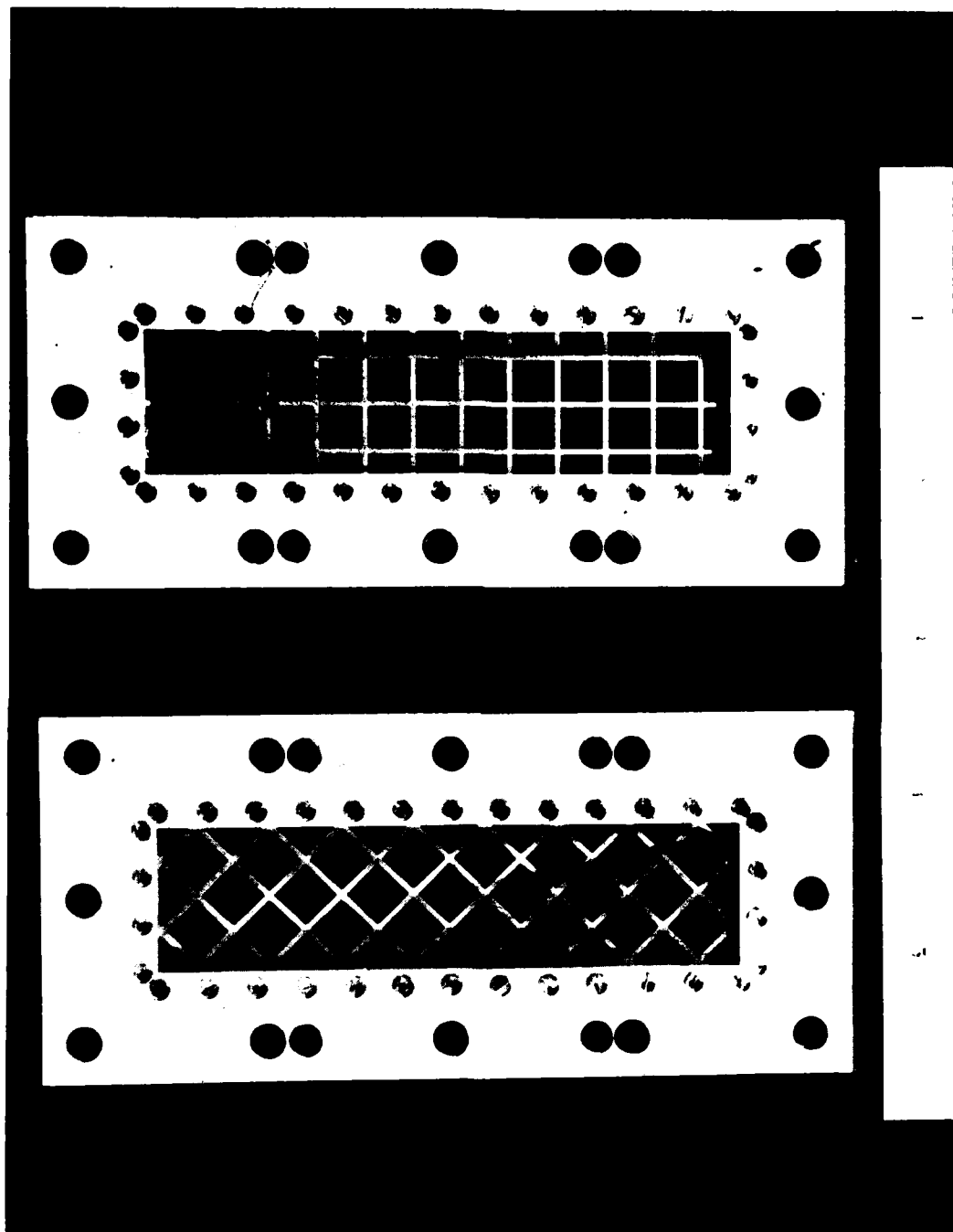


Figure 4-18    Contacting Crossed Strip Samples for  
Near-Broadside Simulator

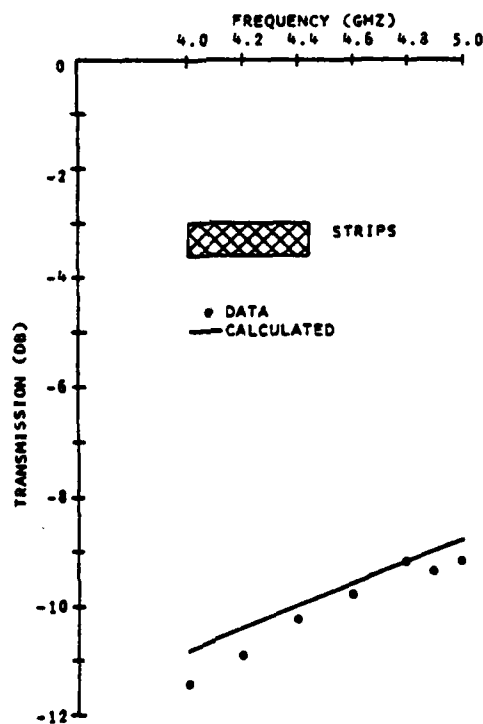
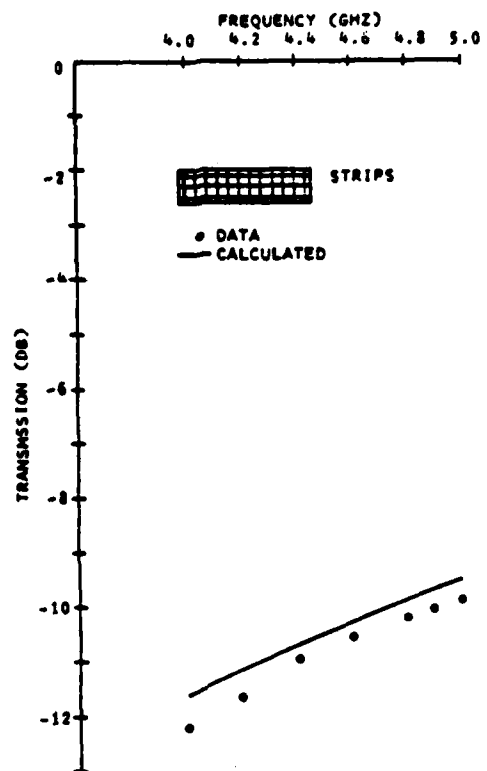


Figure 4-19 Data for Contacting Crossed Strip Samples Near Broadside

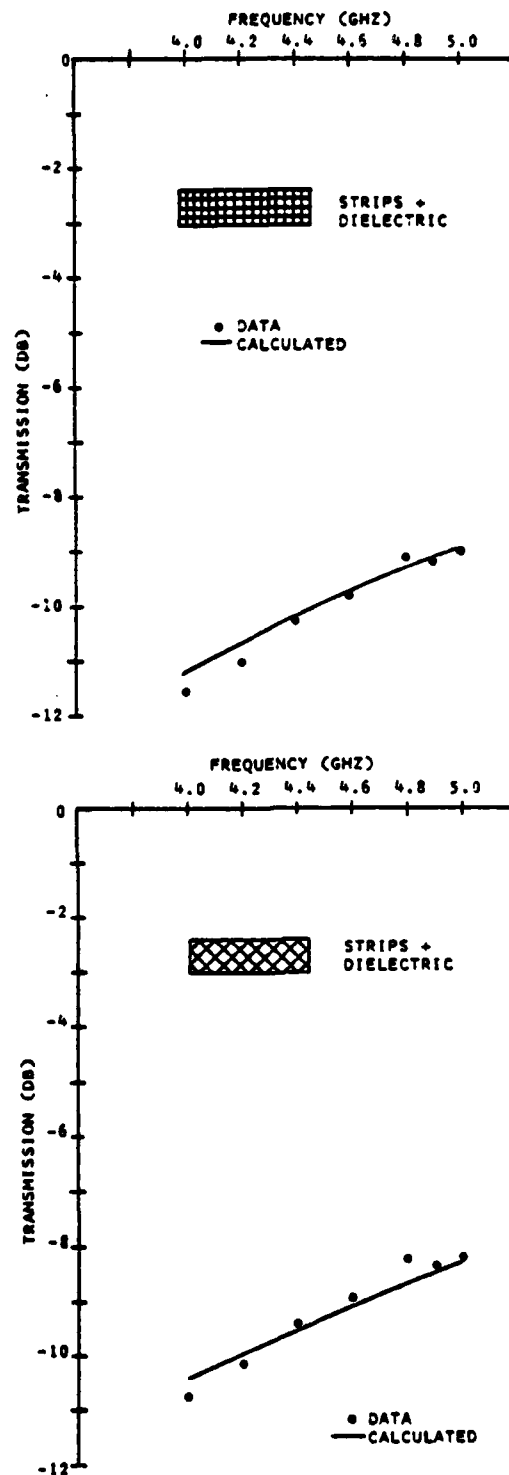


Figure 4-20 Data for Contacting Crossed Strips with Dielectric Near Broadside

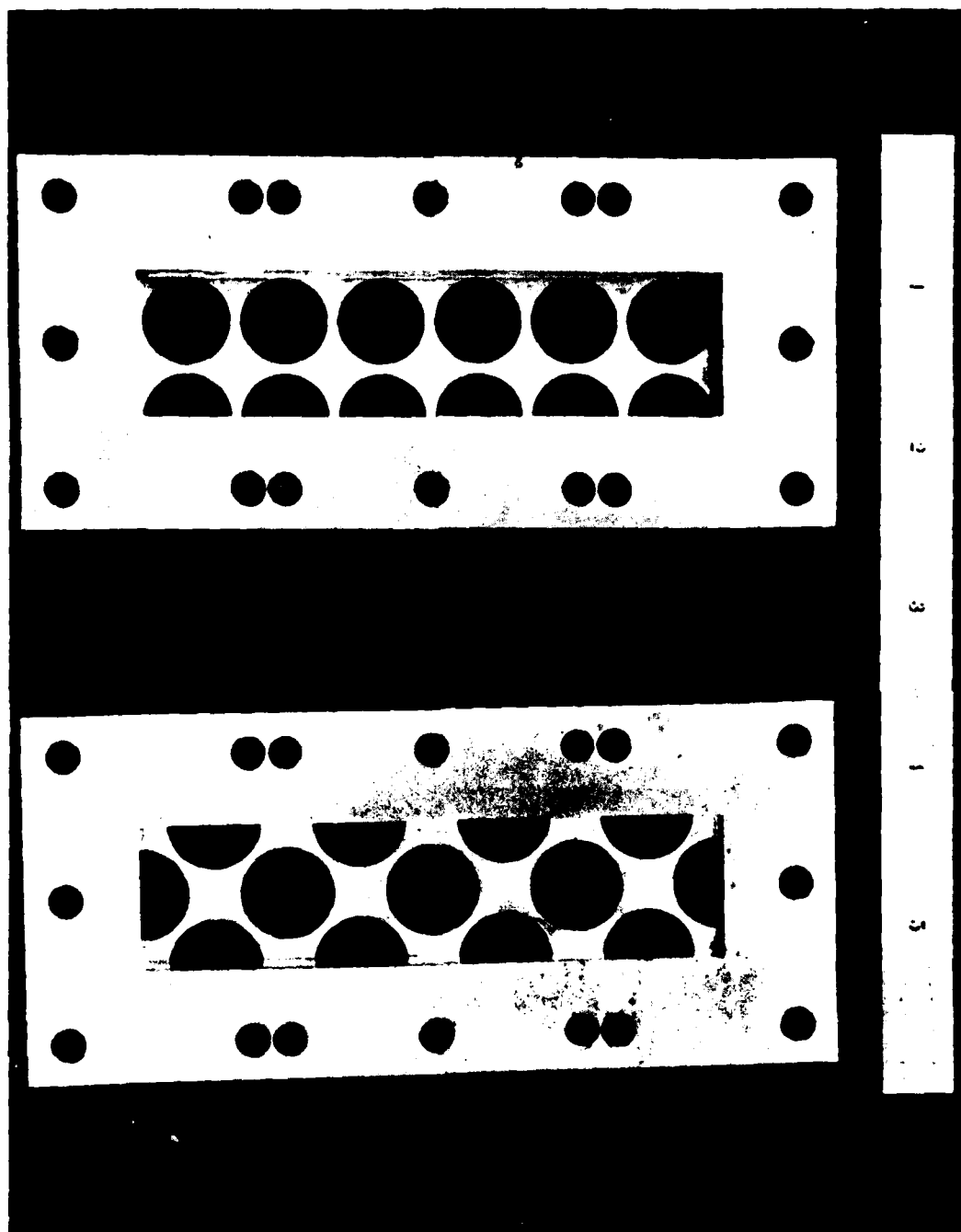


Figure 4-21 Round Hole Samples for Near-Broadside Simulator

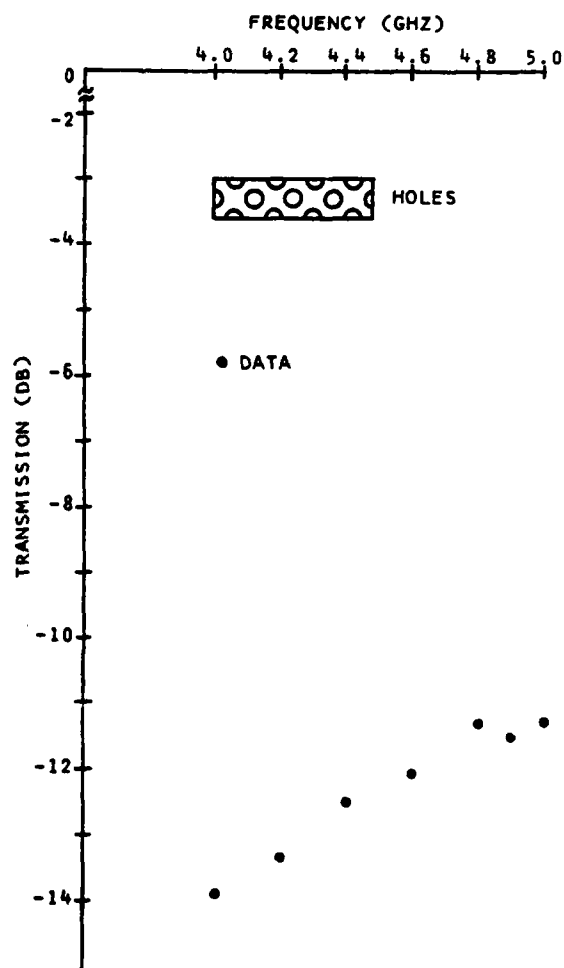
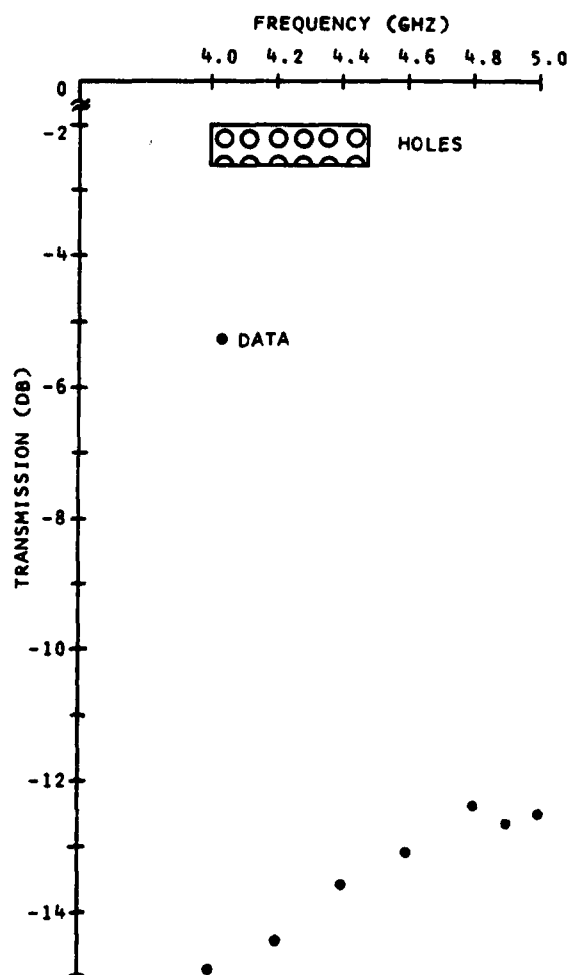


Figure 4-22 Data for Round Holes Near Broadside

computed curve is given. No measurements were made with dielectric added to these holes. Holes such as these have a rather large susceptance, and are likely to be suitable only for the central high-susceptance layers of a spatial filter.

Figure 4-23 shows two samples of larger holes intended to give lower values of susceptance. The spacing of these holes is  $0.37 \lambda$  at 5.0 GHz. The top sample has a web between holes of 0.062 inches and the bottom sample has a 0.020 inch web; both samples have a 0.040 inch thickness for the metal sheet.

Figure 4-24 shows the measured data for these two samples. From this and other data it is estimated that the susceptances at 5.0 GHz are about 2.8 and 2.1 at broadside for these two samples. These values would be sufficiently low for the edge susceptances of some of the "stronger" 3-pole filters, but not for some of the less "strong" ones.

Figure 4-25 shows two sets of measured data in which dielectric having a  $k$  of about 3.5 is added to the hole sample having a 0.020 inch web. The first set of data has the dielectric only filling the holes; the second set has the dielectric also in a 1/16 inch sheet on one side. From this and other data it is estimated that the susceptance at 5.0 GHz has been reduced by the dielectric to about 1.5 and 1.1, respectively. This would be sufficiently low for most of the less "strong" filters. However, it is expected that the 0.020 inch web would be difficult to construct reliably in a large spatial filter panel. At X-band this web scales to about 0.010 inch, which becomes even more difficult.

The web thickness could be increased without increasing the susceptance by a further addition of dielectric, but this would increase the weight, the sensitivity to dielectric material tolerances, and the frequency sensitivity of the filter susceptances. A still greater spacing between the holes could also be considered, but an increase to only  $0.5 \lambda$  would



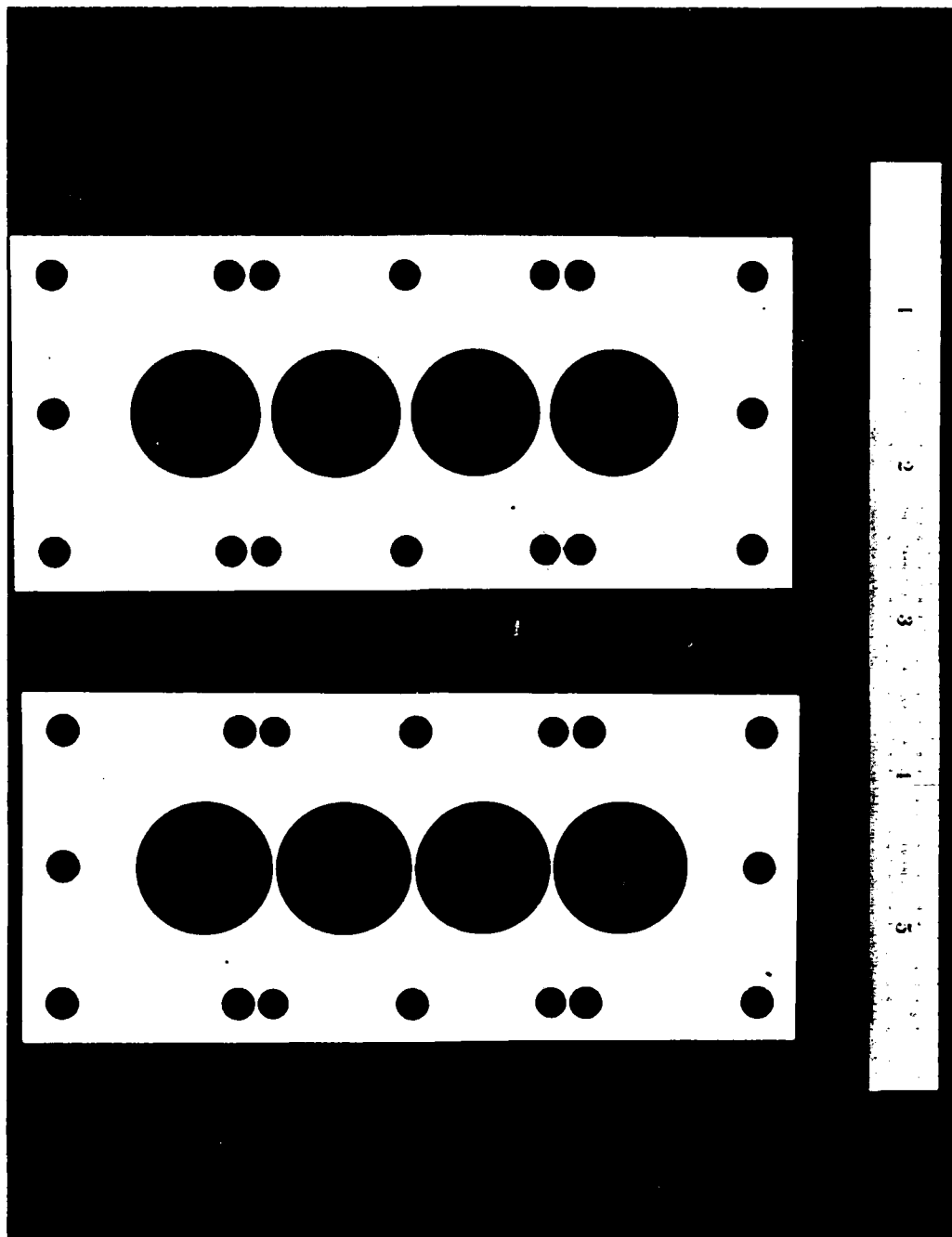


Figure 4-23 Large Round Hole Samples for Near-Broadside Simulator

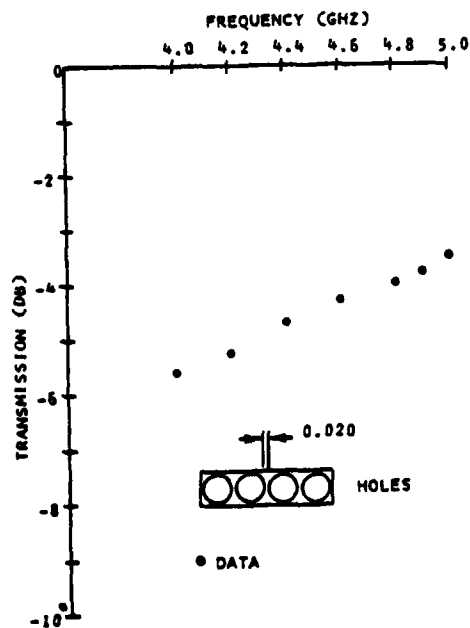
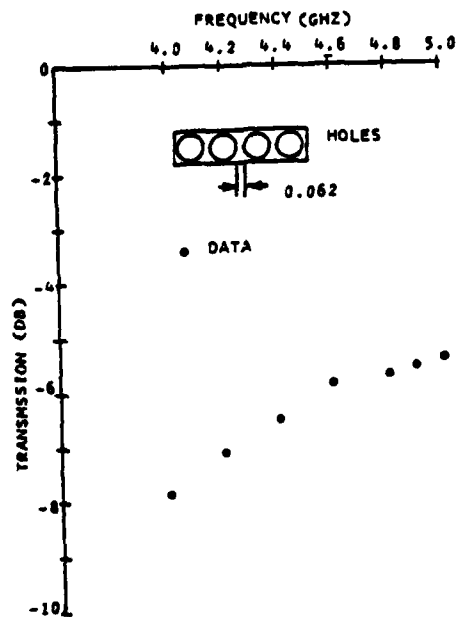


Figure 4-24 Data for Large Round Holes Near Broadside

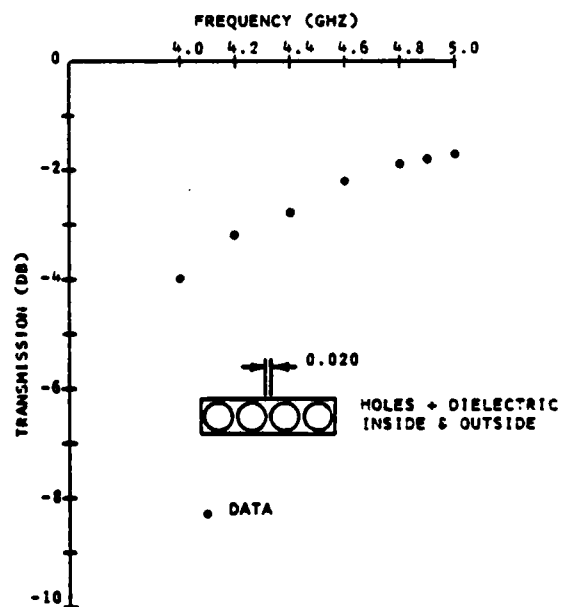
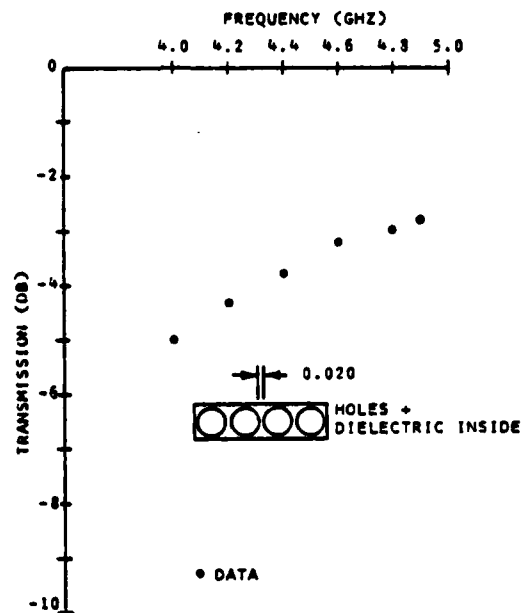


Figure 4-25 Data for Large Round Holes with Dielectric Near Broadside

mark the onset of grating-lobe problems. Another alternative is to employ a square hole instead of a round hole. A square, or nearly-square, hole is feasible to construct by certain methods, and will have substantially lower susceptance for the same web thickness.

Figure 4-26 shows a sample of nearly-square holes in a 0.062 inch thick metal sheet. The web thickness is 0.080 inches, and the web is straight except for a 0.062 inch radius at the corners of the hole. The spacing of these holes is  $0.37 \lambda$  at 5.0 GHz, the same as the previous three sets of holes.

Figure 4-27 shows the measured data for these nearly-square holes. Comparison of these measurements with those at the bottom of Figure 4-24 shows that this sample has about the same performance as the round hole sample that has only 0.020 inch web thickness and 0.040 inch sheet thickness. From this and other measured data it is estimated that the susceptance of the nearly-square hole sample at 5.0 GHz is between 2.1 and 2.2 at broadside.

Also shown in Figure 4-27 is a computed curve. This curve is obtained by neglecting the rounded corners in the nearly-square holes. The grid then becomes a contacting crossed grid of wires having a rectangular cross-section of 0.080 x 0.062 inches. This can be computed in terms of an equivalent diameter of a round cross-section wire (Ref. 11), and the standard susceptance formula can then be used. When this is done, including a small correction factor F for the large spacing (Ref. 6), the susceptance at 5.0 GHz computes to be 2.1 at broadside. The measured data and the computed results, while not in perfect agreement, are reasonably close.

#### Insulated Wire Results

Figure 4-28 shows a sample representing an insulated crossed grid of wires. Only the perpendicular orientation is shown because it has perfect imaging in the simulator walls.

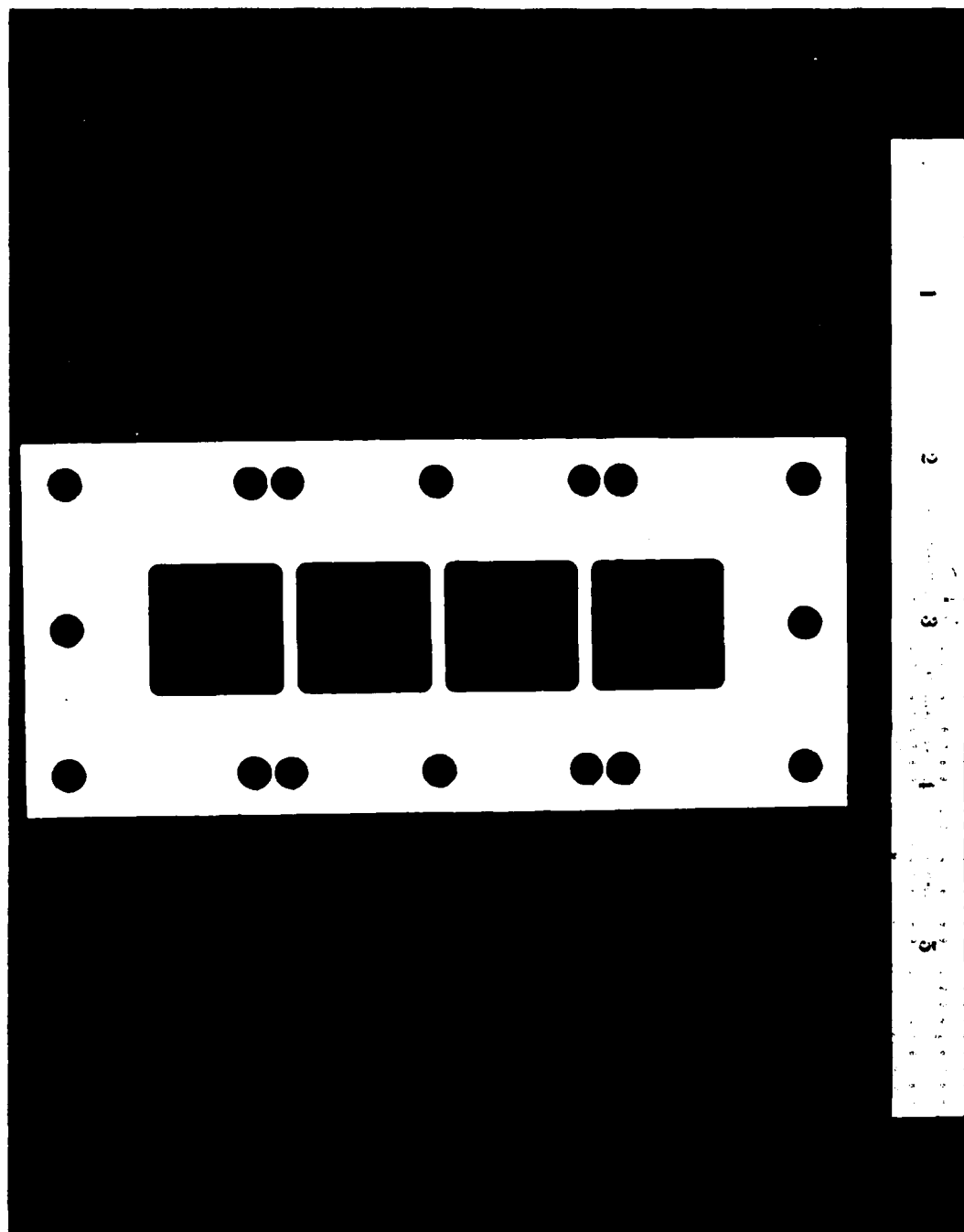


Figure 4-26 Nearly-Square Hole Sample for Near-Broadside Simulator

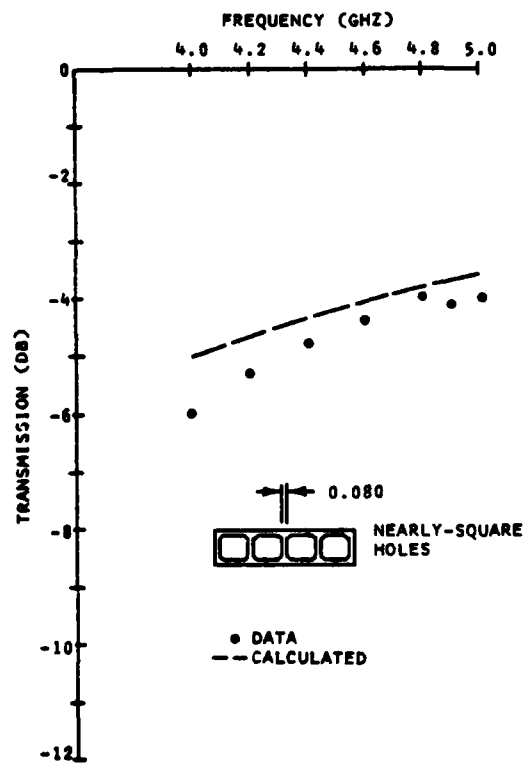


Figure 4-27 Data for Nearly Square Holes Near Broadside

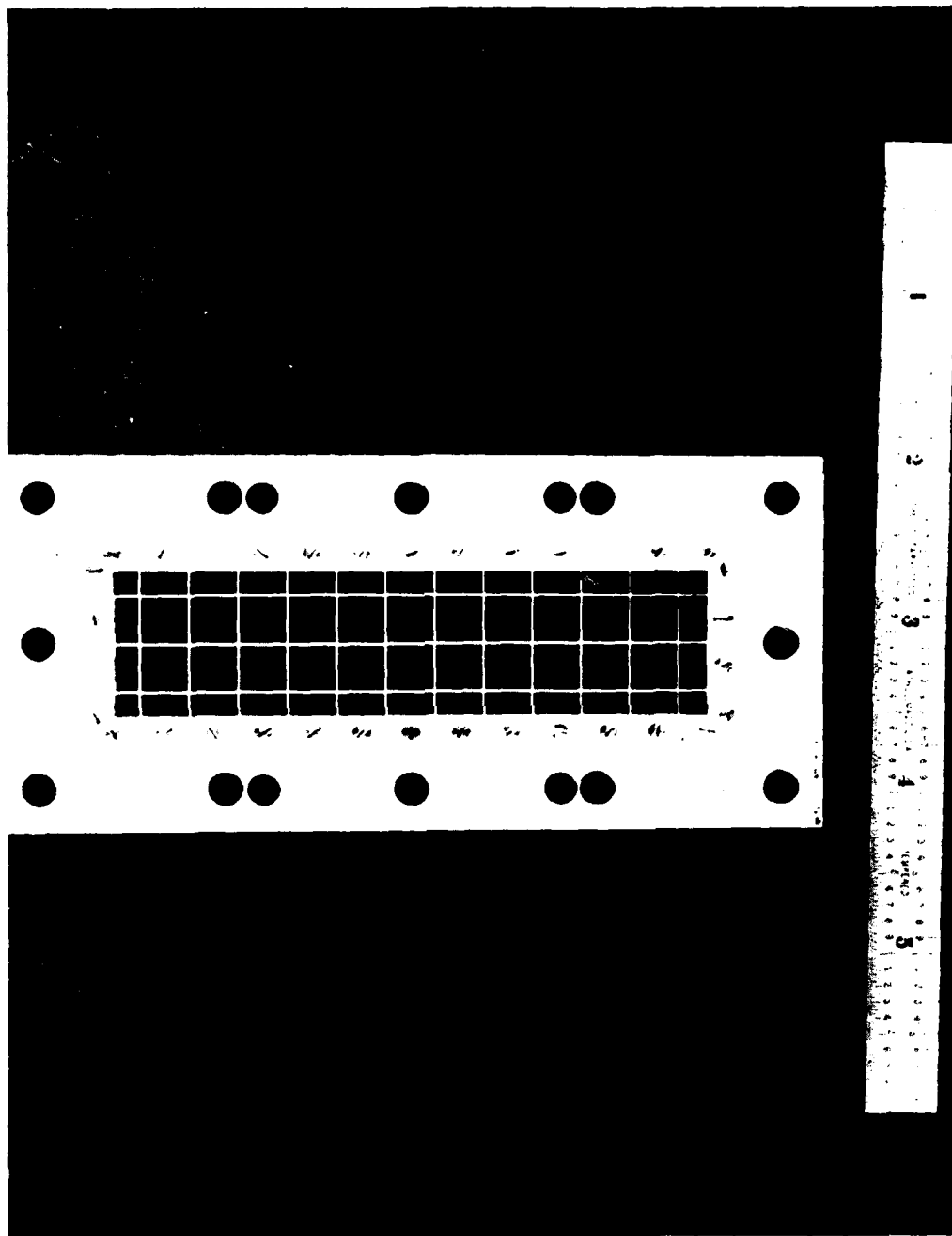


Figure 4-28 Insulated Crossed Wire Sample for Near-Broadside Simulator

As before, the wires are gold-plated steel rods 0.020 inches in diameter. The separation between centerlines of the crossed sets of parallel wires is either 0.030 or 0.090 inches; in the former case there is a minimum air space of 0.010 inches at the crossing points.

Figure 4-29 shows the data points measured for the insulated crossed-wire sample. The results for the two different separations are close, as expected. Also shown is a curve calculated from the grid dimensions using the formula for H-plane incidence given in Section 2.5. The agreement between the measured data and the calculated curve is rather good, and is better than that for the contacting strips. It is interesting that the magnetic-field blocking effect is smaller for the wire case than it is for the strip case, which may in part account for the closer agreement obtained with the wires.

Figure 4-30 shows the data points measured for the wire sample encased in a sheet of dielectric about  $3/32$  inch thick, having a  $k$  of about 3.5. Also shown is a calculated curve based on the approximate formula for capacitive susceptance of a thin dielectric sheet. The measured data agrees reasonably well with the simple calculation, as expected.



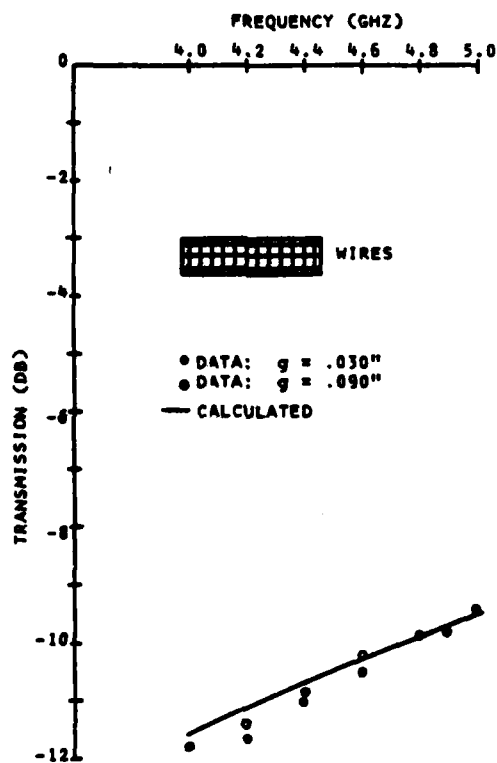


Figure 4-29 Data for Insulated Crossed Wire Sample Near Broadside

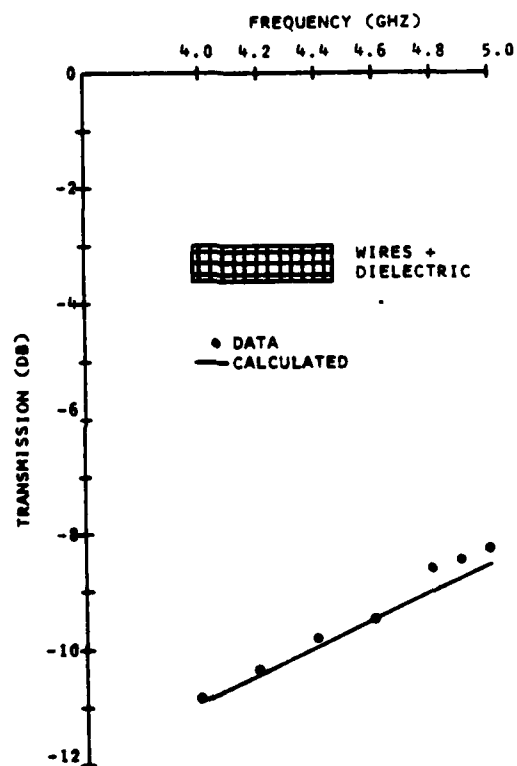


Figure 4-30 Data for Insulated Crossed Wires with Dielectric Near Broadside

## SECTION 5

### CONCLUSIONS

This interim report has described the results obtained in two general areas of investigation. One area is an analysis of the basic design of spatial filters that use metal grids. The other area is an investigation of the properties of metal grids for use in a spatial filter.

From the analysis of basic metal-grid spatial filters, the following results have been obtained:

(1) Two general types of angular passbands are available: a broadside (disk) passband, and an off-broadside (ring) passband. The broadside passband is expected to have more general application.

(2) The frequency bandwidth of a metal-grid spatial filter is directly related to its angular passband size. For a broadside filter, the maximum frequency bandwidth relative to the mid frequency is approximately equal to the passband solid angle at the mid frequency divided by  $\pi$ .

(3) A significant measure of spatial filter performance is the rejection at a specified angle in the stopband. A certain value of this rejection can be obtained with many different combinations of passband width, passband ripple, and number of poles. The rejection increases with an increase of the metal-grid susceptances, regardless of the passband width or ripple, but is greater with a larger number of poles.

(4) Tolerances on the spatial filter lengths and susceptances must be held tighter for filters that provide greater rejection. A critical tolerance is the uniformity of the central lengths, because of the sensitivity of insertion phase to a change of length of a high-Q resonator. Also, small errors in the length values can greatly increase the filter reflection in its passband. Tolerances on the susceptances are

also important, both for insertion phase uniformity and for low reflection in the passband.

(5) A mechanical tolerance that is the tightest that is feasible can be related to a spatial filter rejection value that can be considered to be the greatest rejection that is available in practice. This available rejection is typically greater with filters having more poles. The available rejection also is typically greater when the frequency of operation is lower.

From the investigation of the properties of metal grids, the following conclusions have been drawn:

(1) A crossed metal grid providing inductive susceptance is a good basic element for a spatial filter.

(2) Several mechanical configurations for this crossed metal grid are available. For a contacting crossed grid, the main configurations are printed metal strips and holes in a metal sheet. For an insulated crossed grid the main configurations are metal wires and printed metal strips. All of these configurations involve dielectric material for support.

(3) Simple approximate formulas are available for all of these metal grid configurations except round holes. These formulas give the susceptance of the basic metal grid versus angle for both H-plane and E-plane incidence. The susceptance becomes large near grazing incidence in the H-plane, which is desirable. The susceptance becomes small near grazing incidence in the E-plane, which is not desirable.

(4) A simulator comprising a waveguide operating near cutoff in the TM-11 mode provides an excellent tool for measuring the behavior of metal grids and their dielectric support near grazing incidence in the E-plane. Such a simulator has been successfully developed and operated during this program.

(5) All of the metal grids measured in the near-grazing E-plane simulator exhibited the basic trend of reduced

susceptance or rejection with increasing angle of incidence. The insulated crossed wire grid gave less rejection than that predicted by the approximate formula.

(6) The addition of dielectric supporting skins to the metal grids measured in the near-grazing E-plane simulator gave increased rejection at angles close to grazing but gave reduced rejection at angles further from grazing. This indicates that the dielectric affects the metal-grid behavior in a way that reduces its susceptance for angles of incidence in the E-plane.

(7) There was no evidence of a spurious E-plane passband found in the simulator measurements made with dielectric skins added to the metal grids.

(8) Measurements made with a different simulator providing near-broadside incidence angles indicated good agreement with, or explainable differences from, the simple approximate formulas for metal-grid susceptance. For metal grids such as round holes, where a simple formula for susceptance is not available, this near-broadside simulator provides a tool that can be used for obtaining the grid dimensions when designing a real spatial filter.

The information contained in this report is intended to be valuable for understanding the performance that is available from a metal-grid spatial filter. It is also expected to be useful during the design, construction and testing of a spatial filter that is scheduled for the next part of this program.

## SECTION 6

### REFERENCES

- (1) R. J. Mailloux, "Synthesis of Spatial Filters with Chebyshev Characteristics", IEEE Trans. AP, pp. 174-181; March, 1976.
- (2) J. H. Pozgay, S. Zamoscianyk, L. R. Lewis, "Synthesis of Plane Stratified Dielectric Slab Spatial Filters Using Numerical Optimization Techniques", Final Technical Report RADC-TR-76-408 by Raytheon Co., December, 1976, A037960.
- (3) A. C. Schell et al, "Metallic Grating Spatial Filter for Directional Beamforming Antenna" AD-D002-623; April, 1976.
- (4) E. L. Rope, G. Tricoles, O-C. Yue, "Metallic Angular Filters for Array Economy", IEEE AP-S Int. Symp. Digest, pp. 155-157; 1976.
- (5) E. L. Rope, G. Tricoles, "An Angle Filter Containing Three Periodically Perforated Metallic Layers", IEEE AP-S Int. Symp. Digest, pp. 818-820; 1979.
- (6) G. G. MacFarlane, "Surface Impedance of an Infinite Parallel-Wire Grid at Oblique Angles of Incidence", JIEEE, Vol. 93, Pt. 3A, pp 1523-1527; 1946.
- (7) G. L. Matthaei, L. Young, E. M. T. Jones, "Microwave Filters", Impedance-Matching Networks, and Coupling Structures", McGraw-Hill, pp 85-101, 450-452; 1964.
- (8) M. I. Kontorovich, V. Yu. Pretun'kin, N. A. Yesepkina, M. I. Astrakhan, "The Coefficient of Reflection of a Plane Electromagnetic Wave from a Plane Wire Mesh", Radio Engineering and Electronic Physics (USSR), Vol. 7, No. 2, pp 222-231; February, 1962.
- (9) M. I. Astrakhan, "Reflecting and Screening Properties of Plane Wire Grids", Radio Engineering (USSR), Vol. 23, No. 1 pp 76-83; 1968.
- (10) G. A. Otteni, "Plane Wave Reflection from a Rectangular-Mesh Ground Screen", IEEE Trans. AP, pp 843-851; November, 1973.

- (11) N. Marcuvitz, "Waveguide Handbook" MIT Rad. Lab. Series, Vol. 10, McGraw-Hill, pp 284-288; 1951.
- (12) J. R. Wait, "Reflection at Arbitrary Incidence from a Parallel Wire Grid" Appl. Sci. Res., Sec. B, Vol. 4, pp 393-400; 1955.
- (13) P. W. Hannan and M. A. Balfour, "Simulation of a Phased Array in Waveguide", IEEE Trans. AP, pp 342-353; May, 1965.
- (14) P. W. Hannan, "Discovery of an Array Surface Wave in a Simulator," IEEE Trans. AP, pp 574-576; July, 1967.
- (15) H. A. Wheeler, "A Survey of the Simulator Technique for Designing a Radiating Element in a Phased Array", Phased Array Antenna Symposium, Artech House, pp 132-148; 1970.

## **MISSION of Rome Air Development Center**

RADC plans and executes research, development, test and selected acquisition programs in support of Command, Control Communications and Intelligence (C<sup>3</sup>I) activities. Technical and engineering support within areas of technical competence is provided to ESD Program Offices (POs) and other ESD elements. The principal technical mission areas are communications, electromagnetic guidance and control, surveillance of ground and aerospace objects, intelligence data collection and handling, information system technology, ionospheric propagation, solid state sciences, microwave physics and electronic reliability, maintainability and compatibility.